ISSN 1422 - 1381

MeteoSchweiz

SMA ISM SWI

Veröffentlichungen

Nr. 59

Jean-Marie Bettems

The impact of hypothetical wind profiler networks on numerical weather prediction in the Alpine region

© Schweizerische Meteorologische Anstalt

Mai 1999

Bestellungen an:
Stab und Dienste, Koordination und Information

SMA Schweizerische Meteorologische Anstalt
ISM Institut suisse de météorologie
ISM Istituto svizzero di meteorologia
ISM Institut svizzer da meteorologia
SMI Swiss Meteorological Institute

Krähbühlstrasse 58
Postfach
CH-8044 Zürich

Telefon 01/256 91 11
Telefax 01/256 92 78

ISSN 1422 - 1381

MeteoSchweiz

SMA ISM SMII

Veröffentlichungen

Nr. 59

Jean-Marie Bettems

The impact of hypothetical wind profiler networks on numerical weather prediction in the Alpine region

© Schweizerische Meteorologische Anstalt

Mai 1999

ABSTRACT

This report presents the results of the OSSE'97 project. This project has been funded by the Laboratory for Atmospheric Physics of the Federal Institute of Technology Zurich, and by the Swiss Meteorological Institute (SMI); its main objective is the evaluation of the impact of hypothetical wind profiler networks on the quality of a mesoscale numerical weather prediction (NWP) system in the Alpine region.

This work is based on the observing system simulation experiment (OSSE) technique, implemented with the Swiss Model (SM) and its associated assimilation scheme. The SM is a hydrostatic primitive equation limited-area model, with 14km mesh width, and the assimilation scheme is derived from the nudging method. In order to circumvent the identical twin problem associated to the use of a single NWP model in our OSSE implementation, the reference atmosphere of the OSSE set-up is obtained from the assimilation cycle. A validation of the technique is made by simulating the European network CWINDE and by comparing the impact of simulated and real data.

A case study approach is used. A set of eight cases has been selected, representing six meteorological situations potentially sensitive to wind profiler observations. The importance of the extent and of the density of the wind profiler network, the comparative impact of different instrument types, the comparative impact of a wind profiler network and of the current rawinsonde system are typical questions which are investigated. Some requirements for an effective observing system and some information about the assimilation scheme are also inferred.

The main results of the present work are summarized in eight thesis, which are presented in section 1.3 of the present document.

ZUSAMMENFASSUNG

Dieser Bericht stellt die Resultate des Projekts OSSE'97 vor. Dieses Projekt ist durch das Laboratorium für Atmosphärenphysik der Eidgenössischen Technischen Hochschule Zürich und der Schweizerischen Meteorologischen Anstalt (SMA) finanziert worden; das Hauptziel ist die Evaluation der Auswirkungen von hypothetischen Windprofiler-Netze auf die Qualität eines mesoskaligen numerischen Wetterprognose(NWP)-Systems in der Alpenregion.

Diese Arbeit basiert auf der Technik eines "Observing System Simulation Experiment" (OSSE, Beobachtungssystem-Simulationsexperiment), implementiert mit dem Schweizer Modell (SM) und dem zugehörigen Assimilationsschema. Das SM ist ein hydrostatisches, geographisch limitiertes Grundgleichungs-Modell mit 14 km Maschenweite, und das Assimilationsschema ist aus der "Nudging"-Methode abgeleitet. Um das Problem der "identischen Zwillinge" zu vermeiden, das mit dem Gebrauch eines einzigen NWP-Modells in unserer OSSE-Implementation zusammenhängt, wird die Referenz-Atmosphäre vom Assimilationszyklus für das OSSE-Experiment verwendet. Eine Validierung der Technik wird durch Simulation des europäischen Netzwerkes CWINDE und durch Vergleich der Auswirkungen von simulierten und echten Daten gemacht.

Eine Fallstudie wird durchgeführt. Acht Fälle sind ausgewählt worden, die sechs meteorologische Situationen repräsentieren, die potentiell besonders sensitiv für Windprofiler-Messungen sind. Die Wichtigkeit der Ausdehnung und Dichte des Windprofiler-Netzes, der Vergleich der Auswirkungen unterschiedlicher Instrumententypen, der Vergleich der Auswirkungen eines Windprofiler-Netzwerks gegenüber dem gegenwärtigen Radiosondensystem sind typische Fragen, die untersucht werden. Einige Voraussetzungen für ein wirkungsvolles Messsystem und einige Informationen über das Assimilationsschema werden ebenfalls abgeleitet.

Die wichtigsten Resultate der vorliegenden Arbeit werden in acht Thesen zusammengefasst, die in Abschnitt 1.3 dieser Arbeit vorliegen.

RESUME

Ce rapport présente les résultats du projet OSSE'97. Ce projet a été financé par le Laboratoire de Physique de l'Atmosphère de l'Ecole Polytechnique Fédérale de Zürich et par l'Institut Suisse de Météorologie (ISM); son objectif principal est l'évaluation de l'impact de réseaux hypothétiques de profileurs de vent sur la qualité d'un système de prévision numérique du temps à méso-échelle, particulièrement dans la région alpine.

Ce travail est basé sur la technique dite de simulation de système d'observation (OSSE), implémentée à l'aide du modèle Suisse (SM) et de son schéma d'assimilation. Le SM est un modèle hydrostatique basé sur les équations primitives, à domaine limité, avec une résolution horizontale de l'ordre de 14km; le schéma d'assimilation associé est dérivé de la méthode du 'nudging'. Afin d'éviter le problème des 'jumeaux identiques' associé à l'usage d'un unique modèle dans notre implémentation de la méthode OSSE, l'atmosphère de référence de notre système est dérivée du cycle d'assimilation. Une validation de la technique est effectuée en simulant le réseau européen CWINDE et en comparant l'impact des observations simulées avec l'impact des observations réelles.

Une étude de cas est effectuée. Un ensemble de huit cas a été choisi, représentant six situations météorologiques différentes, potentiellement sensibles à l'information apportée par des profileurs de vent. L'importance de l'étendue et de la densité du réseau de profileurs, l'impact comparatif de divers types d'instruments, l'impact comparatif d'un réseau de profileurs et du systèmes actuel de radiosondage sont des questions typiques abordées dans cette étude. Quelques contraintes que doivent satisfaire un système d'observation effectif ainsi que des informations sur le schéma d'assimilation sont aussi dérivés de cette étude.

Les résultats principaux de ce travail sont résumés en huit thèses présentées dans la section 1.3 de ce document.

RIASSUNTO

Questo rapporto presenta i risultati del progetto OSSE'97. Tale progetto è stato finanziato dal Laboratorio di Fisica dell'Atmosfera della Scuola Politecnica Federale di Zurigo e dall'Istituto Svizzero di Meteorologia (ISM); il suo principale obbiettivo è quello di valutare l'impatto di una ipotetica rete di "wind profilers" sulla qualità di un sistema di previsione numerica del tempo a mesoscala, in particolare nella regione alpina.

Questo lavoro è basato sulla tecnica detta di simulazione dei sistemi d'osservazione (OSSE), implementata con l'ausilio del modello Svizzero (SM) e del suo schema di assimilazione. SM è un modello idrostatico basato sulle equazioni primitive, a dominio limitato, con una risoluzione orizzontale dell'ordine di 14 km; lo schema associato di assimilazione è derivato dal metodo di "nudging". Onde evitare il problema dei "gemelli identici" associato all'uso di un unico modello nella nostra implementazione del metodo OSSE, l'atmosfera di riferimento del suddetto sistema viene derivata dal ciclo di assimilazione. Una validazione di questa tecnica viene effettuata simulando la rete europea CWINDE e confrontando l'impatto delle osservazioni simulate con quello delle osservazioni reali.

Un studio di differenti casi è stato effettuato. Un insieme di otto eventi è stato scelto in rappresentanza di sei situazioni meteorologiche differenti, potenzialmente sensibili all'informazione fornita dai "wind profilers". L'importanza dell'estensione e della densità della rete dei "profilers", l'impatto comparativo di diversi tipi di strumenti, l'impatto comparativo di una rete di "profilers" e del sistema attuale di radiosondaggio sono alcune delle questioni tipo affrontate da questo studio. Le condizioni alle quali deve soddisfare un sistema effettivo di osservazioni come pure alcune informazioni sullo schema di assimilazione vengono pure derivate in questo rapporto.

I risultati principali del lavoro svolto sono riassunte in otto tesi presentate nella sezione 1.3 di questo documento.

TABLE OF CONTENTS

1 Outline of the present work

1.1 Context and objectives

Wind profiling radars (WP) are remote sensing systems measuring vertical profiles of the wind vector up to many kilometres from the ground. They can be complemented with radio acoustic sounding systems (RASS) to provide profiles of temperature, although with a significantly smaller vertical span than that of the corresponding wind profile. While more traditional in-situ upper air sounding systems measure temperature and humidity profiles as well, WP radars do have several advantages: high frequency data, high vertical resolution, Eulerian characteristics, unattended operation in nearly all weather conditions.

Besides direct usage of WP observations for weather monitoring these observations have a priori a great potential to improve mesoscale forecasting by numerical weather prediction (NWP) systems. Current data assimilation schemes are being designed to make best use of high-resolution observations in time (and space). For example the so-called "nudging" method has proved to be a powerful tool to produce high-quality initial conditions for NWP. Thereby, the model atmosphere is continuously forced towards the available observations by adding a special relaxation term to the prognostic equations; the observational data can be used at the proper point in time without any need for temporal interpolation to fixed synoptic times. Wind profiler data are perfectly suited to be injected in a nudging scheme, all the more since the observed quantities have a straightforward relationship with the prognostic fields of the NWP model and do not require any further processing to be assimilated.

It is the main objective of the OSSE'97 project to evaluate the impact of hypothetical WP networks on the quality of the analysis (initial conditions) and forecast of a mesoscale NWP system in the Alpine region; this information will be a very valuable decision tool for the Swiss Meteorological Institute (SMI) in relation with the vision to build a WP network in Switzerland. A second objective is to help define the location of the wind profilers to be deployed during the observing period of the Mesoscale Alpine Programme (MAP – Binder and Rossa, 1996). In order to support the MAP experiment (e.g. aircraft mission planning) real-time high-resolution forecasts will be provided during this period; it is desirable to optimize the usage of the available WP to get the best possible forecasts.

1.2 Methodology and limitations

A useful tool to assess the performance of a proposed observing system – from which there have not yet been any observation – is the observing system simulation experiment technique (OSSE). In this approach *simulated* observations are extracted from a reference atmosphere created by running the best available NWP model; this reference atmosphere represents the "truth". In a second step a less perfect model is used to produce forecasts with and without assimilating the simulated observations. The impact of the proposed observing system is measured by comparing these two forecasts with the "truth" of the reference atmosphere.

The Swiss Model (SM) and its associated assimilation scheme based on the nudging technique have been used to implement the OSSE technique. The SM is an hydrostatic primitive equation, limited area model, with a mesh size of about 14km, and a vertical resolution of about 100m in the low troposphere decreasing to about 1000m at 10km. The SM is calculated on a 2000km×2000km domain centred over Switzerland. Data from the European wind profiler network CWINDE (Oakley et al., 1997) have been used

to validate our implementation of the OSSE technique (a complete description of these tools is presented in section 2).

A set of eight meteorological cases has been selected representing six different meteorological situations potentially sensitive to WP observations:

- one case characterized by a fast moving front in a westerly flow (FASTEX case);
- two episodes of heavy precipitation over the southern Alps, with advection of warm and moist air from the Mediterranean towards the Alps (MAP cases);
- two cases of summer convection;
- one case of south Foehn;
- one case characterized by upper-level cold air drops in an easterly flow;
- one case with opposite-direction northeasterly low level and westerly high level flows, with strong wind shear.

Then different configurations of WP networks have been simulated to investigate the following questions (the experimental set-up is thoroughly described in section 3):

- what is the impact of WP observations on the quality of the SM analysis and forecast; how does it compare with the impact of the current rawinsonde system;
- how does the impact of full-tropospheric radars (FT radars – 400MHz class) compare with the impact of boundary layer radars (BL radars – 1.2GHz class);
- how does the impact of realistic WP network configurations compare with the impact of a "maximum" configuration;
- what is the effect of complementing a Swiss-scale WP network with the European-scale network CWINDE.

It should be remembered that OSSEs measure the combined effect of the observing system *and* of a particular NWP model with its assimilation scheme. Hence OSSEs are also an efficient tool to point out weakness in the assimilation method. On the other hand results must be interpreted with great care when seeking to generalize the conclusions of the experiments to an arbitrary NWP system.

Experience at ECMWF has shown that the impact on NWP forecasts due to changes in the assimilation scheme are much less consistent, over a number of cases, than impact due to changes in the model formulation (Bader and Graham, 1996, section 2.1). In this sense our results are based on a relatively small set of cases and we paid special attention to this fact in drawing our conclusions, in particular by avoiding generalization of statistically non significant results.

Due to limitations in our implementation of the OSSE method (see section 2.3.2 for more details) only the impact of a standalone WP observing system can be studied; no assessments can be made about the impact of WP observations when used to complement the current operational observing system. Moreover, due to practical constraints, no systematic evaluation over a long period has been performed so that it was not possible to derive statistically significant information *about the mean performance* of a specific WP network. However this does not prevent robust conclusions *about the relative performances* of different WP networks or different observing systems.

1.3 Main results

In this section a set of eight thesis summarizing the main results of the project are presented. The results supporting these thesis are described in section 4.

On the impact of hypothetical Swiss wind profiler networks on the NWP system of the Swiss Meteorological Institute:

Thesis A1 WP observations have a positive effect on analysis and very short range forecasts of *wind*. The so-called maximum network – a network of 12 WP regularly spaced over Switzerland – corrects between 30% and 75% of the low-level wind analysis error over Switzerland; this impact is similar to the impact of the current operational rawinsonde network. However, this positive effect mostly disappears after 12 hours of forecast.
The impact on the mass and the temperature fields, if any, is in most cases not significant and no effect on the precipitation field is observed.

Thesis A2 The only observed difference between the impact of FT radars (400MHz class) and of BL radars (1.2GHz class) is the improved mid-tropospheric wind. However mid-tropospheric winds are less depending on the initial conditions and more depending on the governing model (via the lateral boundary conditions) than lower level winds, so that only a limited potential for improvement exists for FT radars.

Thesis A3 Realistic configurations for a network of BL radars (1.2GHz class) bring a substantial part of the correction obtained with the maximum network. For example profiles at Payerne and at the locations of the 3 Swiss weather radars bring in most of the cases between 50% and 100% of the "maximum" low level wind correction.

Thesis A4 Complementing a Swiss-scale network with the European-scale CWINDE network brings a further positive impact on wind forecast in some meteorological situations. This illustrates the importance of upstream observing systems for forecast quality. However the CWINDE network, with its 10 profilers, is not dense enough to have a systematic impact (about this last point see also thesis B2).

Comparison between wind profiler and rawinsonde observing systems – some observing system requirements for effective NWP model initialization:

Compared with the impact of the simulated WP networks the impact of the current operational rawinsonde network (about 60 stations on the SM domain) is characterized by initial conditions which are more *consistent* with the reference atmosphere. Indeed the positive effect on the initial conditions persists much longer in the forecast, and an improvement of the precipitation field is observed in some cases.

Thesis B1 On the meso-β-scale it is not sufficient to assimilate the wind. In order to have a robust assimilation scheme with a visible impact of the observing system on the *forecast*, it is necessary to assimilate observations which directly constrain additional fields of the model. Indeed the mass, temperature and humidity fields do not necessarily adapt to the wind field; in some situations the mass field can even be the dominant factor for improving the analysis.

Thesis B2 The high temporal resolution of WP observations does not compensate for a poor horizontal resolution of the observing system. A sufficient horizontal resolution on the *whole* NWP domain is a prerequisite for bringing a consistent and systematic quality improvement of a meso-β–scale limited area model. A horizontal distance between neighbouring instruments of about 250km produces good results.

On the nudging scheme deployed at the Swiss Meteorological Institute:

Thesis C1 In the low to mid troposphere the vertical influence range of a single-level upper air observation is too broad (observations at the top and bottom of a multi-level report also belong to the single-level upper air category).

Thesis C2 The assimilation of the horizontal wind does not always produce a consistent improvement of initial conditions *and* forecasts. Forcing the model wind towards the observations at some sensitive atmospheric locations may result in a large *negative* impact in the forecast, although the initial conditions of the wind field have been improved. This behaviour is not sensitive to the degree of non-divergence used in the parametrization of the horizontal wind correlation. A small improvement is observed if the horizontal influence range of wind observations is reduced.

In view of these results an optimal configuration for a Swiss WP network, both in terms of cost and impact on the quality of the SM, would consist of 4 to 6 boundary layer radars regularly distributed over Switzerland. In fact the backbone for such a network already exists, albeit in experimental modes, with the profiler at Payerne and the wind profiles derived from the three operational Swiss weather radars (La Dôle, Albis, Monte-Lema – Germann, 1998). However the restricted availability of the profiles above weather radars due to poor sensitivity in clear-air is a drawback of this system.

Moreover, the potential of a Swiss WP network for NWP is limited as long as it is not part of a larger network covering the whole NWP model domain with sufficient horizontal resolution. Another lesson drawn from this work is the massive NWP quality loss which would result from a replacement of the existing rawinsonde observing system with a WP based system; such a scenario should only be considered if the WP system is complemented by other observing systems providing good quality surface pressure and thermodynamic profiles.

Finally the above results – based on the current operational model used at the SMI – should not substantially differ if this model is replaced by a non-hydrostatic model with increased horizontal resolution.

1.4 Related studies

Preliminary results of this work have been presented during the fourth International Symposium on Tropospheric Profiling held in Snowmass (Bettems et al., 1998), and during the fourth MAP Meeting held in Chamonix (Bettems and Binder, 1998).

Other authors have applied the OSSE technique, in conjunction with the nudging scheme, to evaluate the impact of hypothetical WP observing systems on NWP quality:

- Kuo and Guo (1989) performed a *single* case study with an adiabatic version of the PSU/NCAR model, with a 80 km horizontal resolution, to evaluate the impact over the continental United States of a network of 77 evenly distributed WP; they found a positive impact in controlling error growth for large scale circulations and in recovering mesoscale circulations, resulting in improvement of precipitation forecasts; noteworthy is the fact that significantly better results were obtained when wind profiles were complemented with temperature profiles.
- More recently Schraff (1996) performed a *single* case study with the Swiss Model – a cut-off low passing over Germany – to evaluate the impact of a network of 18 evenly distributed WP located in the main precipitation area; he only found a clear positive impact on the forecast of relevant weather elements (position of warm front and

precipitation) when assimilating the temperature profiles in addition to the wind profiles.

In both of these studies WP observations have been simulated with hourly temporal resolution. Sensitivity studies have shown the existence of a critical temporal resolution such that any resolution increase beyond this value does not significantly improve the model analysis and forecasts. In Kuo and Guo this value has been found to be around 3 hours.

Observing system experiments (OSE) based on the US Wind Profiler Demonstration Network (NOAA, 1994) have been conducted by Smith and Benjamin (1994). Assimilation of real data from these 30 profilers has resulted in consistent improvement in the 3 and 6 hour short-range wind forecasts; however, no impact was detectable in the 12 hour forecasts.

Finally Bader and Graham (1996) made an extensive review of recent impact studies completed by an interesting discussion of the OSE and OSSE techniques.

2 Description of the tools

2.1 The Swiss Model

The NWP model deployed in this study is a version of the operational Swiss Model (SM). It is based on the code of the Europa Model (EM) of the German Weather Service (Majewski, 1991). It is an hydrostatic primitive-equation limited-area model cast in a terrain-following coordinate system. Its prognostic variables are surface pressure p_s, the horizontal wind components (u,v), total heat h (the sum of enthalpy and latent heat) and total specific water content q_w (the sum of specific content of water vapour q_v and of liquid water q_c). Assuming water saturation in clouds, the quantities q_v, q_c and the temperature T can be derived from these prognostic variables. The geopotential ϕ and the vertical velocity are diagnostic variables.

The SM is formulated on an Arakawa-C grid using rotated spherical coordinates. In the vertical the atmosphere is resolved in N layers; the layer interfaces are constant pressure levels above a critical pressure level p_T and constant σ levels below this level – σ is the quotient $(p-p_T)/(p_s-p_T)$ where p stands for pressure. The prognostic variables (u,v), h and q_w, as well as the diagnostic variables T, q_v, q_c and the vertical velocity in the pressure system ω are defined at the centre of the layers (*full levels*). The geopotential, the vertical velocity in the hybrid system and the vertical fluxes are evaluated at the layer interfaces (*half levels*). The time stepping is leap-frog with semi-implicit correction and Asselin-filter; both Euler and Semi-Lagrange treatment of the horizontal advection are available. Second order central differences are used for spatial discretization. A linear fourth-order horizontal diffusion of the 3-D prognostic variables is performed along the model levels, with a correction term in the heat equation to account for the slope of the model layers.

The vertical turbulent fluxes are parametrized with a second order closure scheme of hierarchy level 2 for the Ekman layer and the free atmosphere (Mellor and Yamada, 1974). The Dyer-Businger relations as modified by Louis (1979) are used in the surface layer. A δ-two-stream radiation scheme for short- and long-wave fluxes with full cloud-radiation feedback is implemented (Ritter and Geleyn, 1992). A mass flux scheme after Tiedtke (1989) is used for the parametrization of moist convection. The SM also includes grid-scale precipitation with cloud microphysics parametrization and a two-layer soil model after Jacobsen and Heise (1982) with snow and water interception storage.

The SM grid is embedded in the four times coarser EM grid and the lateral boundary conditions (LBC) for the SM are provided by EM fields interpolated to the fine mesh grid; special care is taken to adapt the EM fields to the SM orography (Majewski, 1985). These lateral boundary conditions are then assimilated by a relaxation scheme after Davis (1976) which adjusts the SM prognostic fields towards the prescribed interpolated EM fields in a marginal zone of 8 grid rows (one way nesting). At the model top both a lid-type upper boundary condition (ω=0) and a radiative upper boundary condition (RUBC – Herzog, 1995) are available; the lid-type condition can be combined with vertical nesting – the SM fields are nudged towards the driving EM fields in the upper atmosphere – in order to reduce the noise produced by reflection of vertically travelling gravity waves at the model top.

There are two analyses readily available at the SMI which can be used as initial conditions for the SM. The first possibility is to use the 3-D optimum interpolation analyses (OI) of the EM dynamically interpolated on the SM grid (Majewski, 1985), followed by an adiabatic normal mode initialization. The second possibility consists in a 4-D data assimilation cycle based on the nudging method. This latter method is used in our OSSE set-up and is shortly described in section 2.2.

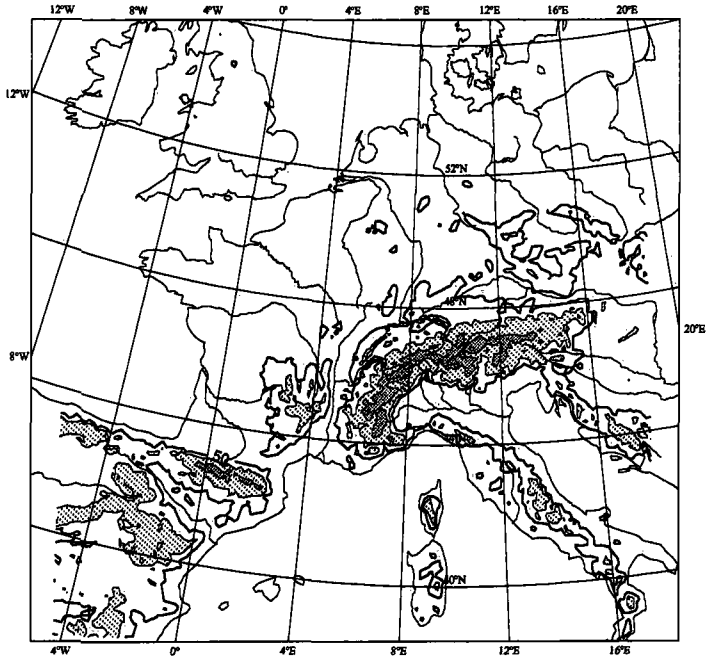

FIGURE 2-1. Swiss Model domain and orography. Isolines at 500, 1000, 2000 and 3000 metres above sea level; light shaded areas between 1000 and 2000m.

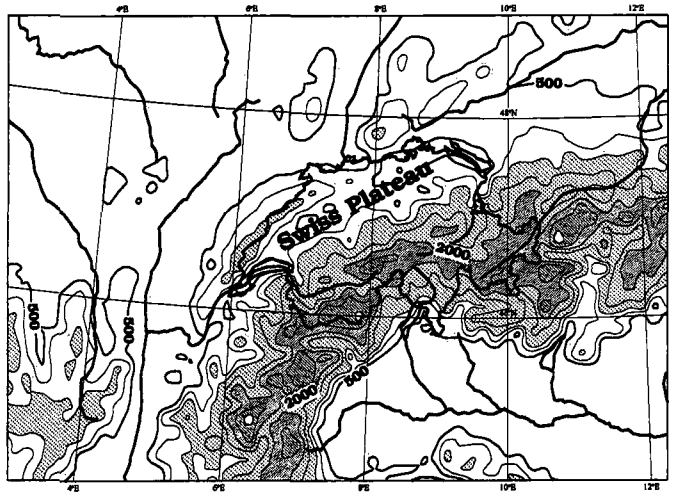

FIGURE 2-2. Swiss Model orography, zoom around Switzerland. Isolines at 500, 750, 1000, 1500, 2000 and 3000 metres above sea level; light shaded areas between 1000 and 2000m.

All experiments performed for the present work are calculated on a 145×145 mesh centred over Switzerland with a 1/8° mesh size, resulting in a horizontal resolution of about 14km. The figures 2-1 and 2-2 depict the SM domain and the model orography; at this resolution only the main Alpine valleys are (partly) resolved and the maximum height for the Alps is around 3100m. In the vertical either a 48 layers configuration (for the reference experiments, see section 2.3) or a 40 layers configuration is used. In both configurations the vertical resolution in the lowest 2km of the atmosphere is about 100m, it then increases smoothly to reach 500m at 4km and 800m at 8km. The exact definition and distribution of the model layers is given in annexe A. In order to minimize spurious smoothing of horizontal gradients the Euler time scheme with a 90 second time step has been preferred to the Semi-Lagrangian scheme. The RUBC has been used at the model top and vertical nesting is not active. (Full) horizontal diffusion along model levels is used.

The model version and the complete set of parameters defining the model configuration are found in annexe B.

2.2 The data assimilation scheme

The assimilation scheme used in this study is based on the nudging or Newtonian relaxation method. A historical overview of the technique can be found in Stauffer and Seaman (1990) and a critical discussion of the method in Bao and Errico (1997). This technique has been implemented in the SM by Schraff (1996, 1997) using relaxation of the SM dynamical fields towards direct observations.

In this scheme the tendency for a SM prognostic field Ψ evaluated at time t and at the grid point $\boldsymbol{x} = (x,y,p)$ is based on the expression

$$\frac{\partial}{\partial t}\Psi(\boldsymbol{x},t) = M(...) + G_\Psi \cdot B(\boldsymbol{x}) \cdot \frac{\sum_{i \in obs} \varepsilon_i \cdot \omega_\Psi^2(\boldsymbol{x},\boldsymbol{x}_i,t-t_i) \cdot [\Psi_i^{obs} - \Psi(\boldsymbol{x}_i,t)]}{\sum_{i \in obs} \omega_\Psi(\boldsymbol{x},\boldsymbol{x}_i,t-t_i)} \qquad (2\text{-}1)$$

The second term on the right hand side represents the nudging term and M(...) represents all other model terms. G_Ψ is the nudging coefficient and $B(\boldsymbol{x})$ a lateral boundary relaxation term, ranging between 0 and 1. The sums in the nudging term run over all observations influencing the model field at the location $(\boldsymbol{x}, t)$. For any observation Ψ_i^{obs} at location $(\boldsymbol{x}_i, t_i)$ the difference $[\Psi_i^{obs} - \Psi(\boldsymbol{x}_i, t)]$ between the observation value and the collocated model field value is the so-called *observation increment*. The correction to the tendency of the model field at the location $(\boldsymbol{x}, t)$ due to the observation Ψ_i^{obs} is proportional to the corresponding observation increment, weighted by a factor ε_i reflecting the observation quality and representativeness and by a factor ω_Ψ reflecting the four-dimensional distance between the location of the observation and the point where the model tendency is evaluated. Both these factors range between 0 and 1.

In the present work G_Ψ is set to 6×10^{-4} s^{-1} which corresponds to an e-folding time of about half an hour[1]. A smaller value of G_Ψ results in poorer control of large-scale error growth (Schraff, 1996). On the other side Bao and Errico (1997) have shown that even for such a small coefficient the nudging terms are a significant contribution to the prognostic tendencies. This means that *the temporal evolution of the model fields is significantly altered compared to what would occur in the absence of nudging.*

The function ω_Ψ defines the way the influence of one observation is spread around the observation location. It is represented by the product of an horizontal part $\omega_{\Psi,r}$, a vertical part $\omega_{\Psi,z}$ and a temporal part $\omega_{\Psi,t}$ which all range between 0 and 1. The parameters used to model these weights are defined separately for each prognostic field and for both upper air and surface observations.

- To define the temporal weight $\omega_{\Psi,t}$ one considers two cases. Firstly, if there are two observations from the same station at times t_1 and t_2 with $t_1 < t < t_2$ and (t_2-t_1) small enough, then a new observation increment for time t is constructed by linear temporal interpolation of the increments at time t_1 and t_2, and the weight $\omega_{\Psi,t}$ is set to 1. Otherwise the temporal weight $\omega_{\Psi,t}(t-t_i)$ is a piecewise linear function, set to 0 outside the domain of influence $[-t_{bwd}, +t_{fwd}]$ and defined in figure 2-3.

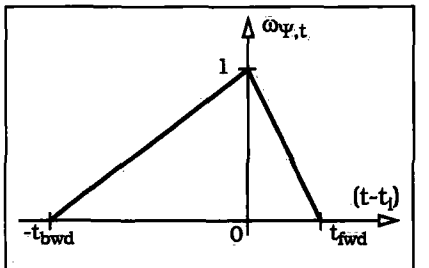

FIGURE 2-3. Temporal weight

[1] If one drops the model term M(...) in equation 2-1 and assumes a single perfect and time invariant observation, then the model field at the observation location approaches the observed state exponentially with an e-folding time of $(1/G_\Psi)$.

Linear temporal interpolation for upper air data takes place when observations are not more than 3 hours apart (respectively 1 hour apart for surface data); the domain of influence of $\omega_{\Psi,t}$ is set to [-3h,+1h] for upper air data and to [-1.5h, 0.5h] for surface data.

- To define the vertical weight $\omega_{\Psi,z}$ one distinguishes multi-level observations from surface or single level upper air observations; note that the bottom and the top of a multi-level report belong to this latter class.
  For a *multi-level report* a vertical interpolation procedure is used to build a 'continuous' profile of observation increments; the observation increment at height p influences only the field tendency at the same height, and the weight $\omega_{\Psi,z}$ for that increment is set to 1. For *single level upper air observations* the weight $\omega_{\Psi,z}$ is a function of the difference $\Delta=(lnp-lnp_i)$; for *surface observations* it is a function of the equivalent potential temperature difference $\Delta=(\theta_e-\theta_{e,i})$. In both cases the vertical weight is modelled by the Gaussian type function $exp[-(\Delta/\sigma_z)^2]$, set to 0 outside of the domain $[-\Delta_{cut},\Delta_{cut}]$, where σ_z and Δ_{cut} are parameters of the scheme. For a single level upper air wind observation, the value of Δ_{cut} is such that the vertical influence radius is about 100hPa at the 500hPa level and 150hPa at the 850hPa level.
  The net effect of this procedure is that the information from upper air observations (multi- or single-level) is spread mainly along isobaric surfaces, whereas information from surface observations is spread mainly along isentropic surfaces.
- The horizontal weight $\omega_{\Psi,r}$ is expressed in term of the horizontal distance $r=[(x-x_i)^2+(y-y_i)^2]^{1/2}$. For *surface pressure* and *thermodynamic fields* it is modelled by the function $(1 + r/\sigma_r) \times exp(-r/\sigma_r)$, set to 0 outside of the domain $[-r_{cut},r_{cut}]$, where r_{cut} is a parameter of the scheme. The scale σ_r depends on $(t-t_i)$ and, for upper air data, on the observation height according to $\sigma_r = \kappa(t-t_i) \times \sigma_{r,0}(p_i)$, where $\sigma_{r,0}$ is derived from OI analysis. The function κ is defined in figure 2-4, and some typical parameters are listed in table 2-1.

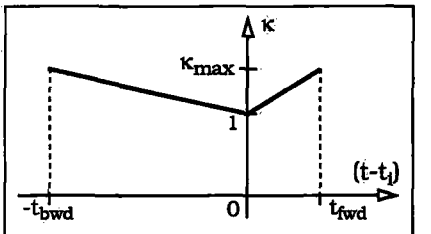

FIGURE 2-4. Temporal variation of horizontal weight

- The horizontal spreading of *wind field* observation increments is based on the decomposition of the horizontal wind vector into a transverse and a longitudinal part (see figure 2-5). The horizontal weight for the longitudinal part is represented by the function $exp(-r/\sigma_r)$ and the weight for the transverse part by $(1 + \gamma \times (r/\sigma_r)) \times exp(-r/\sigma_r)$; both of these functions are set to 0 outside of $[-r_{cut},r_{cut}]$. The parameter r_{cut} and the scale σ_r have been defined in the previous paragraph. The value of γ

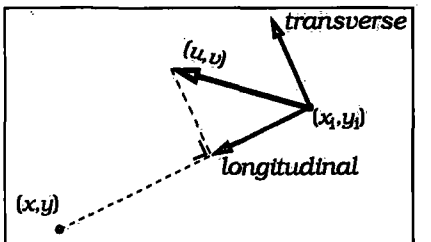

FIGURE 2-5. Wind decomposition for horizontal spreading

	Surface observation			Upper air observation				Both	
	$\sigma_{r,0}$	κ_{max}	r_{cut}	$\sigma_{r,0}$(850hPa)	$\sigma_{r,0}$(500hPa)	κ_{max}	r_{cut}	γ (850hPa)	γ (500hPa)
p_s	83 km	1.1	$2 \times \sigma_r$	–	–	–	–	–	–
(u,v)	70 km	1.0	$2.5 \times \sigma_r$	80 km	100 km	1.3	$3.5 \times \sigma_r$	0.4	0.5
T	100 km	1.0	$2 \times \sigma_r$	65 km	83 km	1.3	$3.5 \times \sigma_r$	–	–
RH	70 km	1.0	$2 \times \sigma_r$	65 km	83 km	1.3	$2.5 \times \sigma_r$	–	–

TABLE 2-1. Parameters defining the horizontal weights for surface and upper air observations. See the text for a full description (*RH* is the relative humidity).

defines the degree of non-divergence of the wind field tendency due to observation increments; it ranges between 0 and 1, a value of 1 being for a fully non-divergent correction.

In order to better assimilate surface pressure a correction of the vertical temperature profile in the lower troposphere is associated to any surface pressure increment. On the other hand, to preserve the mesoscale structures of the wind, *no* geostrophic wind correction is associated to the assimilation of surface pressure observations. Finally the tendency due to a surface pressure increment as expressed in equation 2-1 is corrected by a factor taking into account the height difference between the location of the observation and the point where the surface pressure tendency is calculated.

The set of data used in a standard run of the assimilation cycle is composed of rawinsonde observations (TEMP, PILOT), surface observations (SYNOP, DRIBU, TESAC) and aircraft observations (AIREP, AMDAR). All upper air observations are utilized except humidity data above 300hPa and significant level data of wind and temperature above 150hPa. Temperature from surface observations is not used, and surface level humidity is only assimilated if the height difference between the station and the model orography is less than 160m; the use of 10 meter wind is restricted to stations which are below 500m and for which the same height difference is less than 100m. The surface pressure is used as long as the station is not more than 100m above or 400m below the model orography. Finally a simple quality control is performed by comparing at each time step the observation increments with predefined thresholds.

The version of the nudging code and a complete set of parameters defining the nudging configuration used in the present work are found in annexe C.

2.3 The OSSE technique

2.3.1 Concept

A description of the observing systems simulation experiment methodology can be found in Arnold and Dey (1986) and in Bader and Graham (1996); in the first paper a summary of the history of OSSE is also presented. The basic idea of the OSSE technique, as a tool to assess the performance of an hypothetical observing system, has already been described at the beginning of section 1.2. In the present section a brief description of an optimal implementation of this technique is done; in the next section the implementation used in the present work is described.

OSSEs have a history which can be traced back to Newton (1954). Based on this long experience a state of the art implementation of the technique, schematically represented in figure 2-6, is defined by the following elements:

1. A long model forecast (many days) using the best available NWP model is performed. This is defined to be the *reference* atmosphere and is used both as a starting point to simulate the hypothetical observing system and to represent the 'true' atmospheric state. A property of OSSE is the perfect knowledge of this true atmospheric state, unlike the OSE situation where the true state is the real atmosphere.
2. Synthetic observations extracted from the reference atmosphere are produced for both the hypothetical observing system and the currently used observing system. The observation characteristics (coverage, resolution, errors, ...) should be simulated as realistically as possible; in particular the correlation of errors with the current meteorological situation should be introduced appropriately.

3. Two assimilation cycles are constructed. On the one hand all synthetic observations are assimilated – this is the *test* run; on the other hand only the synthetic observations from the currently used observing system are assimilated – this is the *control* run. The relationship between these two runs and the reference run should be similar to the relationship between the (operational) NWP model and the reality. For that reason the test and control runs should be based on a different model, less sophisticated than the model used for the reference atmosphere.

4. Forecasts based on the control and the test assimilation cycles are calculated every few days. These forecasts are verified against the reference atmosphere to measure the likely impact of the hypothetical observing system. Note that it is necessary to have a representative set of cases in order to draw *statistically significant* conclusions.

5. If a *real* observing system similar to the hypothetical one exists, it is possible to validate the OSSE implementation against an OSE by comparing the impact of simulated data with the impact of genuine data. Moreover a calibration factor can possibly be deduced from such a comparison and applied to further OSSE results.

A first limitation of the OSSE technique is its dependency on the choice of a specific NWP model and assimilation scheme. In particular the results obtained with a particular assimilation system may not be transferable to a very different system. Another limitation is connected to the degree of realism of the reference run. Obviously atmospheric structures *not* present in the reference run (for example due to poor initial conditions) will not be present in the simulated observations either, but could be present in the real observations; in that sense the OSSE technique does not expose the full potential of a new observing system.

2.3.2 Implementation

Due to practical constraints the optimal OSSE configuration described in the previous section could not be applied. Indeed only one NWP model was available, the SM, and the massive computational resources required (one long assimilation cycle for each hypothetical WP network configuration) were incompatible with the time constraint of the project.

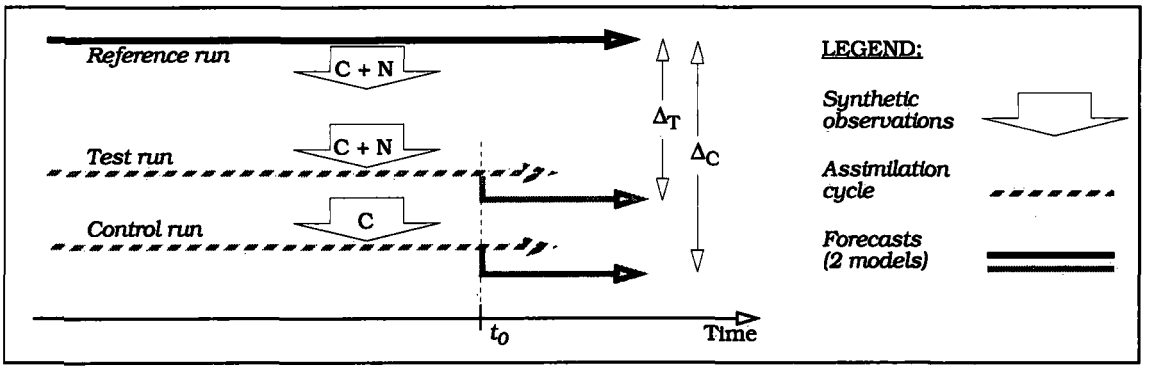

FIGURE 2-6. Optimal OSSE implementation. Synthetic observations for the current (C) and the new (N) observing systems are extracted from the reference run, based on the best available model. They are re-assimilated in the control and the test runs, based on a simplified model. Impact of the new observation system is assessed by comparing the errors of the control forecast (Δ_C) with the error of the test forecast (Δ_T) – errors defined with respect to the reference fields.

Circumventing the identical twins problem.

If the same model for the reference and for the test and control runs is used, the impact of synthetic observations is over-estimated and optimistic conclusions may be drawn from the OSSE (this is the so-called *identical twins problem*). Indeed, in such a case, the characteristics of the synthetic observations, unlike real observations, are fully consistent with the assimilating model; moreover the NWP model deficiencies are not simulated (in other words a situation with a perfect model is considered). In order to circumvents this problem another approach has been chosen, characterized by a reference run based on the SM assimilation cycle. This approach is described in figure 2-7.

With the proposed design the identical twins problem is strongly mitigated: the forcing due to the nudging term substantially alters the evolution of the reference fields compared to what occurs in the test and control runs (section 2.2), and the different distribution of vertical levels (higher resolution) further distinguishes the reference run.

Envisaged inferences.

However, in order to keep this property, it is not possible to follow the optimal OSSE design and to compare the impact of the current with the impact of the complete (current and hypothetical) observing system; *only the impact of the hypothetical observing system alone can be evaluated.* Indeed, assimilating observations from the current observing system in the control run would mean a similar observation forcing for both the reference and the control run; it would also result in a rapid convergence of reference and control fields, and a complete loss of sensitivity to the new observing system.

This limitation in the predictive skill of the OSSE technique does not prevent robust conclusions about the *relative* performances of different hypothetical WP networks, or about the relative performances of some hypothetical WP network and the current rawinsonde network. In this latter case the real rawinsonde observations are directly assimilated in the test run (instead of the synthetic observations, see figure 2-7). Because they represent a (relatively) small subset of the current observing system, the argument about the absence of the identical twins problem still holds.

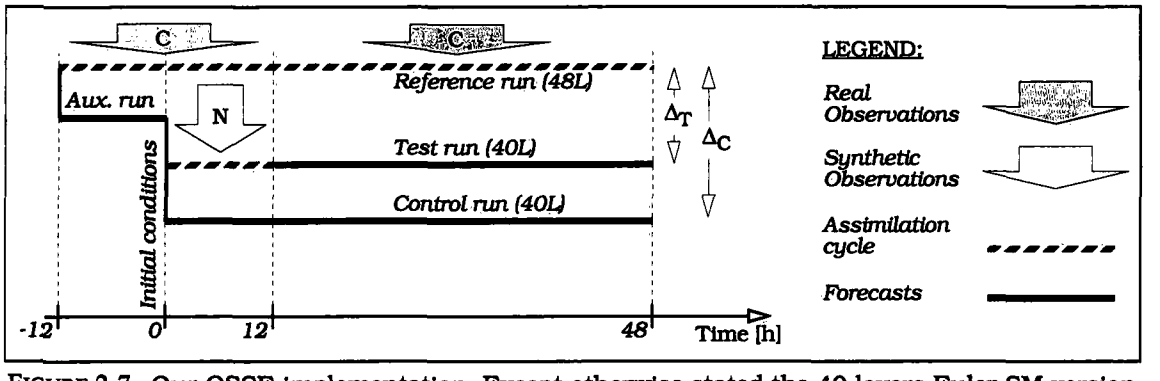

FIGURE 2-7. Our OSSE implementation. Except otherwise stated the 40 layers Euler SM version described in section 2.1 is used and the same LBC are used in all runs. Synthetic observations for the hypothetical WP networks (N) are extracted from the reference run, which is based on a 48 layers version of the SM assimilation cycle, with all conventional data (C) assimilated. A state differing from the reference is built from a 12h run of a semi-Lagrangian SM version; it is used as initial conditions for both control and test runs. The test run is a 12h assimilation cycle, ingesting observations (N), followed by a 36h forecast; the control run is a 48h forecast. Impact of the hypothetical WP network is measured by comparing the errors of the control forecast (Δ_C) with the error of the test forecast (Δ_T) – errors defined with respect to the reference fields.

Initial conditions.

A further point to consider is the dependence of OSSE results on the choice of the initial conditions, at time 0h. They define the initial errors of the test and control fields measured against the reference fields; if these errors are small in the region where the simulated observing system is located, or if they are so large that the build-in quality control rejects the simulated observations, the effect of the simulated observing system will be small. To circumvent this problem, a procedure has been designed to produce initial conditions which are 'reasonably' different from the reference fields: they result from a 12h *forecast* of a semi-Lagrangian SM version (the auxiliary run defined in figure 2-7). Moreover, the acuity of this problem is much lowered if only comparative information is drawn from the OSSE, which is the case in the present study.

Lateral boundary conditions.

Except the auxiliary run, all runs use the same hourly lateral boundary conditions. This means that our OSSE design simulates a system with perfect LBC. This simplifies the interpretation of OSSE by removing a factor interfering with the initial conditions in the determination of the forecast quality, without significantly degrading the value of our conclusions; indeed LBC driven situations (e.g. strong advective cases) are not very sensitive to initial conditions.

LBC are derived from the most recent EM analysis or forecast, a new set of EM analysis and hourly forecasts being available every 12 hours. To ensure a smooth transition between contiguous 12 hour sets, a linear temporal interpolation between the LBC at time +9h of the first set and the LBC at time +0h of the next set is performed. For the auxiliary run this interpolation is not performed: only the LBC of the first set are used. This is done in order to increase the magnitude of the error in the initial conditions.

2.3.3 Characteristics of synthetic wind profiler observations

A report for a synthetic WP observation contains a vertical profile of the horizontal wind velocity and direction, and can be complemented with a temperature profile if simulation of RASS is wanted. Observation errors are also simulated. The profile location (in grid point units), the profile bottom and top (in meters above surface), the vertical resolution of the profile (in meters) and the error characteristics are individually specified for each simulated WP. The observation frequency is *globally* specified for all simulated WP. These synthetic observations, possibly complemented with real observation reports, are stored in AOF format (Martellet, 1978) for later processing. The extensions to the SM code made to allow the generation of synthetic wind profiler observations are described in annexe D.

Synthetic wind and temperature profiles are derived from the model fields at the profile location. Interpolation procedures are defined to be consistent with the SM and the nudging algorithms – a synthetic profile without superimposed errors extracted from a SM integration should have no impact when re-assimilated in a second identically configured SM integration (in a first approximation). The following steps are performed to obtain such synthetic profiles:

1. The geopotential ϕ on each observation level is obtained from the height above ground of this level.
2. The pressure p on each observation level is obtained by linear interpolation of $ln(p)$ with respect to ϕ between the adjacent model *half-levels*[2].

3. The horizontal wind (u,v) and the temperature T on each observation level are obtained by interpolating linearly (u,v) and T with respect to $ln(p)$ between the adjacent model *full-levels*[3].
4. The horizontal wind direction and velocity (dd,ff) are obtained after transforming (u,v) from the rotated coordinate system to the geographic coordinate system.
5. A synthetic error composed of a bias and a random error is superimposed to the values of dd, ff and T in order to obtain the final profiles.

Characteristics of WP errors are generally derived by comparing WP observations with a NWP model analysis or short term forecast, or with rawinsonde observations. Results of such comparisons can be found in Görsdorf (1997) for RASS errors, in Nash and Lyth (1997) or Van Baelen (1998) for wind profile errors. Of course these characteristics depend heavily on the type and specifications of the WP radar and on the algorithm used to process raw observation data. In the present work a simplified model for synthetic errors is used:

1. Observation of wind speed, wind direction and temperature are independent random variables.
2. Observations at two different levels or two different times are independent random variables.
3. Let the observation of a field Ψ at a specified time and level be represented by the random variable Ψ_{obs}, and let Ψ_{mod} be the value of the field derived from the SM; then Ψ_{obs} is defined by $\Psi_{obs} = \Psi_{mod} + \Delta\Psi_{bias} + \Delta\Psi_{rand}$ where $\Delta\Psi_{bias}$ is the bias and $\Delta\Psi_{rand}$ is the random error.
4. The bias $\Delta\Psi_{bias}$ and the standard deviation σ_{rand} depend only on the specified field and on the type of simulated WP. In particular these quantities neither depend on the height of the observation nor on the current state of the atmosphere.
5. The random variable $\Delta\Psi_{rand}$ is defined to be normally distributed with a standard deviation σ_{rand} and a mean Ψ_{mod} [4]. Moreover, to avoid unrealistic large errors the normal distribution is truncated at $2\times\sigma_{rand}$.
6. The standard deviation σ_{rand} for the wind velocity is proportional to the wind velocity itself; this ensures reasonably smooth wind profiles even with low winds. The standard deviation for the other fields and all biases have constant values.
7. The numerical values of the different parameters introduced in this error model have been (loosely) derived from the available literature; they are listed in table 2-2.

The main limitation of the scheme presented in this section is the fixed value of the top of synthetic profiles. In reality this quantity depends on the state of the atmosphere, particularly for profiles from boundary layer radars and from weather radars; with these latter instruments in the absence of scatterers (clear-air situation) no profile at all is available. Consequently the present scheme could lead to too optimistic conclusions for some unfavourable weather situations, for which full synthetic profiles

[2] Consistent with calculation of ϕ on SM full levels – see equations 5.3.6 and 5.3.8 in chap. 2 of EM/DM documentation – and with the derivation of p from ϕ in the nudging routine RPPPMOD.

[3] Consistent with the construction of vertical profiles of observation increments in the nudging routine VIPRASO, if both nudging parameters LYTHICK and LSIGNIF are false.

[4] Strictly speaking a normal distribution is incompatible with a quantity such as the wind direction which takes its values in a strict subset of the real numbers; this is however a reasonable approximation if the standard deviation of the considered distribution is not too large with respect to the size of the subset.

Instrument type	bias(*ff*) [ms^{-1}]	σ_{rand}(*ff*) [ms^{-1}]	bias(*dd*) [°]	σ_{rand}(*dd*) [°]	bias(*T*) [°K]	σ_{rand}(*T*) [°K]
ST radar (50MHz)	-1.0	0.1 × *ff* [ms^{-1}]	+5.0	10.0	-	-
FT radar (480MHz)	+0.5	0.1 × *ff* [ms^{-1}]	+2.0	10.0	-	-
BL radar (1.2GHz) / VAD	+0.5	0.1 × *ff* [ms^{-1}]	+3.0	10.0	0.0	0.5

TABLE 2-2. Standard deviation of the random error (σ_{rand}) and bias characterizing the synthetic errors superimposed on wind force *ff*, wind direction *dd* and temperature *T*. The first row is for strato-tropospheric radars, the second row for full-tropospheric radars, and the third row for boundary layer and weather radars (VAD).

are assimilated although no real observations would be available. In regard of this limitation the rather crude simulation of WP errors is certainly good enough.

2.3.4 Validation of the method

Do synthetic data produced with the OSSE tool have the same impact on the SM as real data? A positive answer to this question would provide a (partial) validation of our OSSE implementation. Real CWINDE data obtained on 12th Feb. 1997 between 12UTC and 24UTC are used to answer this question.

The european CWINDE network (Oakley et al., 1997) is composed of semi-operational and research wind profilers operated in real time, with hourly temporal resolution; the location and characteristics of the profilers are shown in the left panel of figure 2-8. The weather situation of 12th Feb. 1997 is characterized by a low-level atmospheric perturbation accompanied by strong winds, more than 40ms^{-1} gusts close to the ground, travelling from western Europe towards the Swiss Alps (fig. 2-8, right panel).

The CWINDE network is simulated with the OSSE tool. On the other hand a *calibration* run is calculated, similar to the test run defined in figure 2-7 but with assimilation of

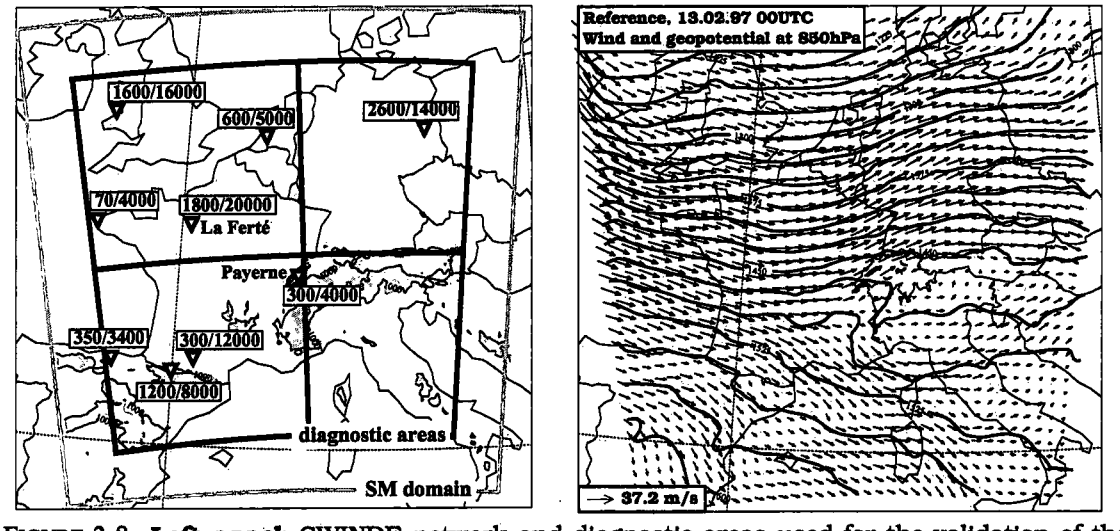

FIGURE 2-8. ***Left panel***: CWINDE network and diagnostic areas used for the validation of the OSSE implementation. Triangles denote the locations of the 9 active CWINDE profilers on 12th Feb. 1997. Specified at each profiler location is bottom and mean top of the corresponding wind profiles, expressed in meters above ground. Four diagnostic areas are defined (north-west, north-east, south-west and south-east). The shaded area denote orography above 1000m. ***Right panel***: 850hPa geopotential and wind fields from the reference experiment, at the end of the assimilation period (13th Feb. 1997, 00UTC).

real instead of synthetic data. Impacts of synthetic and real observations are compared, the impact being measured by the difference between the test or the calibration fields and the control fields. Note that real CWINDE data are also assimilated in the *reference* run, additionally to conventional data, so that the best possible representation of the real atmosphere is obtained at the locations of the CWINDE profilers. This is necessary in order to be sure that any observed differences between the impacts of synthetic and real observations are due to deficiencies in the simulation of WP data, and not to a poor simulation of the real atmosphere by the reference experiment.

Some typical results are presented for the wind field (figures 2-9 and 2-10) and for the temperature field (figures 2-11 and 2-12 – the observed impact is a consequence of wind assimilation alone). In these figures both a subjective comparison of field patterns and an objective comparison of statistical measures are proposed. The impacts of synthetic and real observations are similar, but not identical. However, the observed differences can partly be traced back to the variation of the profile tops and to missing data in the real observations, not simulated in the synthetic observations (for example the top of the Payerne profile fluctuates between 3400m and 5000m and observations at La Ferté-Vidame are missing during the first 6 hours assimilation). These results are

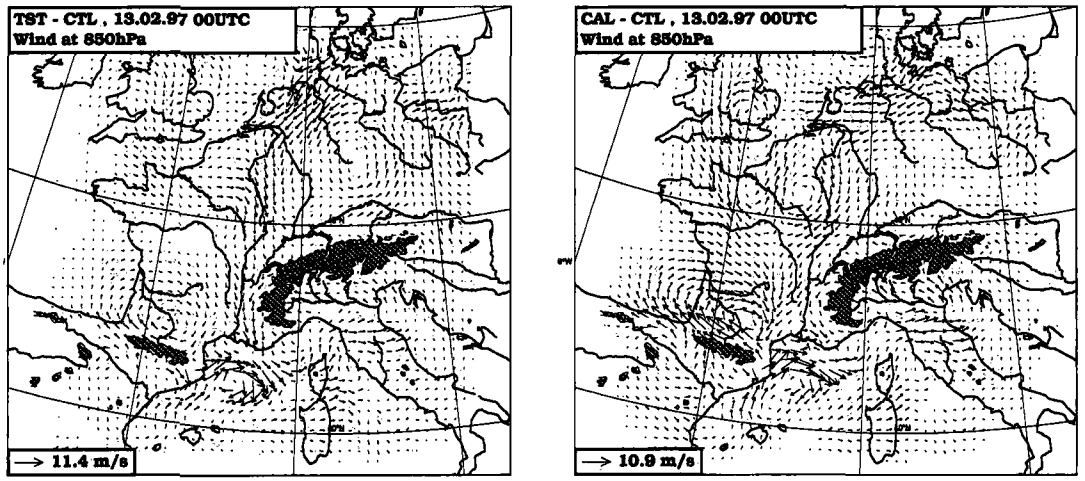

FIGURE 2-9. Impact of synthetic (left panel) and real (right panel) CWINDE data on the 850hPa wind field at the end of the assimilation period on the whole SM domain. Plotted is the difference between the test (TST) or the calibration (CAL) field and the control field (CTL). The shaded areas denote orography above 1500m.

FIGURE 2-10. Impact of real (solid line) and synthetic (dashed line) CWINDE observations on the 850hPa wind field evaluated in the south-western (left panel) and on the south-eastern (right panel) diagnostic areas defined in fig. 2-8. Plotted is the evolution of the mean value of the modulus of the difference fields. Data assimilation takes place during the first 12 hours.

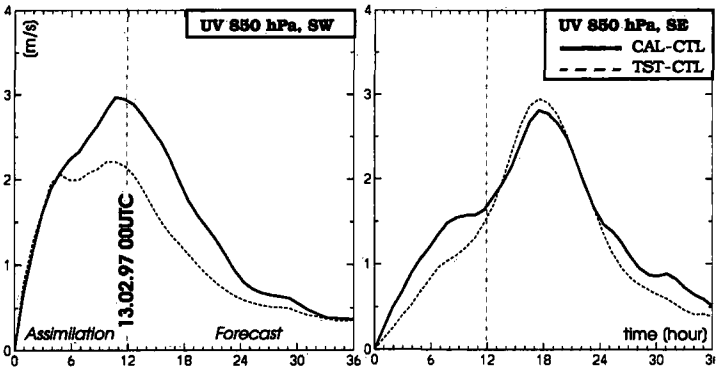

representative of a comprehensive comparison. They concur to the conclusion that our OSSE implementation correctly simulates the impact of WP data.

However, the stronger impact of real observations noticed in the left panels of figures 2-10 and 2-12 is a general trend – in average 20% at analysis time – and is an indication of the "roughness" of real data compared to synthetic data. This fact gives an upper-bound to the accuracy of any quantitative results obtainable by our OSSE implementation.

Finally, another noticeable aspect in figures 2-10 and 2-12 (unrelated with OSSE validation) is the delay of WP observations impact observed in the south-eastern diagnostic area; this reflects the advection of the information from the instrument rich south-western area towards the east.

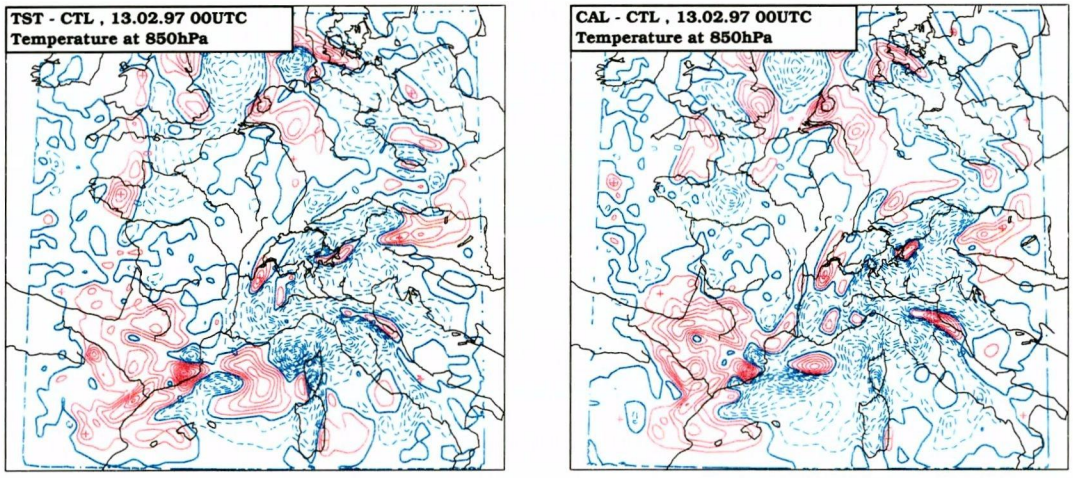

FIGURE 2-11. Impact of synthetic (left panel) and real (right panel) CWINDE data on the 850hPa temperature field at the end of the assimilation period on the whole SM domain. Plotted is the difference between the test (TST) or the calibration (CAL) field and the control field (CTL). Red (resp. blue) isolines represent positive (resp. negative) differences, in 0.2°C interval.

FIGURE 2-12. Impact of real (solid line) and synthetic (dashed line) CWINDE observations on the 850hPa temperature field evaluated in the south-western (left panel) and on the south-eastern (right panel) diagnostic areas. Plotted is the evolution of the standard deviation of the field with respect to the control field. No temperature information is assimilated and the observed impact is a consequence of wind assimilation alone.

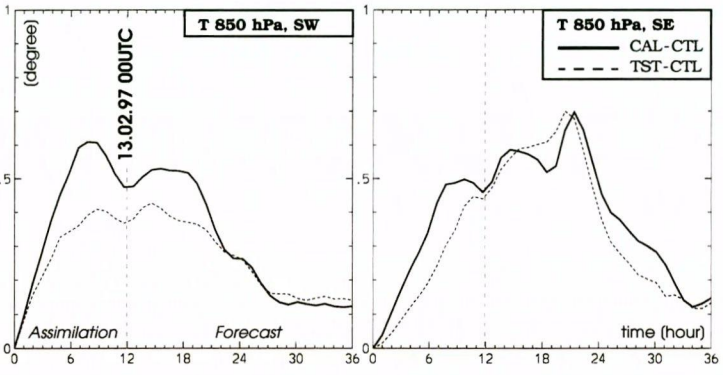

3 Experimental set-up

Three different experimental set-ups have been defined. A first set-up, shortly described in section 2.3.4, is used to validate the OSSE implementation. A second set-up used to evaluate the impact and to help optimize a future MAP SOP wind profiler network (the network deployed during the special observing period of the MAP experiment – Binder and Rossa, 1996) and a third set-up used to evaluate the impact of hypothetical Swiss WP networks are described in this section. In the remaining of this document one will use the terms 'calibration set-up', 'MAP set-up' and 'Swiss set-up' respectively.

3.1 Simulated wind profiler networks

A wind profiler network is characterized by the types and characteristics of the used instruments on the one hand, by their number and geographical distribution on the other hand. In the present work four classes of wind profiler radars are simulated: boundary layer (BL) radar operating around 1.2 GHz, full-tropospheric (FT) radar operating around 480 MHz, strato-tropospheric (ST) radar operating around 50 MHz and Doppler weather radar operating around 5.4 GHz. The first three classes can be complemented with RASS to provide temperature profiles; the last class uses the VAD technique to derive wind profiles from the two highest elevation scans of the weather radar (Germann, 1998). Note that, typically, profilers are designed to operate in two modes: one for low-altitude sampling with high vertical resolution and another for higher-altitude sampling with reduced vertical resolution.

The characteristics of wind or temperature profiles – altitude range, vertical and temporal resolution, accuracy – depend on the exact characteristics of the considered instrument. In the present work hourly temporal resolution and the modelisation of observation errors (bias, random) defined in section 2.3.3 have systematically been used. The other profiler characteristics, if not otherwise specified in the corresponding network definition, are those defined in table 3-1.

Networks for the MAP set-up (see figure 3-1)

Three networks are simulated, fitted into each other. The smallest is composed of the 5 ST radars of the initially planned MAP SOP network, the next one is composed of the whole MAP SOP network and the largest is composed of this latter network

Instrument type	Mode	Vertical range (meter above ground)			Temporal resolution	Errors
		bottom	top	resolution		
ST radar (50MHz)	-	specific to each instrument			1 hour	See table 2-2
FT radar (482MHz)	Low mode	500	8000	250		
	High mode	2600	14000	500		
BL radar (1290MHz)	Low mode	100	2200	60		
	High mode	400	4600	200		
VAD	-	200	4600	200		

TABLE 3-1. Typical characteristics of synthetic wind profiles. The characteristics of the FT radar are based on the Lindenberg profiler, the characteristics of the BL radar is modelled on the Payerne profiler; both profiler modes are simulated (see however the remark at the end of this section, page 24). The VAD characteristics are similar to the high mode of BL radar.

complemented with the CWINDE network. This set-up has been chosen to test the sensitivity of the assimilation procedure to the horizontal scale of the observation network and to the geographical distribution of the instruments.

Note that the configuration of the CWINDE network at the time of the MAP SOP will not exactly correspond to the simulated configuration (e.g. the instrument at Brest will not be present). Furthermore, the final set-up for the MAP SOP network may still be changed. However, this has no effect on the conclusions presented in section 4.4.

Networks for the Swiss set-up (see figure 3-2)

Three Swiss-scale networks representing possible future configurations are simulated: the BL1 network based on the existing profilers (the profiler at Payerne and the 3 SMI

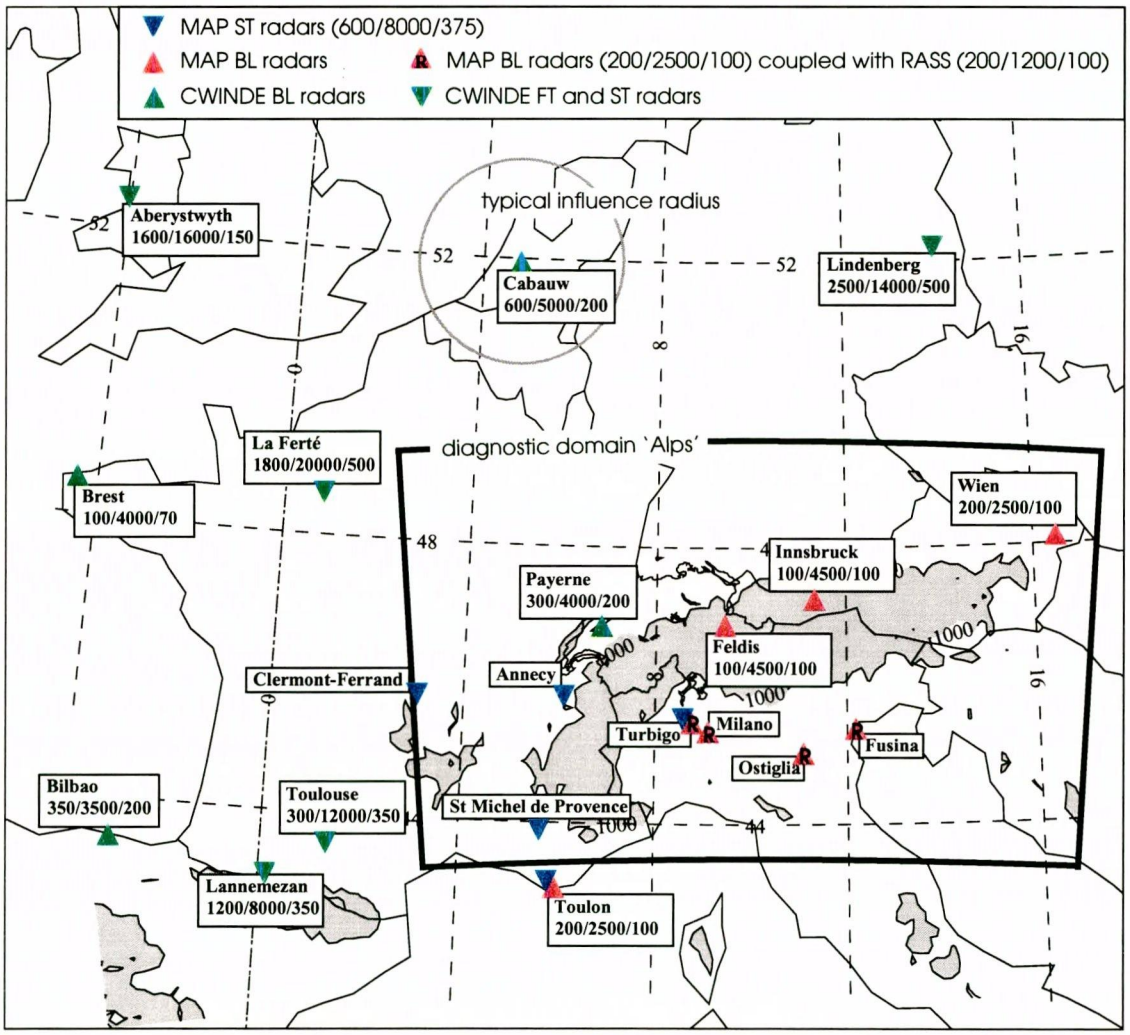

FIGURE 3-1. The 3 networks simulated for the MAP set-up: the MAP ST radars (MAPST – blue symbols), the whole MAP network (MAP – blue and red symbols), the whole MAP network complemented with the CWINDE network (MAP+CWINDE – blue, red and green symbols). Specified at the profiler location (or in the legend box) are the bottom, top and vertical resolution of the corresponding wind or temperature profile, expressed in meters; these values have been derived from the characteristics of the real instrument. The typical influence domain of a 850 hPa wind observation is also represented: from the domain centre to its boundary the weight of the observation in the nudging term is reduced by a factor 10. The diagnostic domain 'Alps' used in the evaluation of the results is pointed out. The shaded areas denote orography above 1000m.

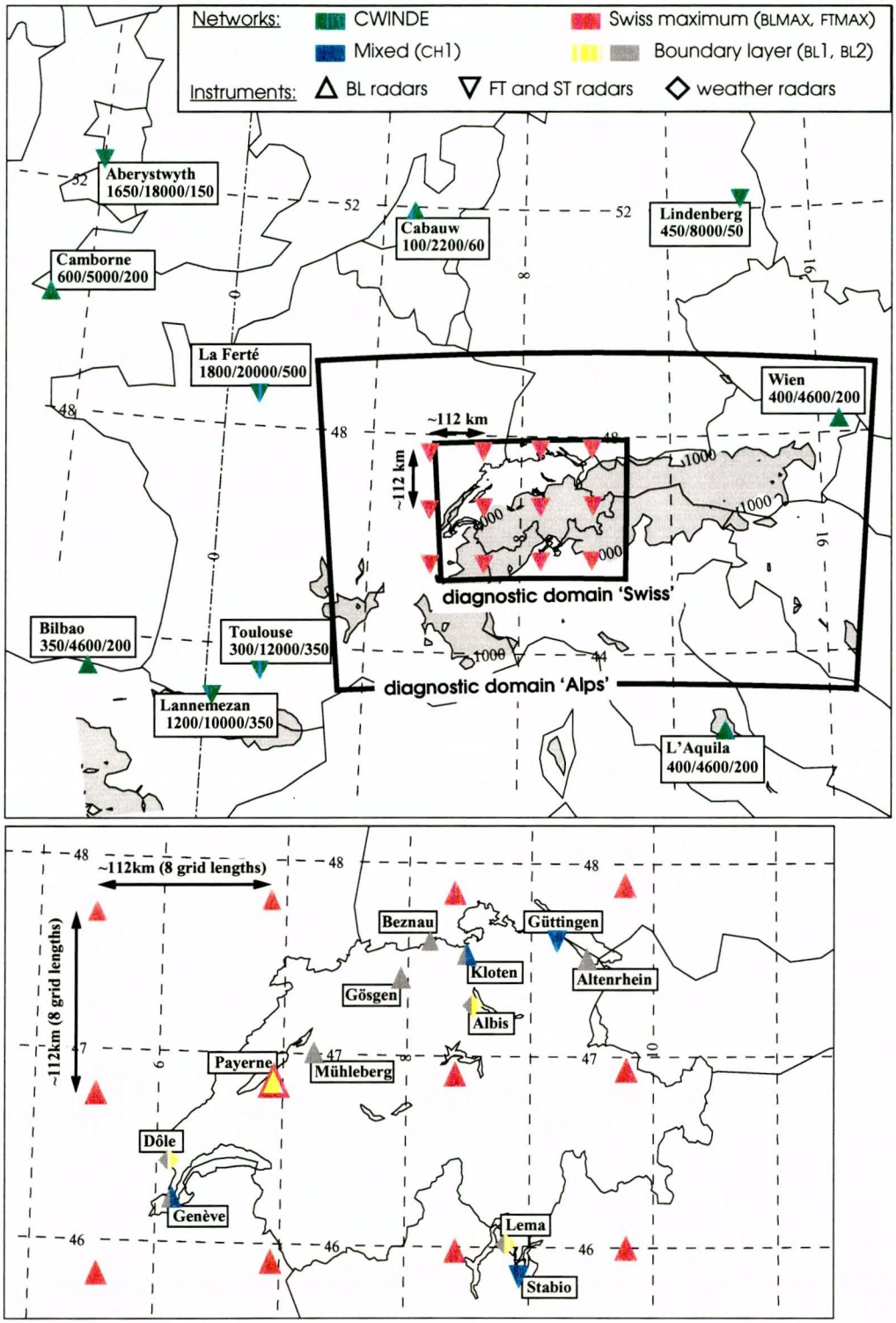

FIGURE 3-2. The 6 networks simulated for the Swiss set-up. ***Top panel***: the CWINDE network (CWINDE – green) and the maximum FT configuration (FTMAX – red). ***Bottom panel***: the maximum BL configuration (BLMAX – red) and the 3 realistic configurations (CH1 – blue, BL1 – yellow, BL2 – grey). If not specified at the profiler location, the bottom, top and vertical resolution of the corresponding wind profile are those defined in table 3-1; all values are expressed in meters. In the top panel, the 2 diagnostic domains used in the evaluation of the results are visible, and the shaded areas denote orography above 1000m.

weather radars), the BL2 network based on the 3 weather radars and on 6 BL radars located at airports and nuclear power plants, and the CH1 network based on a mix of 2 BL and 2 FT instruments, these latter ones being placed on both sides of the Alps. To evaluate the influence of these 'realistic' configurations two 'maximum' regularly spaced BL and FT networks extending over Switzerland are also simulated (BLMAX and FTMAX).

Moreover a future configuration of the CWINDE network is simulated, and *real* observations from the operational rawinsonde network – surface pressure and the wind, temperature and dew-point temperature profiles – are assimilated in a separate test run of our OSSE set-up (see section 2.3.2).

A summary of all simulated observing systems is available in table 3-2. The following comparisons have systematically been performed:

- **FTMAX/CH1**: to measure the impact of a combined BL/FT network;
- **BLMAX/BL1/BL2**: to measure the impact of BL and weather radar networks;
- **CWINDE+FTMAX/FTMAX/BLMAX**: to compare the impacts of FT and BL profilers and to measure the influence of the horizontal scale of the network;
- **CWINDE+FTMAX/TEMP**: to compare wind profiler with rawinsonde impact.

Note that, due to a bug in the assimilation code, only the low modes of the simulated profiles have been assimilated. The main consequence of this fact is a weakening of the impact of BL profilers. On the other hand, because high-level winds (above 8000m) are less depending on initial conditions and more depending on LBC, the consequence of this bug on the impact of FT profilers is small.

3.2 Meteorological cases

In order to assess the benefit of hypothetical observing systems with the OSSE method, two (complementary) approaches are possible: case studies or systematic evaluation over a long period. Due to practical constraints, only the first approach has been chosen in this study. One has selected eight cases for which a significant impact of WP observations is expected (1 case for the calibration set-up, 2 cases for the MAP set-up and 5 cases for the Swiss set-up); typical candidates for such cases are meteorological situations which present mesoscale details not resolved by other observing systems, and which are not dominated by the LBC.

	Name	Instruments	Horizontal scale
1	MAPST	5 ST radars	Southern Alps
2	MAP	5 ST radars, 8 BL radars, 4 RASS	Alps
3	MAP+CWINDE	9 ST radars, 1FT radar, 12 BL radars, 4 RASS	SM domain
4	BL1	1 BL radar, 3 weather radars	Switzerland
5	BL2	6 BL radars, 3 weather radars	Switzerland
6	CH1	2 FT radars, 2 BL radars	Switzerland
7	BLMAX	12 BL radars	Switzerland
8	FTMAX	12 FT radars	Switzerland
9	FTMAX+CWINDE	4 ST radars, 13FT radars, 5 BL radars	SM domain
0	TEMP	About 60 *real* rawinsondes with mostly 12h temporal resolution	SM domain

TABLE 3-2. Characteristics of the simulated observing systems (1–9), and of the operational rawinsonde network, limited to the SM domain (0).

In the remainder of this section one shortly describes the synoptic features of each selected case. Maps of the geopotential, the horizontal wind and the temperature fields on the 500 hPa and 850 hPa levels, coming from the reference SM integration, are also plotted.

Each selected case will be referred to by its *analysis time*, that is by the date and time corresponding to the 12h point on the time scale of figure 2-7. For test runs, the analysis time is preceded by a 12h assimilation period and followed by a 36h forecast.

Cases for the MAP set-up (see figure 3-3)

Two MAP cases, the Piedmont episode and the South-Ticino episode, have been used. Both episodes are characterized by heavy precipitation over the southern Alps, with advection of warm and moist air from the Mediterranean towards the Alps.

Piedmont case (04.11.94 12UTC) and South-Ticino case (13.09.95 12UTC)
The 500hPa geopotential field shows a deep trough over the Western North Atlantic slowly approaching the Alps, associated with a sequence of secondary troughs crossing the Alps in a southwesterly flow. The ridge to the east, associated with an anticyclone over Eastern Europe, remains almost stationary, implying scale contraction and

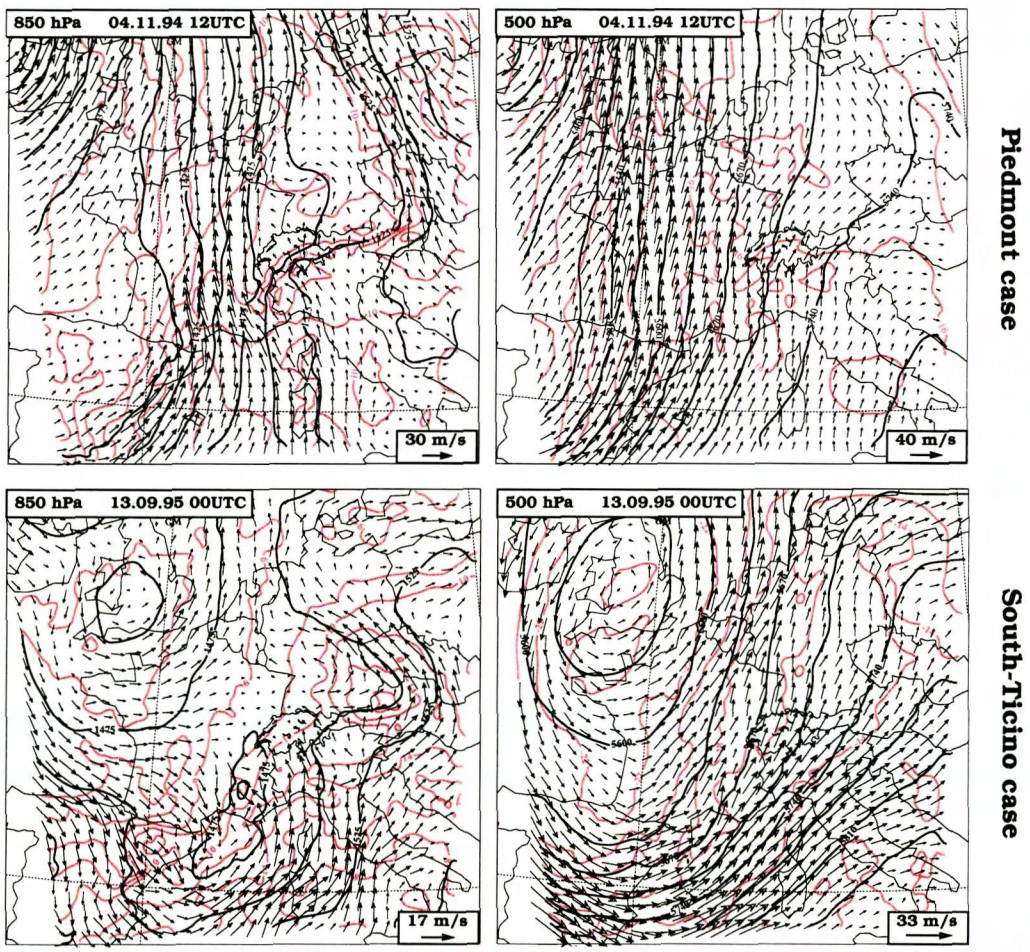

FIGURE 3-3. Geopotential, temperature and wind for each case of the MAP set-up. Reference fields are displayed at analysis time, at the 850hPa and 500hPa levels. Black contours represent the geopotential (in 25m intervals at 850hPa, in 35m interval at 500hPa), red contours represent the temperature (in 2°C intervals) and arrows represent the wind (plotted each 5 grid points).

intensification of the geopotential gradient on the leading edge of the trough.
At lower levels, ahead of the upper-level trough, a narrow and elongated strong southerly airflow extends from the Mediterranean to the Alps. Enhanced ascent over the southern slope of the Alps is observed.

Cases for the Swiss set-up (see figure 3-4)

Opposite flows (26.12.95 12UTC)

The upper level situation is characterized by a trough moving from the English Channel towards the Alps, associated with a strong westerly and confluent flow over central Europe.
Cyclogenesis takes place over the Gulf of Genoa, implying northeasterly winds in the lower atmosphere over Switzerland. This leads to a situation with opposite flows and strong wind shear over the analysed region. This particular state produced unexpected snow fall due to the lifting of the warm and moist upper level air over the cold low level flow.

South Foehn (14.04.98 12UTC)

The principal activity centre is a mature depression extending through the whole troposphere, centred over the North Sea. A secondary trough over Portugal is associated with this depression.
An area with positive vorticity advection moves from Ireland towards central Europe, and merges with the secondary trough, producing a strong southerly flow over the Alps (Foehn). This situation leads to heavy precipitation over the southern slopes of the Alps.

Summer convection (02.07.98 12UTC)

A wide depression over Biscay extends through the whole troposphere. A jet-stream from central Spain to the Pyrenees is associated with this depression, and one observes a moist southwesterly flow over whole Western Europe, nearly parallel to the Alps.
A stationary frontal zone extends from the Balkans to Southern France. A small high pressure ridge moves from the central Alps towards East, leaving the Alpine region more and more influenced by the approaching depression.
Within this southwesterly flow, the development of convective precipitation over Western Switzerland is observed (up to 30 mm per hour).

Summer convection (21.07.98 12UTC)

The upper level situation is characterized by a vast depression over Northern Scotland, and a southwesterly cyclonic circulation over central Europe. A secondary trough moving from the Biscay to the North Sea is also observed. A jet stream extending from Massif Central to Denmark, leaving Switzerland beneath its right entrance, is associated with this situation.
A cold front crosses central Europe from south-west to north-east. The vertical stratification of the atmosphere is very unstable, with a weak inversion between 2700 and 3000m which could increase convective activity when suddenly broken-up. The development of convective precipitation over central Switzerland is observed (up to 25 mm per hour).

Cold air drops (22.09.98 00UTC)

A high pressure centred over the North sea extends in the lower atmosphere till the Alps and middle Italy. In the upper troposphere cold air drops cross the Alps from east to west, at the southern edge of the high pressure. Stable vertical stratification of the atmosphere prevents convective development.

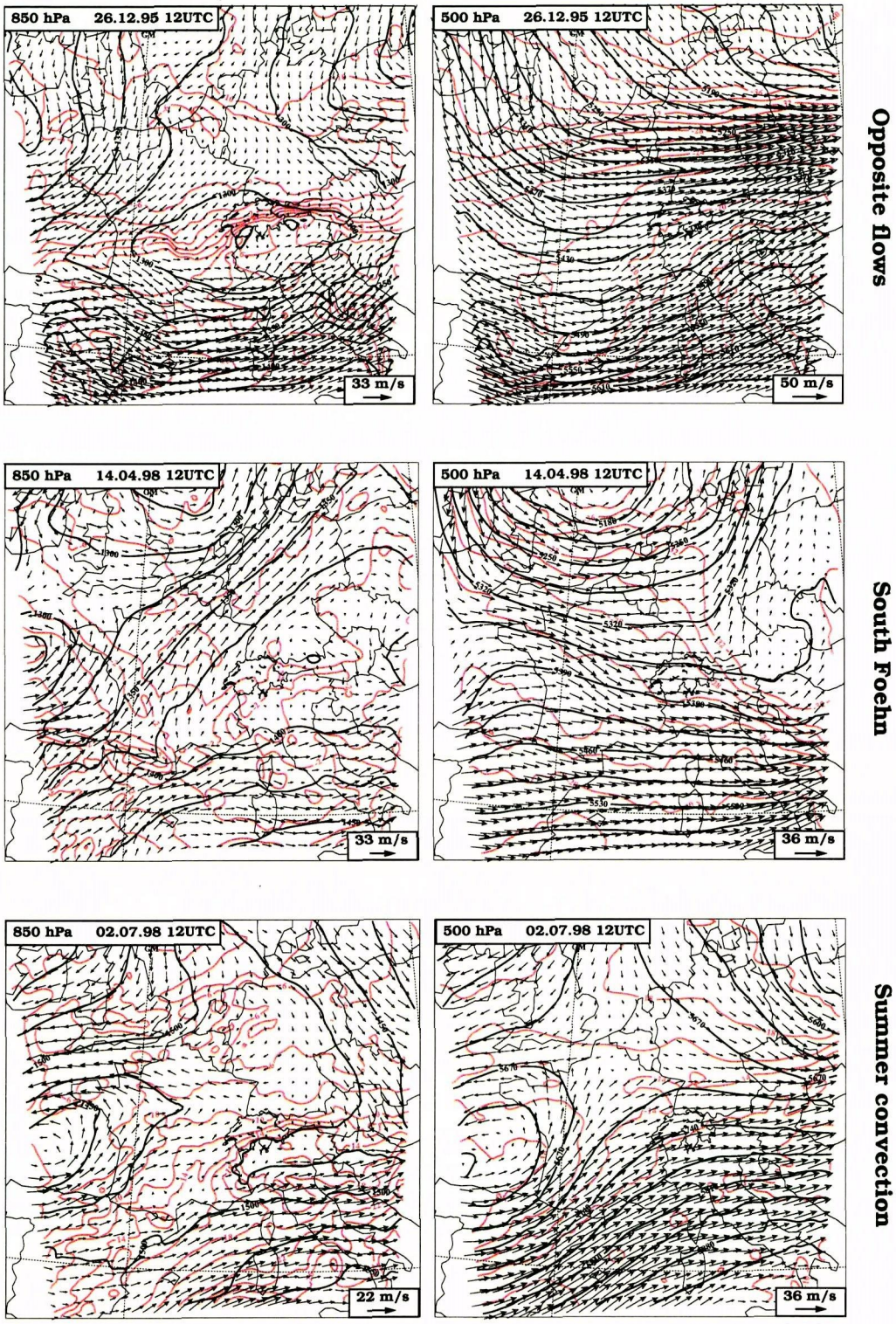

FIGURE 3-4. **Continued on next page**. Geopotential, temperature and wind for each case of the Swiss set-up. Reference fields are displayed at analysis time, at the 850hPa and 500hPa levels. Black contours represent the geopotential (in 25m intervals at 850hPa, in 35m interval at 500hPa), red contours represent the temperature (in 2°C intervals) and arrows represent the wind (plotted every 5 grid points).

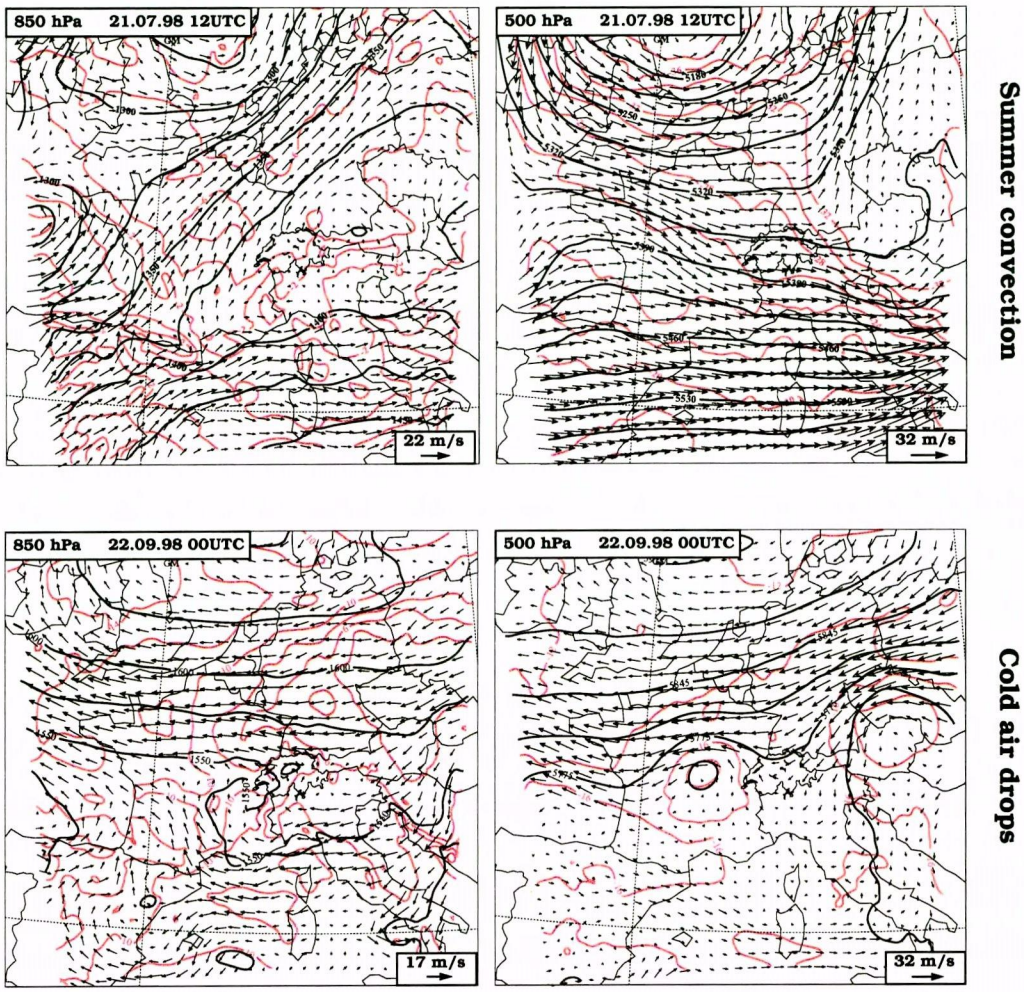

FIGURE 3-4. **Continued from previous page**. Geopotential, temperature and wind for each case of the Swiss set-up. Reference fields are displayed at analysis time, at the 850hPa and 500hPa levels. Black contours represent the geopotential (in 25m intervals at 850hPa, in 35m interval at 500hPa), red contours represent the temperature (in 2°C intervals) and arrows represent the wind (plotted every 5 grid points).

3.3 List of experiments

The list of experiments performed for the OSSE'97 project is summarized in table 3-3. For each case, according to the scheme defined in section 2.3.2, one calculates a reference SM integration, a control integration and a set of test integrations – one for each simulated observing system. Some supplementary SM integrations are also calculated to evaluate the impact of real WP or rawinsonde networks, and to perform sensitivity studies.

TABLE 3-3. Experiments performed for the present study.

Case[a]	Meteorological situation	Experimental set-up	Simulated observing systems[b]	Supplementary studies[c]							
				real WP data	real TEMP data	real TEMP, p_s only	real TEMP, wind only	real TEMP, p_s and wind	vertical corr. length	horizontal corr. length	hor. spreading of wind
97021300	Fast moving front in westerly flow (FASTEX case)	Calibration	CWINDE	✓					✓		
94110412	Moist air advection from Mediterranean towards the Alps (Piedmont MAP case)	MAP	MAPST, MAP, MAP+CWINDE								
95091300	Moist air advection from Mediterranean towards the Alps (South-Ticino MAP case)	MAP	MAPST, MAP, MAP+CWINDE		✓	✓					
95122612	Opposite flows, strong wind shear	Swiss	BL1, BL2, CH1, BLMAX, FTMAX, FTMAX+CWINDE		✓		✓	✓			
98041412	South Foehn	Swiss	BL1, BL2, CH1, BLMAX, FTMAX, FTMAX+CWINDE		✓	✓	✓	✓			
98070212	Summer convection	Swiss	BL1, BL2, CH1, BLMAX, FTMAX, FTMAX+CWINDE		✓				✓	✓	
98072112	Summer convection	Swiss	BL1, BL2, CH1, BLMAX, FTMAX, FTMAX+CWINDE		✓				✓	✓	
98092200	Cold air drops, in easterly flow	Swiss	BL1, BL2, CH1, BLMAX, FTMAX, FTMAX+CWINDE		✓		✓	✓	✓	✓	✓

[a] The tag used to specify a case is the date at the end of the 12h assimilation of the test run (see fig. 2-7), expressed in the format <*year*><*month*><*day*><*hour*> (2 digits each).

[b] See table 3-2 for the characteristics of each system.

[c] The first two columns are impact studies, the next three are sensitivity studies to different parameters measured by rawinsondes, and the last three columns are sensitivity studies related to some parameters of the nudging scheme (respectively σ_z, σ_r, and γ – see section 2.2).

3.4 Evaluation methodology

As explained in section 2.2, the evaluation of an OSSE is based on the verification of the control and test experiments against the reference experiment; in this context *one defines the error of any control or test quantity as the difference between this quantity and the corresponding reference quantity*. The impact of a specific observing system is

then assessed by comparing the associated test error with the control error. Because of the considerable amount of data produced by OSSEs – about hundred SM integrations have been calculated for the present study – it is necessary to use a synthetic and objective measure of these errors:

- 2 diagnostic domains are defined: the whole SM domain (excluding a narrow strip along the domain boundary) and a domain centred over the Alps for the MAP set-up (see figure 3-1), the domain centred over the Alps and a domain centred over Switzerland for the Swiss set-up (see figure 3-2)[1].
- 3 pressure levels are used: 850 hPa, 700 hPa and 500hPa.
- for the horizontal wind field one considers a measure defined by the mean value of the modulus of the wind error, evaluated in each diagnostic domain and on all 3 pressure levels; this measure is sensitive to errors of both the wind velocity and the wind direction.
- for the surface pressure, the humidity and the temperature fields one considers the measures defined by the bias and the standard deviation of the corresponding field, evaluated in each diagnostic domain and, for the thermodynamic fields, on all 3 pressure levels.

The temporal evolution of these measures is systematically calculated; together with measures specific to the meteorological situation they are used to assess the OSSE results. When necessary these objective measures are complemented with subjective comparison of field patterns in order to gain more insight into specific questions.

[1] The coordinates of the lower-left and upper-right corners of these diagnostic domains, expressed in rotated longitude-latitude system, are (-10,-17;4,-3) for the whole domain, (-5,-14;5,-8) for the 'Alps' domain, and (-3,-12;0.5,-9.5) for the 'Swiss' domain.

4 Results

The main results derived from the present work have been presented as theses in section 1.3. In this section each thesis is illustrated by a selection of results. Moreover the consequences of this work for the future MAP SOP network are also presented.

All the nomenclature used in this section has been introduced in section 3. In particular, a short description of the simulated networks is available in tables 3-1 and 3-2; the *analysis time* for a specific experiment is the date and time corresponding to the 12h point on the time scale of the figure 2-7 (end of assimilation period for the test experiment), and the *test* or *control error* is the difference between test or control fields and the corresponding reference fields. One will also use the tags 'SM', 'Alps', and 'Swiss' for the 3 diagnostic domains introduced in section 3.4.

4.1 On the impact of hypothetical Swiss wind profiler networks

Thesis A1

WP observations have a positive effect on analysis and very short range forecasts of wind. The so-called maximum network – a network of 12 WP regularly spaced over Switzerland – corrects between 30% and 75% of the low-level wind analysis error over Switzerland; this impact is similar to the impact of the current operational rawinsonde network. However, this positive effect mostly disappears after 12 hours of forecast.
The impact on the mass and the temperature fields, if any, is in most cases not significant and no effect on the precipitation field is observed.

In table 4-1 the impact of WP observations on the quality of the wind *analysis* is summarized. A marked positive impact is observed: measured in the diagnostic domain 'Swiss', the FTMAX network corrects about half of the control error of the low-tropospheric wind. This effect is comparable to the correction brought by the current operational rawinsonde network. Moreover, for some episodes, the impact of WP observations is characterized by a drastic correction of the flow pattern. Such a case is presented in figure 4-1, where the FTMAX network is able to correct a temporal phase

	wind 850hPa		wind 700hPa		wind 500hPa	
	FTMAX	TEMP	FTMAX	TEMP	FTMAX	TEMP
Opposite flows (26.12.95)	30% 6h	50% 30h	30% 6h	50% 27h	20% 6h	30% 24h
South Foehn (14.04.98)	55% 12h	55% 30h	40% 6h	55% 33h	25% 6h	30% 36h
Convection (02.07.98)	40% 21h	40% 36h	35% 4h	30% 10h	40% 6h	40% 9h
Convection (21.07.98)	35% 2h	35% 36h	35% 3h	35% 28h	< 5% 6h	< 5% 8h
Cold air drops (22.09.98)	55% 21h	50% 25h	75% 8h	55% 27h	75% 13h	55% 36h
Mean correction	*45%*	*45%*	*45%*	*45%*	*30%*	*30%*

TABLE 4-1. Impact of the FTMAX network and of the operational TEMP network on the wind *analysis* error, measured on the diagnostic domain 'Swiss', expressed in percentage of the correction of the control error. Both the mean correction over all cases of the Swiss set-up and the individual corrections are listed. The duration of this positive impact, expressed in forecast hours, is also given for both networks.

error in a Foehn episode. On the other hand, the impact of the FTMAX network measured on the diagnostic domain 'Alps' is significantly weaker (figure 4-2 gives an illustration of this fact), in particular it is much smaller than the impact of the TEMP network. This fact is due to the limited horizontal extension of the FTMAX network; this is a point which is further discussed in thesis B2.

Another noticeable aspect in table 4-1 is the reduced impact of WP and rawinsonde observations on the mid-tropospheric winds, in comparison with the impact of these observations on lower level winds (note also the higher variability of this impact). This is possibly due to the stronger advection at higher levels, inducing a faster outflow of the information brought by the assimilation procedure and a stronger dependence of the fields on the lateral boundary conditions.

The observed improvement of the wind field at analysis time has of course a positive impact on the quality of the wind field in the *forecast*, but only for a limited and relatively short period of time as it can be seen from the values listed in table 4-1. A typical illustration of this phenomenon is given by figure 4-2: for this South Foehn case the (positive) effect of the synthetic WP observations is limited to the first 12 forecast hours. Note that this limited impact in the forecast is not a weakness of our assimilation procedure but is related to the set of assimilated observations. Indeed improvement brought by the TEMP network persists much longer in the forecast (this last point will be further discussed in section 4.2).

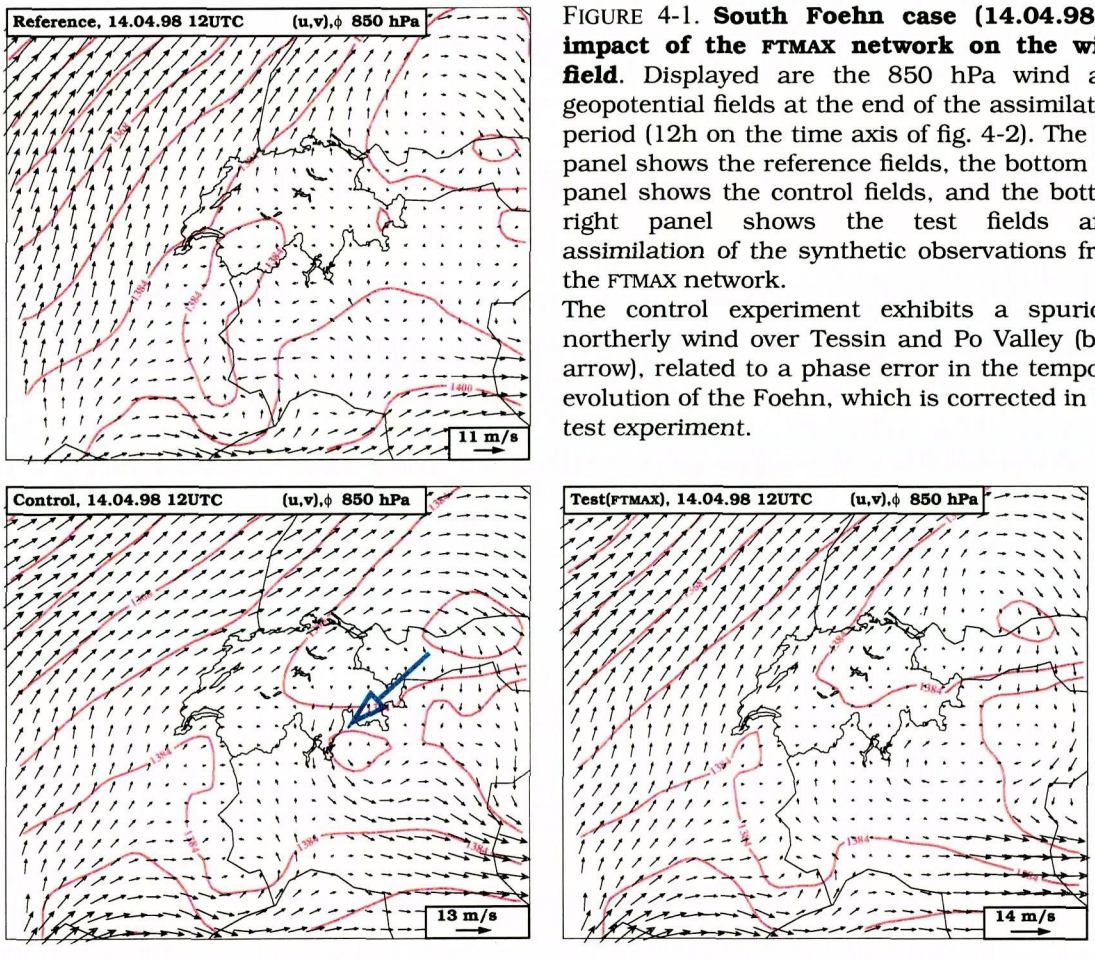

FIGURE 4-1. **South Foehn case (14.04.98) – impact of the FTMAX network on the wind field**. Displayed are the 850 hPa wind and geopotential fields at the end of the assimilation period (12h on the time axis of fig. 4-2). The left panel shows the reference fields, the bottom left panel shows the control fields, and the bottom right panel shows the test fields after assimilation of the synthetic observations from the FTMAX network.
The control experiment exhibits a spurious northerly wind over Tessin and Po Valley (blue arrow), related to a phase error in the temporal evolution of the Foehn, which is corrected in the test experiment.

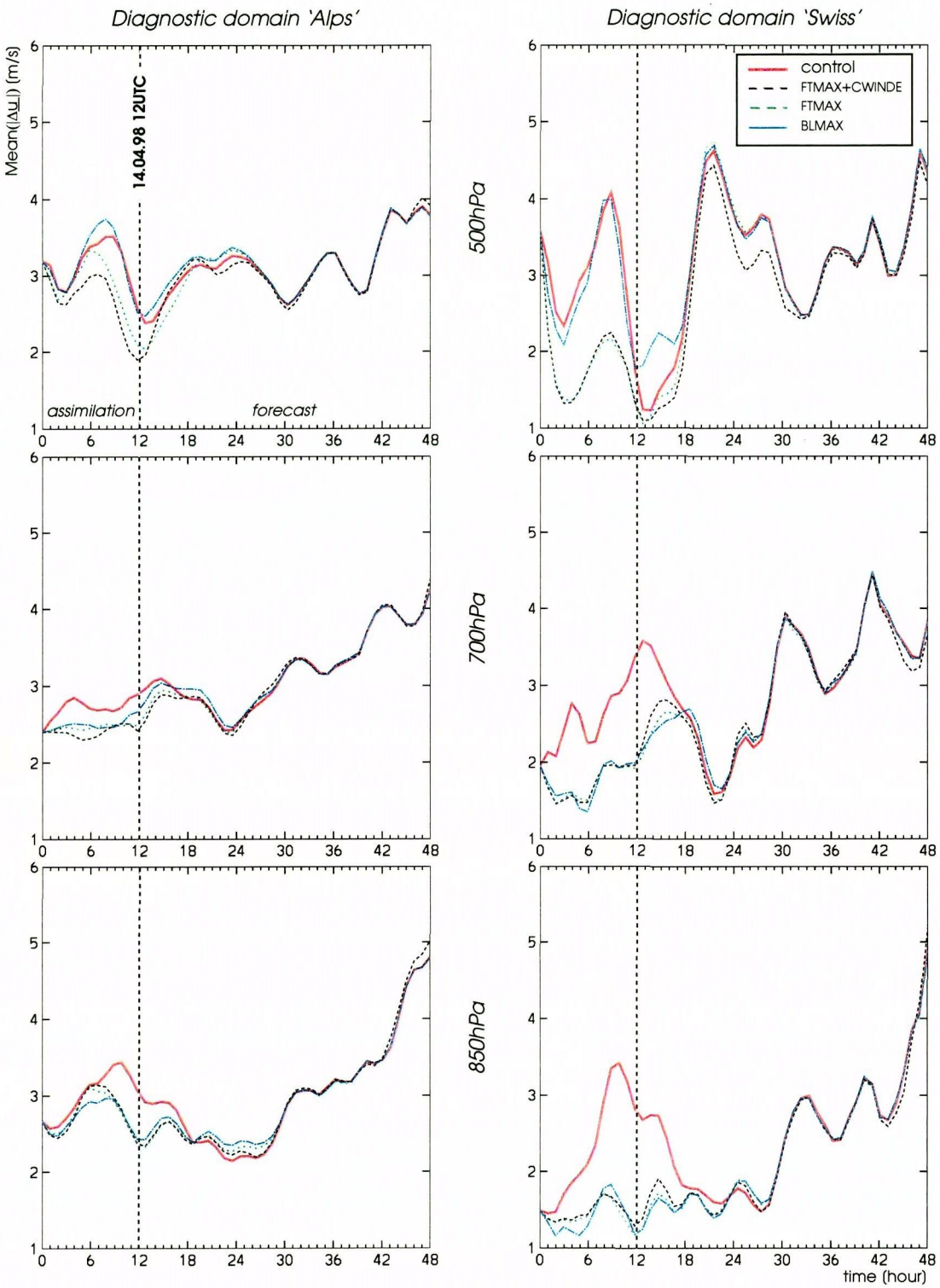

FIGURE 4-2. **South Foehn case (14.04.98) – impact of WP observations on the wind field error**. Displayed is the temporal evolution of our measure of the wind error (see section 3.4), evaluated on 3 pressure levels and in both the 'Alps' and the 'Swiss' diagnostic domains. The red line denotes the error of the control experiment, the other lines denote the error after assimilation of synthetic observations from the FTMAX+CWINDE network (black curve), from the FTMAX network (green curve), and from the BLMAX network (blue curve). Data assimilation takes place during the first 12 hours.

The impact of WP observations on other variables than the wind field is in most cases not significant. One exception is the South Ticino episode: here the assimilation of the winds from the synthetic WP observations brings a strong improvement not only of the wind field, but also of the reduced surface pressure (see figures 4-3 and 4-4) and of the temperature fields. This improvement persists at least 12 hours in the forecast. However, as in all other cases, the impact on the precipitation fields is negligible.

Finally, two remarks about the figures presented here. In figure 4-2, the negative impact of the BLMAX network on the 500hPa wind field is due to a too broad nudging vertical weight ($\omega_{\Psi,z}$, see page 12) and will be discussed in thesis C1. In figures 4-3 and 4-4, the relative impact of the different synthetic observing systems is discussed in relation with thesis A4.

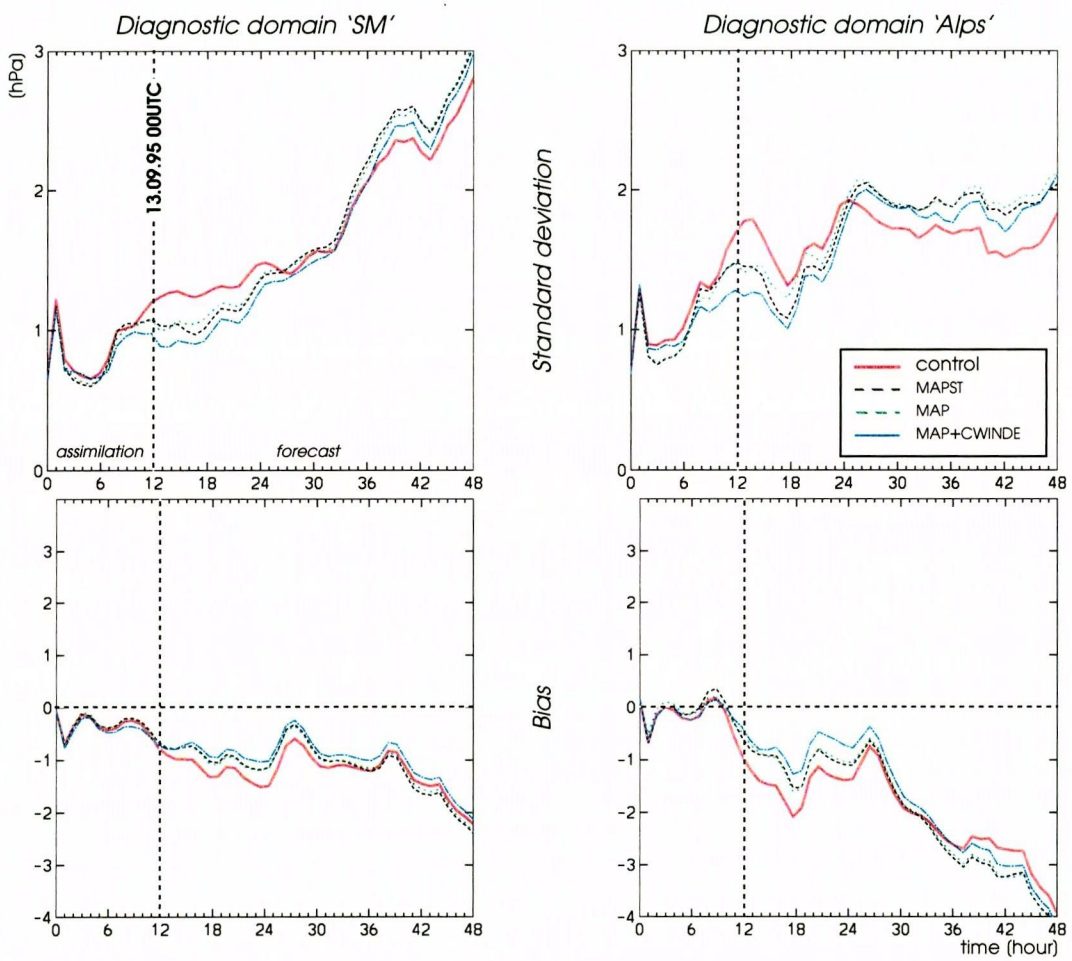

FIGURE 4-3. **South Ticino case (13.09.95) – impact of WP observations on reduced surface pressure error.** Temporal evolution of the bias and of the standard deviation of the reduced surface pressure, evaluated in both diagnostic domains of the MAP set-up. The red line denotes the error of the control experiment, the other lines denote the error after assimilation of synthetic observations from the MAPST network (black curve), from the MAP network (green curve), and from the MAP+CWINDE network (blue curve). Data assimilation takes place during the first 12 hours. *See also the figure 4-4 for instantaneous representations of the reduced surface pressure error plotted on the whole SM domain.*

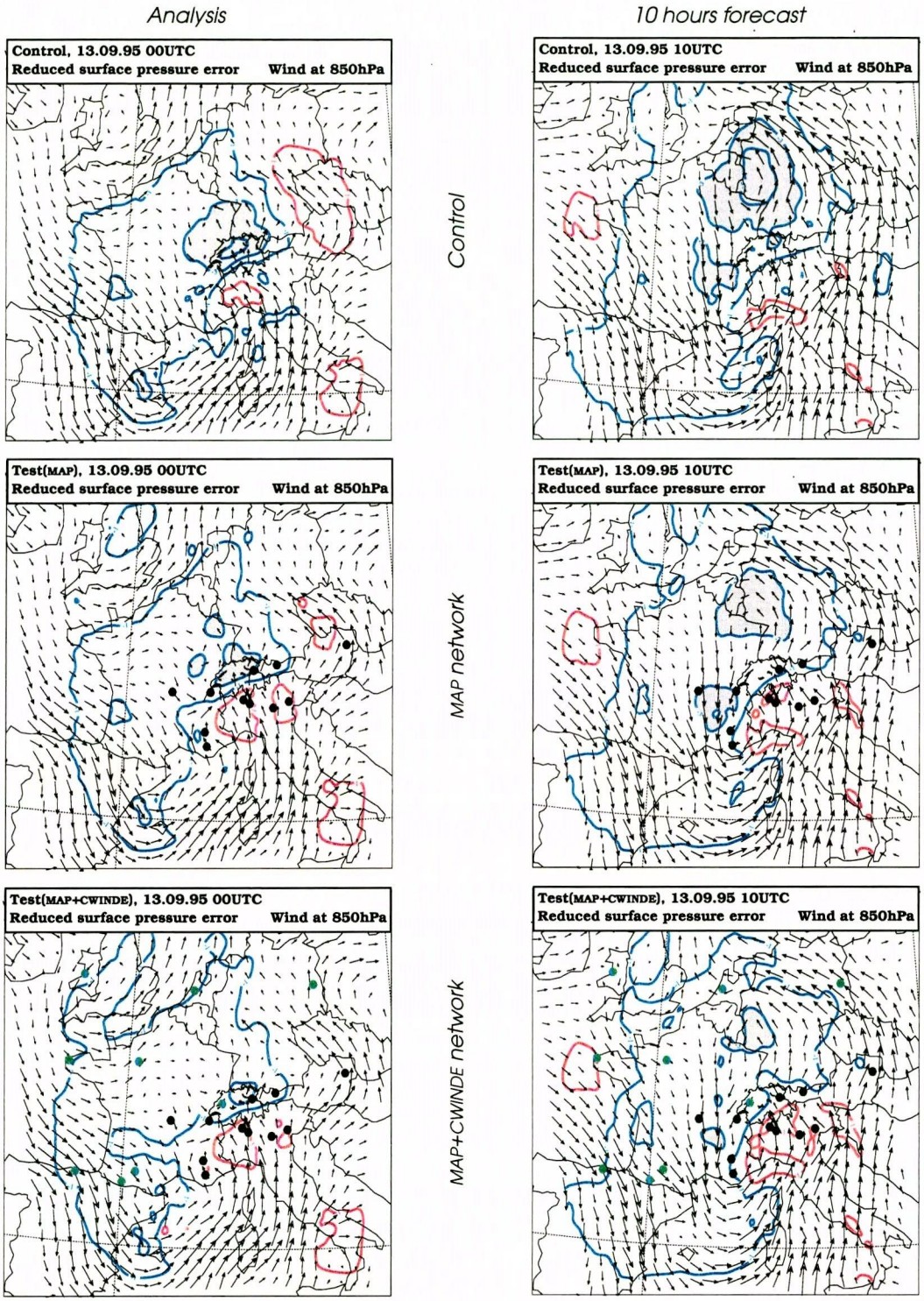

FIGURE 4-4. **South Ticino case (13.09.95) – impact of WP observations on reduced surface pressure error**. Isolines denote the reduced surface pressure error at the end of the assimilation period (left panels) and after 10h forecast (right panels), expressed in hPa, in 2hPa interval. The upper row is for the control experiment, the middle row shows the effect of the MAP network, and the lower row shows the effect of the MAP+CWINDE network. Shaded areas denote errors larger than 3hPa. Also plotted is the 850hPa wind field of the corresponding experiment and the location of the instruments in the MAP network (black dots) and in the CWINDE network (green dots).

Thesis A2

The only observed difference between the impact of FT radars (400MHz class) and of BL radars (1.2GHz class) is the improved mid-tropospheric wind. However mid-tropospheric winds are less depending on the initial conditions and more depending on the governing model (via the lateral boundary conditions) than lower level winds, so that only a limited potential for improvement exists for FT radars.

In table 4-2 the comparative impact of FT and BL radars on the quality of the wind *analysis* is summarized. Although FT radars have a vertical resolution about 4 times coarser than BL radars (low mode only – see table 3-1), both networks have a very similar impact on the low-tropospheric wind. This is further illustrated in figure 4-2, on page 32: one observes similar effects of the BLMAX and FTMAX networks on the 850hPa and 700hPa wind fields, not only at analysis time but also during the forecast. It is however probable that the higher vertical resolution of BL radars is beneficial in the case of a strong vertical gradient of the horizontal wind, but this point has not been investigated in the present study.

Due to the higher vertical span of FT radars, it is not surprising to observe a larger impact on mid-tropospheric wind with the FTMAX network than with the BLMAX network. More surprising is the fact that this better mid-tropospheric wind does not induce other improvements of the meteorological fields (this is however in line with the second part of the thesis A1).

The limited potential for mid-tropospheric wind improvement, in comparison with improvement of lower level winds, is a point which has already been observed and discussed in relation with the thesis A1. This further constrains the possible advantage of FT radars over BL radars for NWP model initialization.

Thesis A3

Realistic configurations for a network of BL radars (1.2GHz class) bring a substantial part of the correction obtained with the maximum network. For example profiles at Payerne and at the locations of the 3 Swiss weather radars bring in most of the cases between 50% and 100% of the "maximum" low level wind correction.

In table 4-3 the percentage of the "maximum" correction obtained with the smallest BL radar network is summarized. At analysis time, the 4 instruments of the BL1 network have an effect on the 850hPa wind which is very similar to the 12 instruments of the

	wind 850hPa		**wind 700hPa**		**wind 500hPa**	
	FTMAX	**BLMAX**	**FTMAX**	**BLMAX**	**FTMAX**	**BLMAX**
Opposite flows (26.12.95)	30%	30%	30%	30%	20%	10%
South Foehn (14.04.98)	55%	55%	40%	40%	25%	< 5%
Convection (02.07.98)	40%	40%	35%	30%	40%	20%
Convection (21.07.98)	35%	35%	35%	35%	< 5%	< 5%
Cold air drops (22.09.98)	55%	40%	75%	60%	75%	< 5%
Mean correction	*45%*	*40%*	*45%*	*40%*	*30%*	*6%*

TABLE 4-2. Impact of the FTMAX and of the BLMAX networks on the wind *analysis* error, measured on the diagnostic domain 'Swiss', expressed in percentage of the correction of the control error. Both the mean correction over all cases of the Swiss set-up, and the individual corrections are listed.
Note: due to a bug in the assimilation code (see page 24) the impact of the BLMAX network on the 500hPa wind is significantly underestimated.

	wind 850hPa	wind 700hPa
	BL1 / BLMAX	BL1 / BLMAX
Opposite flows (26.12.95)	85%	75%
South Foehn (14.04.98)	85%	70%
Convection (02.07.98)	100%	50%
Convection (21.07.98)	100%	0%
Cold air drops (22.09.98)	100%	90%

TABLE 4-3. Comparative effect of the BLMAX network and of the BL1 network on the wind *analysis* error, measured on the diagnostic domain 'Swiss', expressed in percentage of the BLMAX correction brought by the BL1 network.

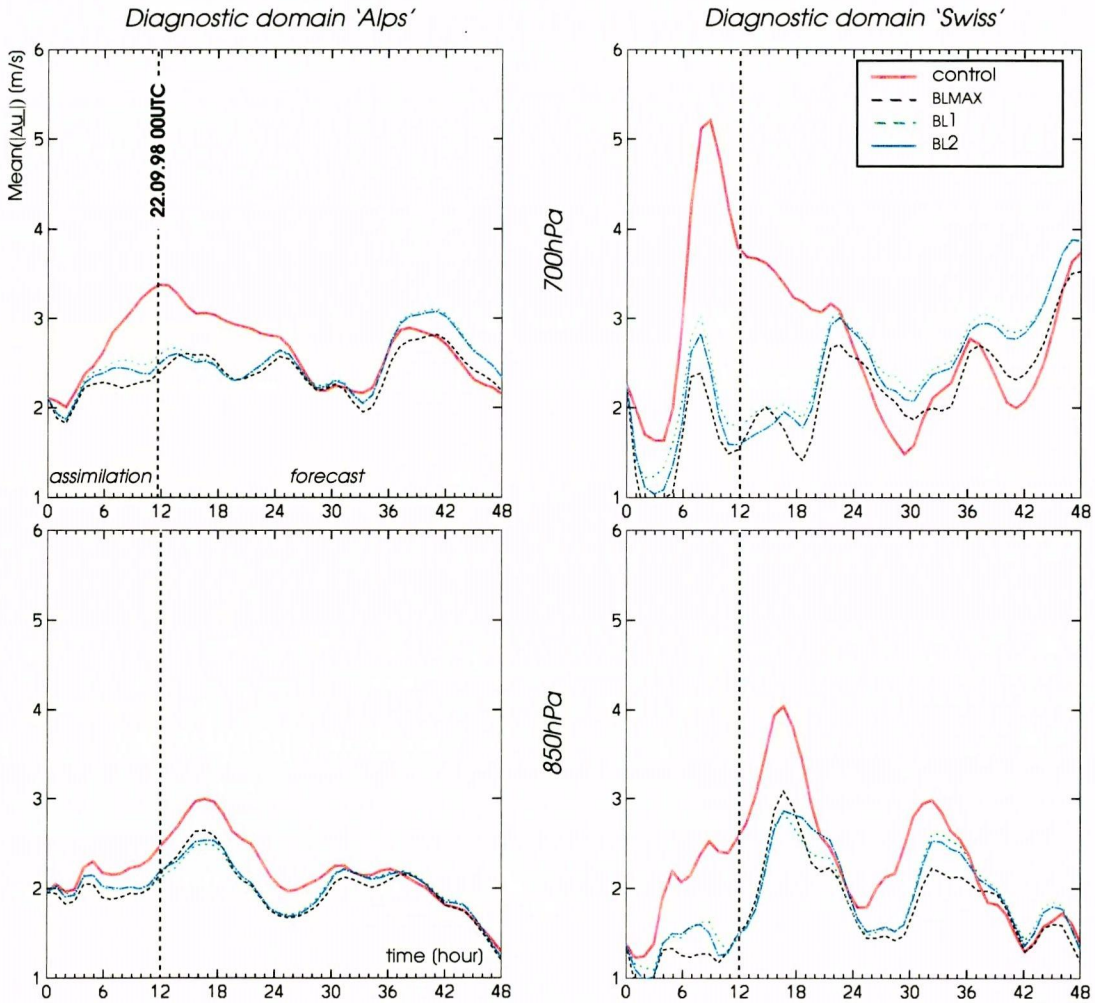

FIGURE 4-5. **Cold air drops case (22.09.98) – impact of maximum and realistic BL radar networks on the wind field**. Displayed is the temporal evolution of our measure of the wind error (see section 3.4), evaluated on 2 pressure levels and in both the 'Alps' and the 'Swiss' diagnostic domains. The red line denotes the error of the control experiment, the other lines denote the error after assimilation of synthetic observations from the BLMAX network (black curve), from the BL1 network (4 radars configuration – green curve), and from the BL2 network (9 radars configuration – blue curve). Data assimilation takes place during the first 12 hours.

BLMAX network. On the 700hPa wind these effects are more differentiated, but, except for the second convective case, at least 50% of the "maximum" correction is obtained with the BL1 network.

A typical illustration of the comparative effects of the different simulated BL radar networks is given by the cold air drops case, in figure 4-5. Although very similar effects are observed at analysis time, the maximum network produces meteorological fields which are more consistent with the reference atmosphere. Indeed a better forecast is obtained after assimilation of observations from the BLMAX network than after assimilation of observations from the BL1 or BL2 networks.

Thesis A4

Complementing a Swiss-scale network with the European-scale CWINDE network brings a further positive impact on wind forecast in some meteorological situations. This illustrates the importance of upstream observing systems for forecast quality. However the CWINDE network, with its 10 profilers, is not dense enough to have a systematic impact (about this last point see also thesis B2).

An illustration of the additional positive impact produced by complementing the Swiss network FTMAX with the European-scale network CWINDE is presented in figure 4-6, for one of the summer convection cases. Although no significant additional effect is observed at analysis time, at least on the diagnostic domain 'Swiss', the 10 instruments of the CWINDE network produce a significant improvement of the *predicted* 700hPa wind. The advection of the information brought by the CWINDE instruments located upstream of the diagnostic domain is responsible for this behaviour: this information needs a certain amount of time to reach the diagnostic domain, resulting in the delayed additional positive impact observed in the right panel of figure 4-6. A rough estimation of this delay, based on the mean wind velocity, supports this explanation.

A similar behaviour is observed in the South Ticino episode, presented in figures 4-3 and 4-4 (page 34). The smallest network configuration, the 5 ST radars of the MAPST

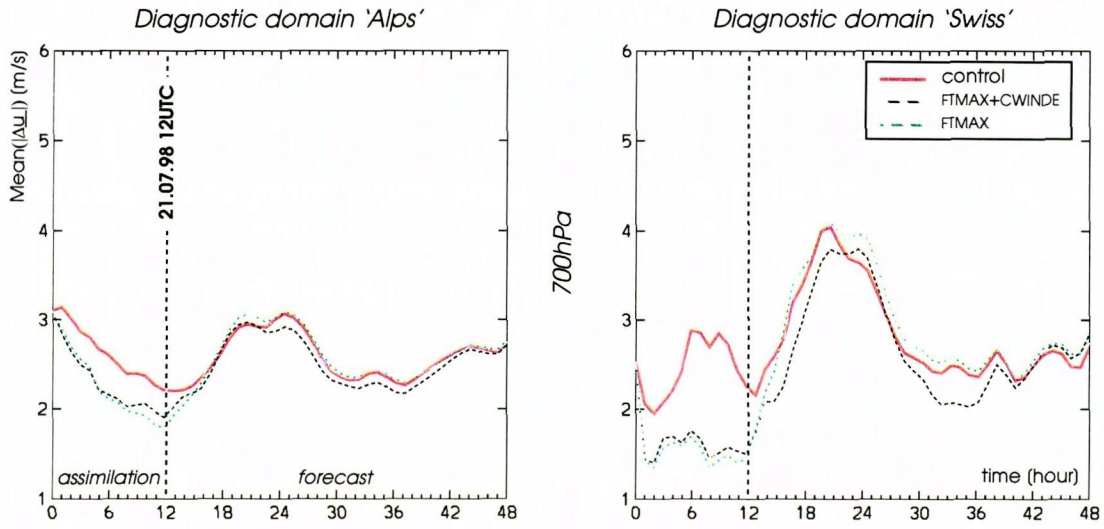

FIGURE 4-6. **Summer convection case (21.07.98) - impact of European and Swiss-scale networks on the wind field**. Displayed is the temporal evolution of our measure of the 700hPa wind error (see section 3.4), evaluated in both the 'Alps' and the 'Swiss' diagnostic domains. The red line denotes the error of the control experiment, the other lines denote the error after assimilation of synthetic observations from the FTMAX+CWINDE network (black curve) and from the FTMAX network alone (green curve). Data assimilation takes place during the first 12 hours.

network, brings about the same improvement as the whole MAP network with its 13 instruments. On the other hand the complete MAP+CWINDE network gives consistently better results than the 2 other configurations and – with respect to the MAP network alone – substantially improves the quality of the SM fields. This shows again the importance of the upstream observing system for the quality of the forecast. Indeed, with respect to the MAPST network, the additional instruments in the MAP network are mostly placed inside the diagnostic area (and therefore no additional impact is observed), whereas the supplementary instruments brought by the CWINDE network are partly placed upstream of the diagnostic area (see figures 3-1 and 3-3).

Finally, one observes that the CWINDE network does not *systematically* produce a clear additional positive impact. It is shown in thesis B2 that the coarse horizontal resolution of this network, with its 10 instruments unevenly distributed over the whole SM domain, is partly responsible for that limitation.

4.2 Some requirements for an effective observing system

In order to gain more insight into the impact of WP networks on NWP quality, it is useful to compare this impact with the effect of an existing observing system; such a comparison also provides a gauge for the evaluation of the WP impact. In the present study the largest simulated WP network (FTMAX+CWINDE) has been compared with the present operational rawinsonde network (TEMP)[1]. The synthetic WP network is characterized by a high temporal resolution (hourly observations versus 12h rhythm for the rawinsonde observations), but, except over Switzerland, has a relatively coarse horizontal resolution (22 instruments spread over the whole SM domain, versus 60 sounding stations for the TEMP network). During a 12 hours period the FTMAX+CWINDE network provides about 290 wind profiles, whereas the TEMP network provides about 120 profiles.

In thesis A1 it has been shown that the FTMAX network and the TEMP network produce similar impacts on the wind analysis, when this impact is measured in the diagnostic domain 'Swiss'. The situation is quite different when the diagnostic domain 'Alps' is considered: in this case the TEMP network has usually a larger impact than the FTMAX+CWINDE network (see figure 4-8 for an illustration). Moreover the positive effect induced by the TEMP network persists much longer in the forecast (see the table 4-1 on page 31 and the figure 4-8), and a positive impact on the surface pressure and on the temperature fields is also observed. In one case the TEMP network is even able to significantly correct the precipitation pattern (see figure 4-7).

This shows that the SM state obtained after assimilation of TEMP observations is much more consistent with the reference atmosphere than the state obtained after assimilation of FTMAX+CWINDE observations (in other words, measured in the SM phase space, the former state is closer to the reference than the latter state). Sensitivity studies have been performed to understand the causes of this fact, resulting in the two theses discussed below.

Thesis B1

On the meso-β-scale it is not sufficient to assimilate the wind. In order to have a robust assimilation scheme with a visible impact of the observing system on the forecast, it is necessary to assimilate observations which directly constrain additional fields of the model. Indeed the mass, temperature and humidity fields do not necessarily adapt to the

[1] For that purpose the *real* TEMP observations – surface pressure and the wind, temperature and dew-point temperature profiles – are assimilated in the test run of our OSSE set-up (see section 2.3.2).

wind field; in some situations the mass field can even be the dominant factor for improving the analysis.

A first sensitivity study based on the TEMP network is presented in figure 4-9. In this experiment, taking place during the south Foehn episode, the impacts of the surface pressure and of the wind observations on the 850hPa wind field are compared. At analysis time both types of observation have a similar positive effect; however, the improvement due to the wind information is limited to the first 12 forecast hours, whereas the improvement due to the surface pressure information persists during the whole forecast. One should stress that in this latter case *no* wind observations are assimilated, so that the observed wind improvement is a consequence of the dynamic adaptation of the SM wind field to the surface pressure field (no geostrophic wind correction is associated to the surface pressure increments in our assimilation scheme – see section 2.2). Note that the inverse is not true: the assimilation of the wind field alone does not induce an improvement of the surface pressure.

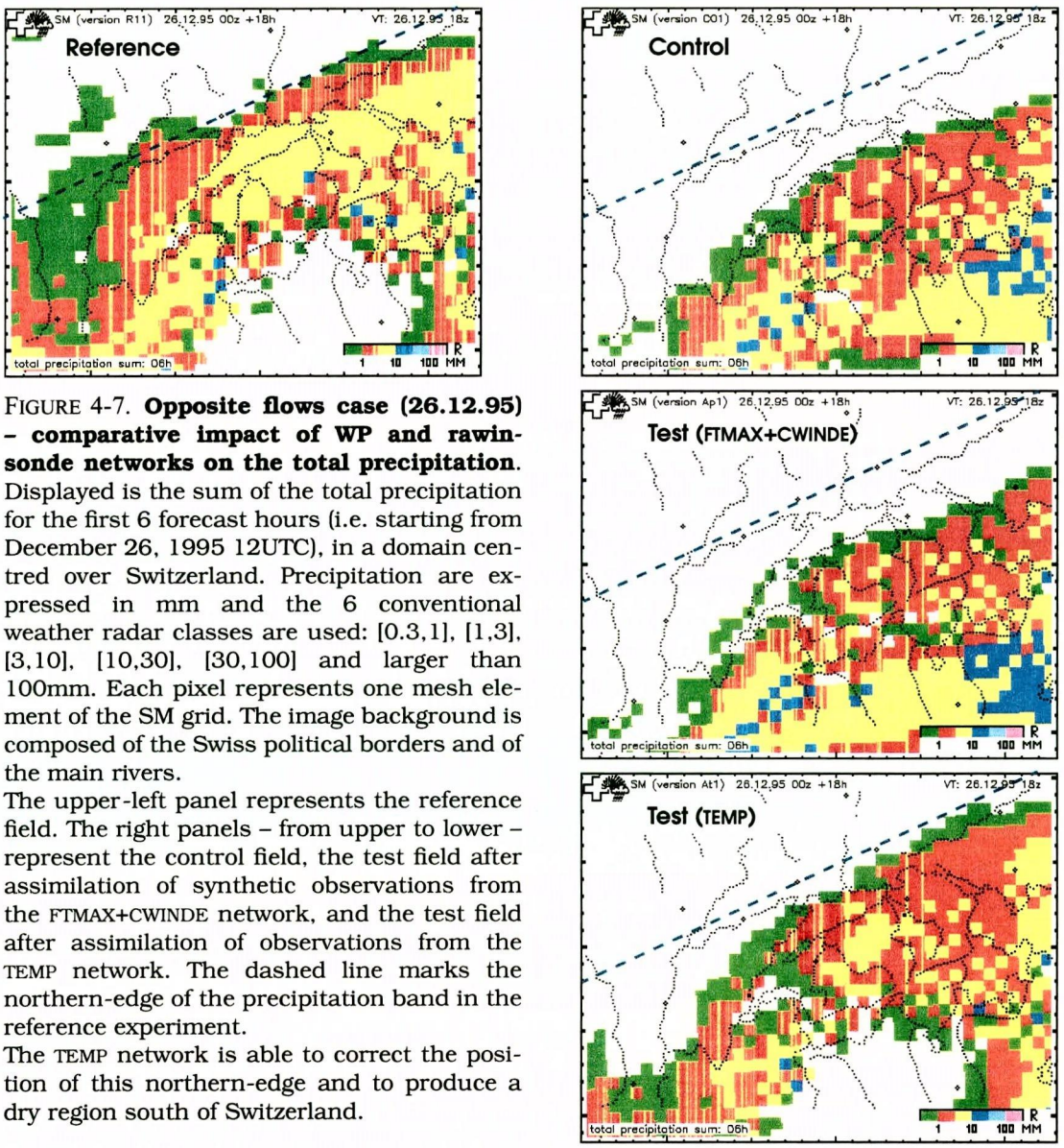

FIGURE 4-7. **Opposite flows case (26.12.95) – comparative impact of WP and rawinsonde networks on the total precipitation**. Displayed is the sum of the total precipitation for the first 6 forecast hours (i.e. starting from December 26, 1995 12UTC), in a domain centred over Switzerland. Precipitation are expressed in mm and the 6 conventional weather radar classes are used: [0.3,1], [1,3], [3,10], [10,30], [30,100] and larger than 100mm. Each pixel represents one mesh element of the SM grid. The image background is composed of the Swiss political borders and of the main rivers.
The upper-left panel represents the reference field. The right panels – from upper to lower – represent the control field, the test field after assimilation of synthetic observations from the FTMAX+CWINDE network, and the test field after assimilation of observations from the TEMP network. The dashed line marks the northern-edge of the precipitation band in the reference experiment.
The TEMP network is able to correct the position of this northern-edge and to produce a dry region south of Switzerland.

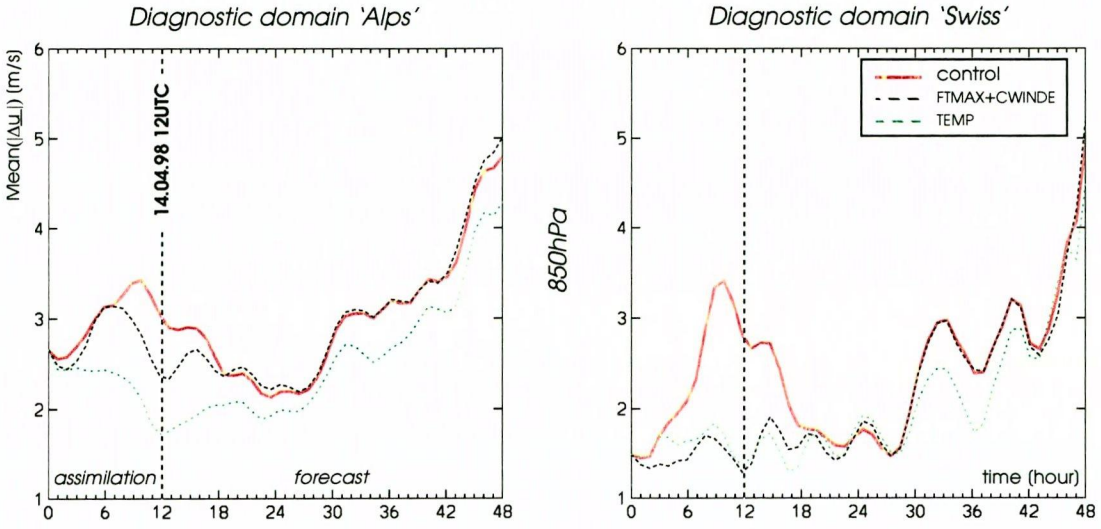

FIGURE 4-8. **South Foehn case (14.04.98) – comparative impact of WP and rawinsonde networks on the wind field**. Displayed is the temporal evolution of our measure of the 850hPa wind error (see section 3.4), evaluated in both the 'Alps' and the 'Swiss' diagnostic domains. The red line denotes the error of the control experiment, the other lines denote the error after assimilation of synthetic observations from the FTMAX+CWINDE network (black curve) and from the TEMP network (green curve). Data assimilation takes place during the first 12 hours.

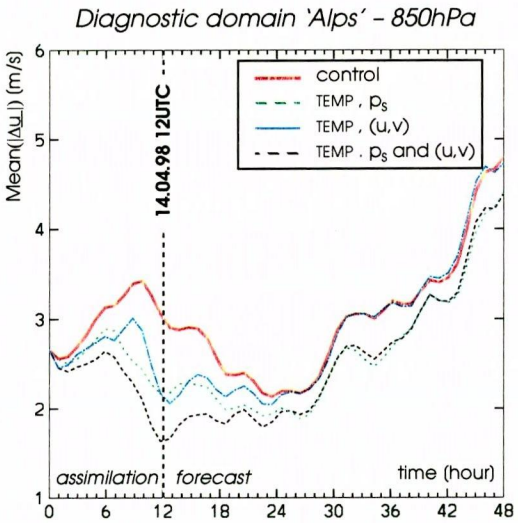

FIGURE 4-9. **South Foehn case (14.04.98) – impact of the TEMP network on the wind field, sensitivity study.** Measure of the 850hPa wind error (see section 3.4), evaluated in the diagnostic domain 'Alps'. The red line denotes the error of the control experiment, the other lines denote the error after assimilation of TEMP observations. The green line is the result of assimilating the surface pressure only, the blue line is the result of assimilating the wind only, and the black line is the result of assimilating the surface pressure and the wind.

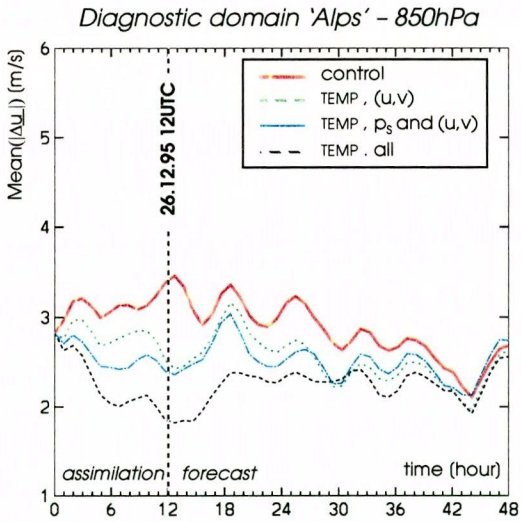

FIGURE 4-10. **Opposite flows case (26.12.95) – impact of the TEMP network on the wind field, sensitivity study.** Measure of the 850hPa wind error (see section 3.4), evaluated in the diagnostic domain 'Alps'. The red line denotes the error of the control experiment, the other lines denote the error after assimilation of TEMP observations. The green line is the result of assimilating the wind only, the blue line is the result of assimilating the surface pressure and the wind, and the black line is the result of assimilating all TEMP information.

In fact, in the second part of the forecast, the 850hPa wind field improvement induced by the assimilation of the complete TEMP profile is entirely due to the surface pressure information. This behaviour is of course related to the meteorological situation under investigation, the surface pressure gradient across the Alps being one of the dominant aspects in the Foehn dynamics.

Unlike the previous case, the South Ticino case presented in figures 4-3 and 4-4 (page 34) shows a situation where a correction of the wind field induces a substantial correction of the surface pressure field. Yet another behaviour is presented in figure 4-10 (page 41) for the 'opposite flows' case. Here the surface pressure does not play a significant role for the correction of the control error; on the other hand the thermodynamic quantities – the temperature and the dew point profiles – have a marked positive impact on both the analysed and the predicted 850hPa wind.

These examples clearly show that a reasonably *systematic* impact on the quality of the forecast fields can only be obtained with an observing system which constrains all the prognostic model fields. Such an observing system also produces consistently better analysis than an observing system providing wind observations only.

Thesis B2

The high temporal resolution of WP observations does not compensate for a poor horizontal resolution of the observing system. A sufficient horizontal resolution on the whole NWP domain is a prerequisite for bringing a consistent and systematic quality improvement of a meso-β-scale limited area model. A horizontal distance between neighbouring instruments of about 250km produces good results.

In order to assess the relative importance of the horizontal resolution and of the temporal resolution of the observing system, one compares the impact of the wind observations coming on the one hand from the FTMAX+CWINDE network, on the other hand from the TEMP network. One should stress that, from this latter network, *only* the wind information is used. Some results are presented in figures 4-11 and 4-12 for the 'opposite flows' case and for the cold air drops case. In both cases the TEMP network has a much larger positive impact than the WP network, in particular on the wind *forecast*, although the number of assimilated profiles is about two and a half times smaller for the TEMP network than for the WP network. This shows that the high temporal resolution of the WP network does not compensate for its poor horizontal resolution, at least in the Alpine region.

Another conclusion to draw from these experiments is the importance of the network horizontal resolution and spatial extent for the construction of a *consistent* model analysis, so that the positive impact of the observing system on the analysis persists during the forecast. The figure 4-12 is a good illustration of this point: the three considered networks have about the same impact on the analysed wind, but only the analysis obtained with the TEMP network generates a forecast which is significantly improved. This could be traced back to the restricted spatial extent of the FTMAX network and to the poor horizontal resolution of the CWINDE network, especially in the eastern part of the SM domain (the cold air drops case is characterized by an easterly flow), and is related to the importance of the upstream information for the forecast quality, already mentioned in thesis A4.

It is possible to obtain a rough estimation of an 'optimal' value for the horizontal resolution of the observing system if one considers that (1) the CWINDE network is clearly not dense enough, with a typical distance between neighbouring instruments of about 600km (10 instruments over a 2000km×2000km domain) (2) the TEMP network brings good results, with a typical distance between neighbouring instruments of about 250km (60 instruments) (3) the BLMAX network, with a typical distance between neighbouring instruments of about 110km, is clearly redundant, as shown by the fact

that the 4 instruments of the BL1 network bring a substantial part of the BLMAX correction (thesis A3).

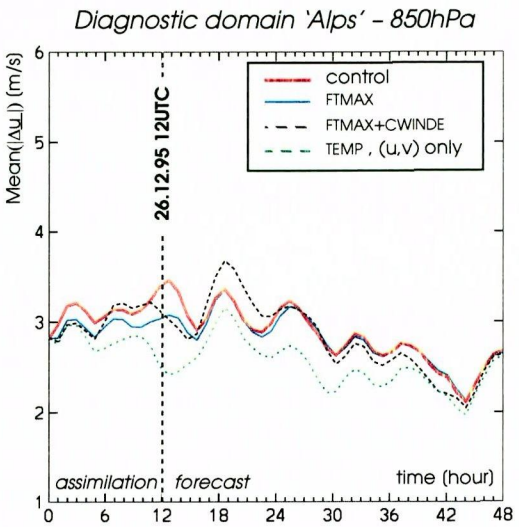

FIGURE 4-11. **Opposite flows case (26.12.95) – impact of the network resolution on the wind field.** Measure of the 850hPa wind error (see section 3.4), evaluated in the diagnostic domain 'Alps'. The red line denotes the error of the control experiment. The blue line denote the error after assimilation of FTMAX observations, the black line denote the error after assimilation of FTMAX+CWINDE observations, and the green line denote the error after assimilating the wind observations from the TEMP network. Data assimilation takes place during the first 12 hours.

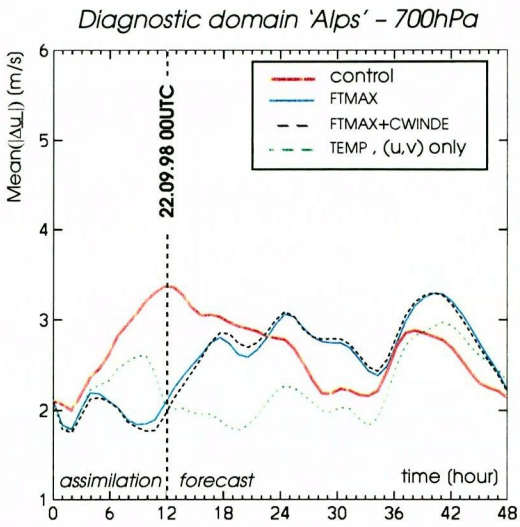

FIGURE 4-12. **Cold air drops case (22.09.98) – impact of the network resolution on the wind field.** Measure of the 700hPa wind error (see section 3.4), evaluated in the diagnostic domain 'Alps'. The red line denotes the error of the control experiment. The blue line denote the error after assimilation of FTMAX observations, the black line denote the error after assimilation of FTMAX+CWINDE observations, and the green line denote the error after assimilating the wind observations from the TEMP network. Data assimilation takes place during the first 12 hours.

4.3 On the nudging scheme

One has mentioned in section 1.2 that an OSSE measures the combined effect of the simulated observing system and of the associated data assimilation scheme (the nudging technique in this study). In fact, because of the fully controlled experimental environment defined in the OSSE context – characterized by a perfect knowledge of the reference state and the use of synthetic observations – OSSEs are well suited to point out problems in the assimilation scheme. Two such problems are discussed in this section.

Thesis C1

In the low to mid troposphere the vertical influence range of a single-level upper air observation is too broad (observations at the top and bottom of a multi-level report also belong to the single-level upper air category).

In section 2.2 the nudging vertical weight $\omega_{\Psi,z}$ has been introduced; this quantity defines the way the influence of one observation is vertically spread. In the original form of our assimilation scheme the width of this function for a single-level upper air wind observation, defined by the parameter σ_z, had been set to 0.33.

With this original parametrization a marked *negative* impact of WP observations on the wind analysis has sometimes been noted. An example is given in figure 4-13 for the FASTEX case (the case used to calibrate our OSSE set-up): a negative impact of the CWINDE network on the 850hPa wind is observed, especially visible around the location of the Lindenberg instrument.

Note that the bottom of the synthetic wind profile over Lindenberg is set to 2600m above ground (about 730hPa), and an observation at the bottom of this profile contributes to the 850hPa wind field tendency with a weight equal to 0.93. By narrowing the vertical weight $\omega_{\Psi,z}$, setting σ_z to 0.04, this latter value is reduced to 0.56 and the observed negative impact is significantly reduced. This clearly shows that a too broad vertical weight is responsible for this negative impact. In fact a strong vertical gradient of the horizontal wind is observed over Lindenberg in this case, so that the observation increments calculated at the profile bottom are *not* representative of the wind error on the 850hPa level.

In the low to mid troposphere such a strong vertical gradient of the horizontal wind is not uncommon, so that the reduced σ_z value has been used for all other experiments calculated during the OSSE project. However, in spite of this corrected vertical weight, a similar negative impact on the wind analysis is still visible in some situations (see for example the BLMAX impact on the 500hPa wind in the Foehn case, in figure 4-2). This shows that further tuning of the vertical nudging weight is still required.

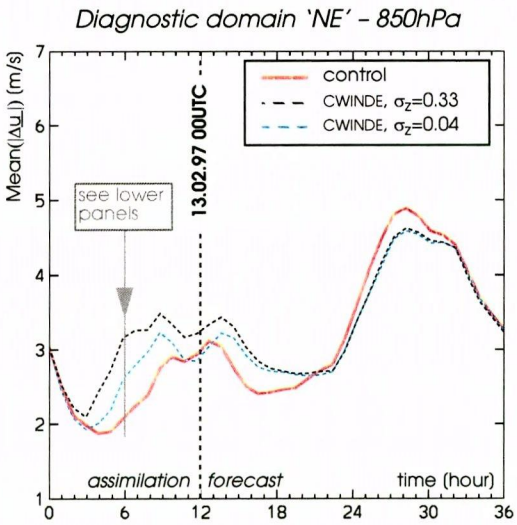

FIGURE 4-13. **FASTEX case (13.02.97) - sensitivity of wind error to the vertical nudging weight.** ***Left panel***: measure of the 850hPa wind error (see section 3.4), evaluated in the north-eastern diagnostic area defined in fig. 2-8. The red line denotes the error of the control experiment, the other lines denote the error after assimilation of CWINDE observations. The black line is obtained with a broad vertical nudging weight, the blue line is obtained with a narrower vertical weight. ***Lower panels:*** 850hPa wind *error* in the middle of the assimilation period, displayed on the whole SM domain. The lower-left panel shows the control error; the lower-right panel shows the test error, the CWINDE observations being assimilated with the broad vertical weight (σ_z=0.33). The location of the synthetic profiler located at Lindenberg is marked by a red triangle. The shaded areas denote orography above 1500m.

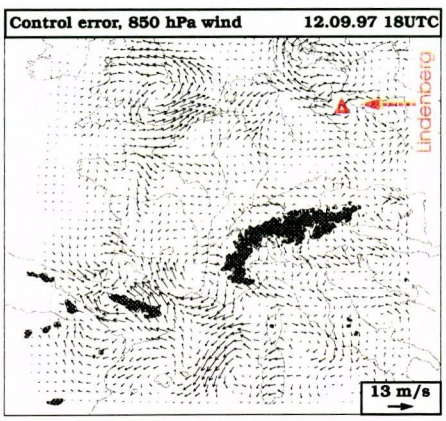

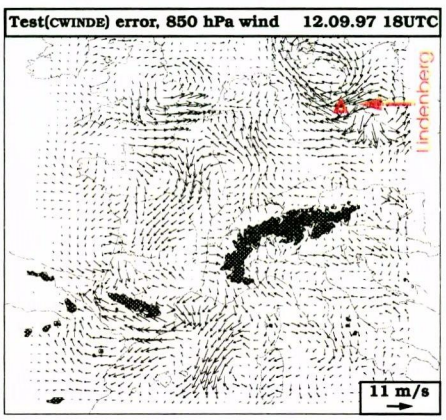

Thesis C2

The assimilation of the horizontal wind does not always produce a consistent improvement of initial conditions and forecasts. Forcing the model wind towards the observations at some sensitive atmospheric locations may result in a large negative impact in the forecast, although the initial conditions of the wind field have been improved. This behaviour is not sensitive to the degree of non-divergence used in the parametrization of the horizontal wind correlation. A small improvement is observed if the horizontal influence range of wind observations is reduced.

An example of the sometimes detrimental effect of WP observations on the quality of the SM forecast is given in figure 4-14 for the cold air drops case. In this figure the 700hPa wind field error measured over the diagnostic domain 'Swiss' is plotted; although the FTMAX+CWINDE network has a large positive impact on the wind analysis, the quality of the subsequent wind forecast is strongly degraded.

For a better understanding of this behaviour, the evolution of the 700hPa wind and geopotential fields in a domain centred over Switzerland is presented in figure 4-15. At analysis time the control experiment is unable to simulate the small ridge of the geopotential field over northern Switzerland, and the wind field in this region exhibits significant errors (north-easterly instead of south-easterly flow at some locations). The FTMAX+CWINDE network corrects the geopotential *pattern* and the wind field error, resulting in the positive impact observed in figure 4-14, but introduces a large bias in the geopotential field. As a consequence, the high over northern Europe extends further east (see the 3135m line in figure 4-15), and the formation of a subsequent cut-off low is delayed. After 12 hours of forecast, this results in a large phase and amplitude error for that cut-off low, and produces the negative impact on the wind field observed in figure 4-14.

This case demonstrates that the assimilation of wind observations with the nudging technique may degrade the quality of other prognostic fields. Sensitivity studies have shown that this behaviour is not sensitive to the degree of non-divergence introduced in the horizontal spreading of wind field increments (the factor γ defined in section 2.2), and is moderately sensitive to the width of the horizontal nudging weight (σ_r, also defined in section 2.2). On the other hand a decisive factor is the location of the observation profile: as shown in figure 4-14, a single profiler at Güttingen (northern part of Switzerland, see figure 3-2) has a similar negative impact as the one of the FTMAX+CWINDE network, whereas a single profiler at Stabio (southern part of Switzerland) produces a consistent improvement of analysis and forecast.

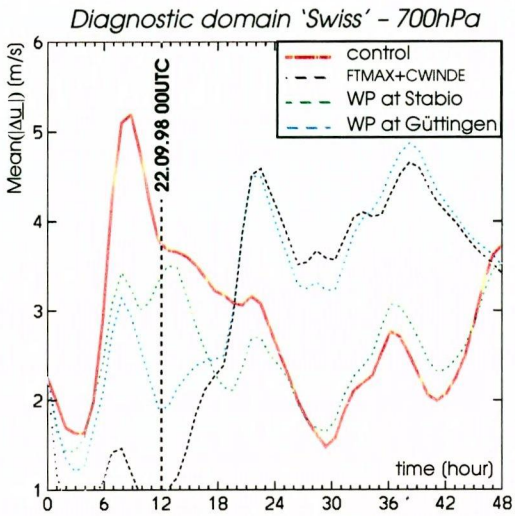

FIGURE 4-14. **Cold air drops case (22.09.98) – sensitivity of wind error to WP locations**. Displayed is the temporal evolution of our measure of the 700hPa wind error (see section 3.4), evaluated in the diagnostic domain 'Swiss'. The red line denotes the error of the control experiment, the black line denotes the error after assimilation of synthetic observations from the FTMAX+CWINDE network. The effect of a *single* WP located at Stabio (green line) or at Güttingen (blue line) are shown (these locations are defined in figure 3-2). Data assimilation takes place during the first 12 hours.

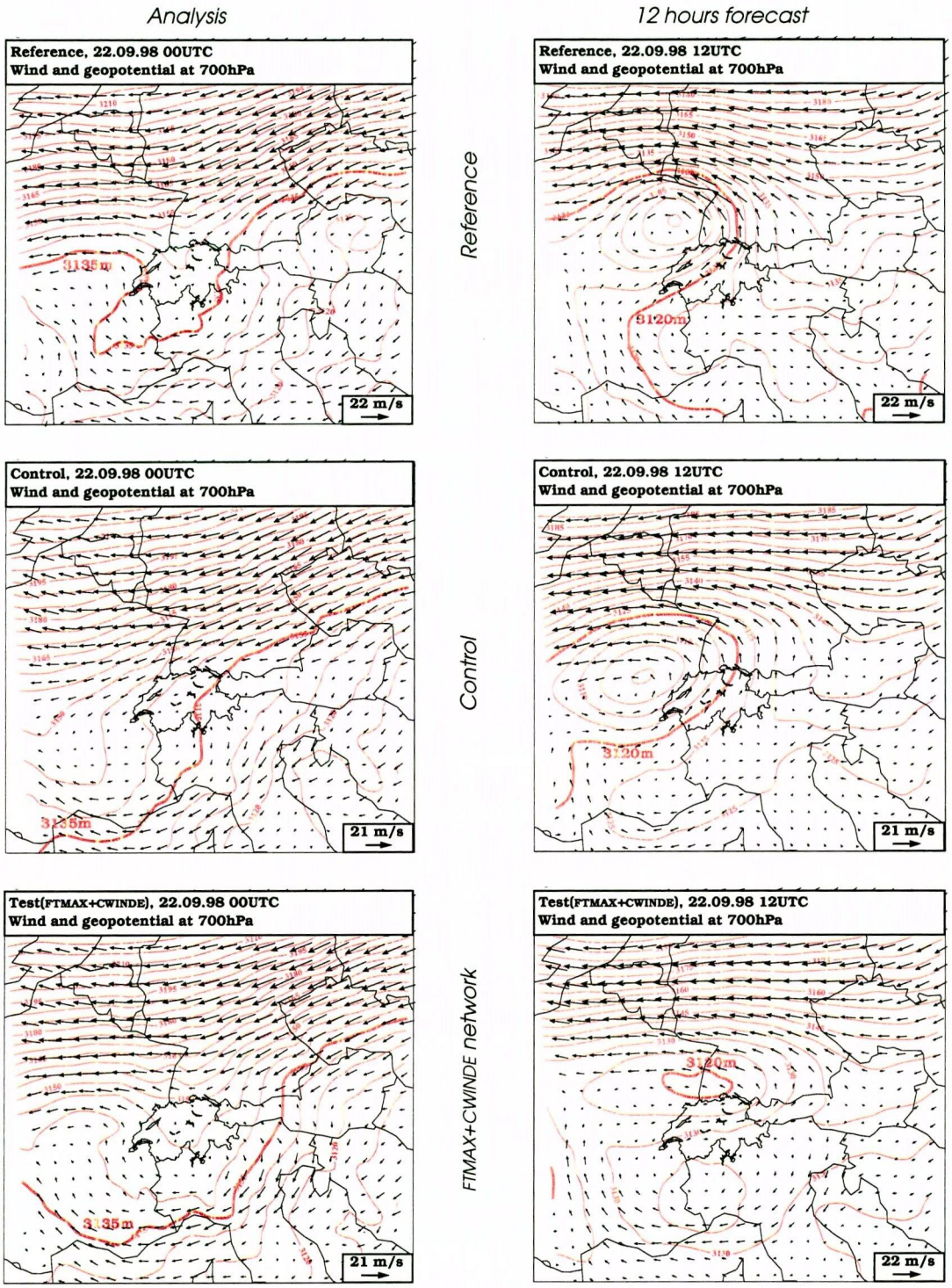

FIGURE 4-15. **Cold air drops case (22.09.98) – detrimental effect of WP observations on the wind and geopotential fields**. Displayed are the 700hPa wind and geopotential fields, in a region centred over Switzerland, at the end of the assimilation period (left panels) and after 12h forecast (right panels). The geopotential is represented by red isolines in 5 meters interval.The upper row is for the reference experiment, the middle row is for the control experiment, and the lower row shows the effect of the FTMAX+CWINDE network.

It is still an open question whether this behaviour can be cured with an improved algorithm for the assimilation of horizontal wind observations, or whether the set of observations used in this case is simply too incomplete to produce a consistent improvement of the analysis (in particular the absence of thermodynamic information could be a decisive factor). The fact that the TEMP network is able to consistently correct both the analysis and the forecast (see figure 4-16) is an element in favour of this latter hypothesis.

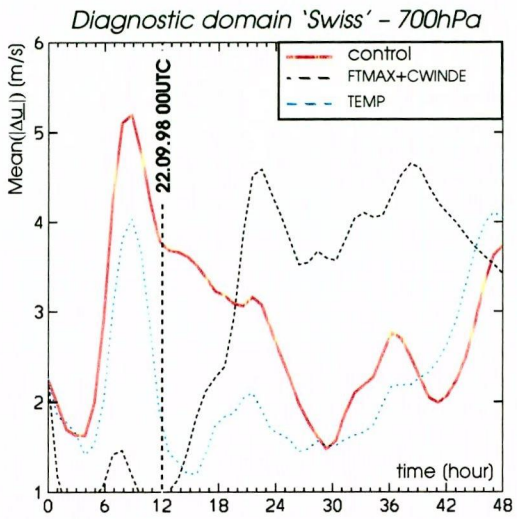

FIGURE 4-16. **Cold air drops case (22.09.98) - comparative impact of WP and rawinsonde networks on the wind field**. Displayed is the temporal evolution of our measure of the 700hPa wind error (see section 3.4), evaluated in the diagnostic domain 'Swiss'. The red line denotes the error of the control experiment, the black line denotes the error after assimilation of synthetic observations from the FTMAX+CWINDE network, and the blue line denotes the error after assimilation of observations from the TEMP network. Data assimilation takes place during the first 12 hours.

4.4 On the MAP SOP wind profiler network

A secondary objective of the present work was to help define the location of the wind profilers to be deployed during the observing period of the Mesoscale Alpine Programme (the MAP SOP). For that purpose the experimental MAP set-up described in section 3 has been introduced, and both the South Ticino and the Piedmont episodes have been included in the set of simulated cases.

The single most important element of this study which is relevant for the definition of the MAP SOP wind profiler network is the importance of upstream observations for forecast quality. This is a point which has been discussed in relation with the thesis A4, and which is illustrated in figures 4-3 and 4-4. Because many of the weather situations targeted by the MAP SOP are characterized by southerly to westerly flows (e.g. intense precipitation over the southern slope of the Alps, Foehn episodes), the instruments located to the south and west of the Alps are important for the quality of the Alpine forecasts during the MAP SOP.

A practical consequence of this fact has been the decision to let the WP located at Lannemezan at its current location (see figure 3-1), instead of relocating it to Annecy as initially planned.

ANNEXES

ANNEXES

A Vertical structure of the Swiss Model

In the vertical the SM is resolved in 40 or 48 layers defined in the hybrid σ-p coordinate system. An estimation of the height above sea level for each layer can be obtained by using the standard atmosphere approximation.

Distribution of layers for the 40 layers configuration, for a surface pressure of 1000hPa:

	p[hPa]	height[m]	width[m]
Half lev.(1)	20.	26481.	
Full lev.	40.	22000.	dh=7062.
Half lev.(2)	60.	19419.	
Full lev.	80.	17595.	dh=3239.
Half lev.(3)	100.	16180.	
Full lev.	120.	15023.	dh=2134.
Half lev.(4)	140.	14046.	
Full lev.	161.	13160.	dh=1664.
Half lev.(5)	182.	12382.	
Full lev.	203.	11690.	dh=1317.
Half lev.(6)	224.	11065.	
Full lev.	245.	10493.	dh=1106.
Half lev.(7)	266.	9960.	
Full lev.	287.	9459.	dh= 972.
Half lev.(8)	308.	8987.	
Full lev.	329.	8541.	dh= 870.
Half lev.(9)	350.	8117.	
Full lev.	371.	7714.	dh= 789.
Half lev.(10)	392.	7328.	
Full lev.	413.	6959.	dh= 724.
Half lev.(11)	434.	6604.	
Full lev.	455.	6264.	dh= 669.
Half lev.(12)	476.	5935.	
Full lev.	497.	5619.	dh= 623.
Half lev.(13)	518.	5313.	
Full lev.	539.	5017.	dh= 583.
Half lev.(14)	560.	4730.	
Full lev.	581.	4451.	dh= 549.
Half lev.(15)	602.	4181.	
Full lev.	622.	3931.	dh= 494.
Half lev.(16)	642.	3687.	
Full lev.	660.	3472.	dh= 424.
Half lev.(17)	678.	3262.	
Full lev.	693.	3091.	dh= 340.
Half lev.(18)	708.	2923.	
Full lev.	720.	2790.	dh= 263.
Half lev.(19)	732.	2659.	
Full lev.	741.	2562.	dh= 193.
Half lev.(20)	750.	2466.	
Full lev.	757.	2392.	dh= 148.
Half lev.(21)	764.	2319.	
Full lev.	770.	2256.	dh= 125.
Half lev.(22)	776.	2194.	
Full lev.	782.	2132.	dh= 123.
Half lev.(23)	788.	2071.	
Full lev.	794.	2010.	dh= 122.
Half lev.(24)	800.	1949.	
Full lev.	806.	1889.	dh= 120.
Half lev.(25)	812.	1829.	
Full lev.	818.	1769.	dh= 119.
Half lev.(26)	824.	1710.	
Full lev.	830.	1651.	dh= 117.
Half lev.(27)	836.	1593.	
Full lev.	842.	1534.	dh= 116.
Half lev.(28)	848.	1477.	
Full lev.	854.	1419.	dh= 115.
Half lev.(29)	860.	1362.	
Full lev.	866.	1305.	dh= 113.
Half lev.(30)	872.	1248.	
Full lev.	878.	1192.	dh= 112.
Half lev.(31)	884.	1136.	
Full lev.	890.	1081.	dh= 111.
Half lev.(32)	896.	1025.	
Full lev.	902.	970.	dh= 110.
Half lev.(33)	908.	915.	
Full lev.	914.	861.	dh= 109.
Half lev.(34)	920.	807.	
Full lev.	926.	753.	dh= 107.
Half lev.(35)	932.	699.	
Full lev.	938.	646.	dh= 106.
Half lev.(36)	944.	593.	
Full lev.	950.	540.	dh= 105.
Half lev.(37)	956.	488.	
Full lev.	962.	436.	dh= 104.
Half lev.(38)	968.	384.	
Full lev.	974.	332.	dh= 103.
Half lev.(39)	980.	281.	
Full lev.	986.	229.	dh= 102.
Half lev.(40)	992.	178.	
Full lev.	996.	145.	dh= 68.
Half lev.(41)	1000.	111.	

The definition of the vertical structure of the SM is made in the configuration file of the program EMTOHM, in the Fortran namelist HMGRID[1]. The value of PINTF defines the critical pressure level where the transition between σ and p levels takes place. The value of PNF defines the set of half-levels in pressure coordinate, for a reference surface pressure defined by PSURF. All values are expressed in hPa.

Definition of half levels for the 48 layers configurations:

```
KEHM= 48,
PINTF= 214.,
PSURF= 1000.,
PNF =  20., 55., 90., 130., 172., 214., 256., 298.,
       338., 378., 416., 454., 490., 526., 560., 592.,
       622., 649., 673., 693., 710., 724., 736., 748.,
       760., 770., 780., 790., 800., 810., 820., 830.,
       840., 850., 860., 870., 880., 890., 900., 910.,
       920., 930., 940., 950., 960., 970., 980., 992.,
       1000.,
```

Definition of half levels for the 40 layers configurations:

```
KEHM= 40,
PINTF= 214.,
PSURF= 1000.,
PNF=   20., 60., 100., 140., 182., 224., 266., 308.,
       350., 392., 434., 476., 518., 560., 602., 642.,
       678., 708., 732., 750., 764., 776., 788., 800.,
       812., 824., 836., 848., 860., 872., 884., 896.,
       908., 920., 932., 944., 956., 968., 980., 992.,
       1000.,
```

[1] A Fortran namelist is a CRAY Fortran input/output structure, which is used to initialize the values of a set of variables.

B Configuration of the Swiss Model

The SM code used for the present work is based on the version 2.25.1.1 of the DM/SM code, with nudging extensions based on the November 1997 version of the DM nudging and with further extensions written specifically for the OSSE project (annexe D).

The SM configuration is defined in a set of Fortran namelists. The configuration for a reference experiment (see Figure 2-7, page 15) is given below; a description of each parameter is found in the EM/DM documentation.

```
&EMGRID
  POLPHI=32.5, POLLAM=-170.0,
  IE=145, JE=145, KE=48,
  PHILU=-19., RLALU=-12., DLAM=0.125, DPHI=0.125,
&END
&RUNCTL
  YADAT='21099812',   NHANF=0, NHENDE=48, DT=90.0,
  LHRM=.true, YMNAME='HRM', LDEBUG=.false,
  LRANA=.false, LQWR=.true, NHDR=1, NHDMXN=3,
  NHEAA= 0, NHDEA=1, NHDAA= 9999, NHDDA=9999,
  NHFORA=12, NHDFOR=12, NHTAA= 9999, NHDTA=9999,
  IADGB=55, IEDGB=111, JADGB=45, JEDGB=87,
&END
&DYNCTL
  LSITS=.true, EPSASS=0.15, LSLA=.false, LVNEST=.false, LORB=.true.,
&END
&PHYCTL
  LPHY=.true, LVDIF=.true, LKON=.true, LSKN=.true, LBOD=.true,
  LRAD=.true, HDRAD=1.0, NJSRAD=2, NDVDIF=3, NLWB=2,
  LHDIF_P=.false, LHDIF_4=.true, DPS_THR=0., HDIF_Q = 1., 1., 1., 1.,
&END
&NMICTL
  LANMI=.false, LDNMI=.false, NVM=3, NITNMI=2, DTNMI=10.0, LWRITEI=.true,
&END
&DIACTL
  LDIA  =.true, HDIAA = 0., HDDIA= 1.,
  LDIMSK=.false, LDILM=.false, LDIDYN=.false, LDIPHY=.false, LDIRAD=.false,
  IADIA =  1, 9,  55, 80, IEDIA = 145, 137,  111, 80,
  JADIA =  1, 9,  45, 68, JEDIA = 145, 137,  87, 68,
  LSPD  =.true, HSPDA=0.0, HDSPD= 1.0, NWLGR = 150000,
  LGPK1 =.true, LGPK3=.false, HGPKA=0.0, HDGPK= 1.0,
  IGPK= 20,53,20,35,80,68,68,89,11,48, 96,114,112,131,132,93,117, 71, 69,119,
  JGPK=130,113,89,57,68,60,42,29,25,27,52, 61, 38, 15, 80,82,111,112,101, 94,
&END
&PRICTL
  LPRDIA=.true, HAPRD= 0.0, HDPRD= 1.0,
  LPRSPD=.true, HAPRS= 0.0, HDPRS= 1.0,
  LPRGPK1=.true,
  LPRGPK3=.false, HAPRG= 0.0, HDPRG= 1.0,
  LPRAD=.false, LPRRD=.false, LPRED=.false,
&END
&DATEN
  YADEN='L48', NAVERS=1, YADTYP='FILE', NLAWB=2,
  YADCAT='$SCRATCH/jmb/wd/98092112_R11/', YADCID='YMP',
  YRDEN='L48', NRVERS=1, YRDTYP='FILE', NLRWB=2,
  YRDCAT='$SCRATCH/jmb/wd/98092112_R11/', YRDCID='YMP',
  YEDEN='R11', NEVERS= 1, YEDTYP='FILE', NTYPEM=52,
  YEDCAT='$SCRATCH/jmb/wd/98092112_R11/', YEDCID='YMP',
  YDDCAT='$SCRATCH/jmb/wd/98092112_R11/', NTYPED=52, YDDCID='YMP',
  YFDCAT='$SCRATCH/jmb/wd/98092112_R11/', YFDCID='YMP',
  YTDCAT='$SCRATCH/jmb/wd/98092112_R11/', YTDCID='YMP',
  YVDCAT='$SCRATCH/jmb/wd/98092112_R11/', YVDCID='YMP',
  NTWAIT=36000, NDTWAIT=180,
&END
```

C Configuration of the assimilation scheme

The nudging code used for the present work is based on the November 1997 version of the DM nudging.

The configuration of the nudging scheme is defined in a set of Fortran namelists. The configuration for a reference experiment (see Figure 2-7, page 15) is given below; a description of these parameters and a complete list of default values is found later on in this annexe.

```
&NUDGE
  LNUDGE  = .true. , NUDGEND = 48,
  NNEWBC  = 4, NBCSTEP = 3, NEWBCDT = 12, LFTOA = .true.,
  THAIRT  = 0.25  , THAIRH  = 50., THAIRV  = 55.,
  QCC     = 0., 500., 0., .6,   QCVF = 5., 0., 10., 0.,  QCTF  = .2,  .2,  .2,  .2,
  NTPSCOR = 3, KTPSTOP = 400, LUVGCOR = .false., QGEO = 0.5,  DVPSMX = 0.3,
  GNUDG   = .0006, .0006, .0006, .0006,     GNUDGAR = .0006, .0000, .0006, .0006,
  LTIPOL  = .true., TIPOLMX = 3.,
  WTUKRSA = 3.0, WTUKRSE = 1.0, WTUKARA = 3.0, WTUKARE = 1.0,
  MSPRPAR = 2,
  CNONDIV = 0.1, FNONDIV = 0.8, TNONDIV = 1.1,
  RHINFL  = 0.0, 83.3,  0.0,   0.0,  RHVFAC = 1.000, 0.000, 0.833, 0.833,
  RHTFAC  = 1.3,  1.3,  1.3,   1.3,  CUTOFR = 3.5, 3.5, 3.5, 2.5,
  DSPRD   = 2500., 2500., 2500., 2500.,  ALODP  =100.,100.,100.,100.,
  DSPRDS  = 1196.,   0.,  27.7,  27.7,    ALODPS = .04, 0. , .04, .04,
  VCUTOF  = 0.75, .0, 1. , 1. ,   WRSABL  = 1. , 1. , 1. , 1. ,
  LSVCORL = .true. , FSVCUT  = .9,
  LCONAI  = .true., NCONBOX = 600,
  YOBSFIL = '/modhome/jmb/sm/nl/osse_R11/FILTER',
&END
&NUDSY
  ALTOPSY =  500., 4000., 4000., 4000.,
  QCSC    = 12. , 500. ,  12. ,   .6,   QCSTF  = .2,  .2,  .2,  .2,
  GNUDGSY = .0006, .0006, .0000, .0006,
  LTIPLSY = .true., TIPSYMX = 1., WTUKSYA = 1.5, WTUKSYE = 0.5,
  MSPRSYP = 2,
  RIFLSY  = 70., 83.3, 100.,  70.,   RHTFSY = 1., 1.1, 1., 1.,    CUTOFS  = 2. ,  2.5,  2.,   2.,
  DPSYLT  = .33, .0 , .11, .11,  DTSYLT = 2. , 0. , 1. , 1. ,
&END
&OUTRS
  LTIMSER = .true.,   LRSPRI = .false.,
&END
&SPRRS
  TOPOBS = 1050., 1050.,  699.,  699.,    BOTMOD = 1050., 1050., 1050., 1050.,
  LSCADJ =.true.,.true.,.true.,.false.,
  IONL = 80, JONL = 68, IONL2 = 69, JONL2 = 60,
&END
&OUTSY
  LSYPRI = .false.,
&END
&NAMANA
  LANADM = .true.,
  LSURFA = .false.,
  LSYNOP = .true. , LAIRCF = .true., LSATOB = .false., LDRIBU = .true., LTEMP  = .true.,
  LPILOT = .true.,   LSATEM = .false.,   LPAOB  = .false.,
  LPRAOF = .false.,  LPRODR = .true.,
  DINLAT = 48.0, DISLAT = 45.5, DIWLON = 6.0, DIELON = 10.5,
  NOCTRQ = 1,
&END
```

Description and default values for the main nudging parameters (courtesy of C.Schraff)

Variable	Default	Description
("+" denotes parameters which are active even if LNUDGE is false)		
NAMELIST /NUDGE/ : GENERAL PARAMETERS AND PARAMETERS FOR UPPER-AIR DATA		
General		
+ LNUDGE	.F.	ON/OFF SWITCH FOR NUDGING
NUDGEND	0	END OF NUDGING PERIOD IN 'MODEL INTEGRATION HOURS'
OBSHEND	999.	LAST ASSIMILATED OBS. IN 'MODEL INTEGRATION HOURS'
+ NEWBCDT	6	INTERVAL [HRS] AT WHICH LATERAL BOUNDARY CONDITIONS (LBC) ARE DERIVED FROM (NEWEST) EM-ANALYSIS
+ NNEWBC	0	NUMBER OF TIMES THAT LBC ARE EM-ANALYSES AFTER 1 HR ((NNEWBC.GE.12) : DO NOT LEVSPRD, HSPREAD,..)
+ NBCSTEP	1	INTERVAL [HRS] OF TRANSITION FROM LBC DERIVED FROM 'OLD' EM-RUN TO LBC DERIVED FROM LATER EM-ANALYSIS
NOLBC	8	NUMBER OF GRID ROWS AT LATERAL BOUNDARIES WHERE OBS ARE NEGLECTED
+ LFTOA	.F.	INITIAL FIELD FROM F-FILES EVEN IF NHANF.EQ.0
+ VRPHD	1.	FACTOR TO GEOPOT. IN REFERENCE PROFILE FOR THE HORIZONTAL DIFFUSION
LCONAI	.F.	TRUE ONLY IF ANALYSIS INCREMENTS BY NUDGING ARE HELD CONSTANT OVER A PERIOD (TIME BOX) 'NCONBOX'
NCONBOX	600	TIME BOX OF CONSTANT ANALYSIS INCREMENTS IN SECONDS
CNONDIV	.9	CONSTANT PART OF THE FACTOR TO THE NON-DIVERGENCE CORRECTION ('FANODICOR') IN 2-DIM WIND CORRELATIONS
FNONDIV	0.	MULTIPLICATION FACTOR TO THE VERTICALLY VARYING PART OF THE 'FANODICOR' AS DEFINED IN SUBR *SETQCT*
TNONDIV	1.	MULTIPLICATION FACTOR TO THE 'FANODICOR' FOR THE BEGINNING AND END OF THE NUDGING PERIOD FOR 1 OBS. RELATIVE TO THE 'FANODICOR' AT THE OBS. TIME (AS GIVEN BY CNONDIV, FNONDIV)
LMX2OBS	.T.	.T. ==> NO MORE (IN TIME) THAN 2 PRESENTLY ACTIVE OBS. REPORTS OF SAME TYPE PER STATION
Size of observation data records (ODR)		
MAXRSO	1000	MAX. NUMBER OF MULTI-LEVEL (M-L) REPORTS (IN ODR)
MAXRSL	200	MAX. NUMBER OF LEVELS IN MULTI-LEVEL REPORTS IN ODR
MAXSYO	20000	MAX. NUMBER OF SURFACE SINGLE-LEVEL (S-L) REPORTS
MAXSLO	5000	MAX. NUMBER OF UPPER-AIR SINGLE-LEVEL (S-L) REPORTS
Corrections for increased balancing of analysis increments		
NTPSCOR	0	SWITCH FOR TEMPERATURE CORRECTION WITH PS-NUDGING 0: ONLY ADIABATIC TEMPERATURE CORRECTION 1-4: TEMPERATURE CORRECTIONS SO THAT THE FINAL GEOPOT. CHANGE DUE TO SURFACE PRESSURE NUDGING IS ZERO AT HIGH LEVELS. 1: CORRELATION OF GEOPOT. CHANGES AT LEVEL K TO THE SURFACE: CFI = .5*BKH(K)*(1+BKH(K)) (CF. UKMO) 2: AS 1, BUT CFI = CK(K)^2 * EXP((1.-CK(K)^3)/4) WHERE CK = (BK-BK(KTOPP)) / (1 -BK(KTOPP)) ALSO: LATERAL SPREADING OF PS-OBS.-INCREMENTS APPROXIMATELY CONSISTENT WITH TEMP. CORRECTION 3: AS 2, BUT CK = (PK- KTPSTOP) / (PS- KTPSTOP) ALSO: LATERAL SPREADING OF PS-OBS.-INCREMENTS IS MADE CONSISTENT WITH THE TEMPERATURE CORRECT'N BY ACCOUNING FOR THE GEOPOT. CORRELATION 'CFI' 5-7: AS 1-3, BUT WITH APPROXIMATION SO THAT THE FINAL GEOPOT. CHANGE DUE TO PS-NUDGING IS NOT EXACTLY ZERO (ERROR ~ 8%), AND THE LATERAL SPREADING OF PS-OBS-INCR. NOT MADE CONSISTENT
KTPSTOP	2	UPPER BOUNDARY OF TEMPERATURE CORRECTION; UNITS: NTPSCOR=2 --> P[HPA] (TAKE NEXT LEVEL BELOW) NTPSCOR=3 --> P[HPA]
FTPSCOR	1.	GLOBAL WEIGHT FACTOR (<=1) TO TEMPERATURE CORRECT.
LUVGCOR	.F.	.T. ==> GEOSTROPHIC WIND CORRECTION APPLIED
QGEO	.5	GLOBAL FACTOR TO THE GEOSTROPHIC WIND INCREMENTS
DVPSMX	.1	WIND SPEED OF GEOSTROPHIC WIND INCREMENTS IS SET TO 'DVPSMX' WHERE COMPUTED INCREMENTS ARE LARGER
Varia		
YOBSFIL	' '	FILE CONTAING OBSERVATION RECORDS FILTER (SEE ROUTINE 'INIREC' FOR FORMAT DESCRIPTION)
PQMIN	29999.	PRESSURE THRESHOLD [P] BELOW WHICH NO MOISTURE DATA ARE USED
RHTSAT	.96	REL HUM. THRESHOLD FOR SATURATION WITH REAL DATA
NDTSORT	600	TIME STEP [S] FOR SORTING / ADMINISTRATING THE DATA

Variable	Default	Description
Vertical profiles	*(RS means rawinsonde / most of these parameters also apply to aircraft data)*	
	(4 dimension arrays are for the fields 1:(u,v), 2:p or ps, 3:T, 4:RH)	
GNUDG	4*.0006	NUDGING COEFFICIENTS FOR TEMP / PILOT DATA [1/S]
RHINFL	0.,130.,0.,0.	CONSTANT PART OF THE 'CORRELATION SCALE OF AUTO-REGRESSIVE HORIZ. STRUCTURE FUNC.'(='COSAS') [KM]
RHTFAC	4* 1.	MULTIPLICATION FACTOR OF THE TOTAL 'COSAS' FOR THE BEGINNING AND END OF NUDGING PERIOD FOR 1 OBS RELATIVE TO THE 'COSAS' AT THE OBS. TIME (AS SPECIFIED BY RHINFL, RHVFAC)
CUTOFR	4* 3.5	CUT OFF IN 'COSAS' UNITS OF THE HORIZ. WEIGHT FN.
QCC	12.,500.,8., .6	CONSTANT PARTS OF QUALITY CONTROL THRESHOLDS ('QC-THR'). (U,V):[m/s], T: [K], RH: [], PS: [Pa]
QCTF	4* .2	FRACTION (OF THE 'QC-THR' AT THE OBS. TIME, GIVEN BY 'QCC', 'QCVF') WHICH IS ADDED TO THE 'QC-THR' FOR EACH HOUR OF DIFFER. BETW. OBS AND MODEL TIME
	(4 dimension arrays are for the fields 1:(u,v), 2:–, 3:T, 4:RH)	
RHVFAC	4* 1.	MULTIPLICATION FACTOR TO THE VERTICALLY VARYING PART OF THE 'COSAS' AS DEFINED IN SUBR *SETQCT*
ALODP	4* 100.	SQUARE OF GAUSSIAN VERTICAL LN(P) INFLUENCE 'RADIUS' IF SPREADING OF INTERPOLATED MULTI-LEVEL DATA IS NOT ALONG ISOBARIC SURFACES. THIS DETERMINES THE NON-ISOTROPY OF HORIZ. STRUCTURE FUNC.
ALODPS	4*.333	SQUARE OF GAUSSIAN VERTICAL LN(P) INFLUENCE 'RADIUS' FOR UPPER-LEVEL SINGLE-LEVEL DATA
DSPRD	4*2500.	SQUARE OF GAUSSIAN VERTICAL THETA(E) INFLUENCE 'RADIUS' IF SPREADING OF INTERPOLATED MULTI-LEVEL DATA IS NOT ALONG ISENTROPIC SURFACES.THIS DETERMINES THE NON-ISOTROPY OF HORIZ. STRUCTURE FUNC.
DSPRDS	4* 27.7	SQUARE OF GAUSSIAN VERTICAL THETA(E) INFLUENCE 'RADIUS' FOR UPPER-LEVEL SINGLE-LEVEL DATA
VCUTOF	4* .75	CUT-OFF OF VERTICAL CORRELATION. UNITS VALUE OF CORRELATION AT CUT-OFF IS [EXP(-VCUTOF)] (C.F UKMO CUT-OFF AT | LN(P/POBS)) | = 0.5 CORREL. FN EXP(-3 *(LN(P/POBS))**2) ==> VALUE OF CORREL. AT CUT-OFF EXP(-.75))
WRSABL	4* 1.	FACTOR TO WEIGHTS WITHIN THE ABL (ATMOSPHERIC BOUNDARY LAYER, I.E. MORE PRECISELY MIXED LAYER)
QCVF	5., 0.,10., 0.	MULTIPLICATION FACTOR TO THE VERTICALLY VARYING PART OF 'QC-THR' AS DEFINED IN SUBR *SETQCT* (NOT AVAILABLE FOR RH (AND PS) !)
	Some parameters related to lateral spreading of observation increments	
MSPRPAR	0	SWITCH WHICH SPECIFIES BOTH - THE SURFACE ALONG WHICH OBS. INCREMENTS OF VERTICAL PROFILES ARE SPREAD - THE PARAMETERS WHICH SCALE THE VERTICAL DISTANCE BETWEEN INTERPOLATED OBSERVATION SITE AND TARGET GRID PT. AND ON WHICH NUDGING WEIGHTS MAY DEPEND. 0 : SPREADING ALONG MODEL LEVELS (K CONSTANT), WEIGHTS DEPEND ON 'LN(P)' AND 'TH' DIFFERENES 2 : SPREADING ALONG ISOBARS ('P' CONSTANT), WEIGHTS DEPEND ON 'TH' DIFFERENCES 4 : SPREADING ALONG ISENTROPES ('TH' CONSTANT) WEIGHTS DEPEND ON 'LN(P)' DIFFERENCES WHERE 'TH' : APPROXIMATE POTENTIAL TEMPERATURE 'THE': APPROX. EQUIVALENT POTENT. TEMPERATURE LN(P): NAT. LOG(PRESSURE)
THRESH1	16.39	THRESHOLD VALUE OF VERTICAL GRAD. OF THE SPREADING PARAMETER (IF MSPRPAR.GE.4) ABOVE WHICH INCREMENTS ARE SPREAD SOLELY ALONG THE SPECIFIED PARAMETER
THRESH2	0.0	THRESHOLD VALUE OF VERTICAL GRAD. OF THE SPREADING PARAMETER (IF MSPRPAR.GE.4) BELOW WHICH INCREMENTS ARE SPREAD ALONG CONSTANT PRESSURE SURFACES.
	Some other parameters	
LTIPOL	.F.	.T. ==> LINEAR INTERPOLATION IN TIME OF VERTICAL PROFILES WHICH ARE .LE. 'TIPOLMX' (SEE BELOW) APART
TIPOLMX	3.0	MAX. TIME SPAN (HRS) ALLOWED FOR LINEAR INTERPOLAT. FOR TEMP / PILOT (TIPOLMX = 0 , IF NOT LTIPOL)
WTUKRSA	2.5	FOR SAW-TOOTH-SHAPED TEMPORAL WEIGHTS TEMPORAL RADIUS OF INFLUENCE TOWARDS THE PAST RELATIVE TO THE OBS. TIME . FOR TEMP / PILOT
WTUKRSE	0.5	FOR SAW-TOOTH-SHAPED TEMPORAL WEIGHTS TEMPORAL RADIUS OF INFLUENCE TOWARDS THE FUTURE RELATIVE TO THE OBS. TIME . FOR TEMP / PILOT
RTEMPMX	1.414	HORIZONTAL SEARCH RADIUS FOR GRID PTS. TO ASSIGN A TEMP / PILOT TO A GRID PT. (FOR 'RTEMPMX' NEGATIVE, THE SEARCH IS LIMITED TO THE 4 NEIGHBOUR. GRID PTS)

Variable	Default	Description
DHMAXPO	400.	MAXIMUM HEIGHT DIFFERENCE BETWEEN MODEL SURFACE AND STATION HEIGHT ALLOWED FOR THE DERIVATION OF A (PS) SURFACE PRESSURE OBS. INCREMENT FROM TEMPS (IN [M])
DHRADPO	500.	GAUSSIAN RADIUS OF HEIGHT DIFFERENCES BETWEEN MODEL SURFACE AND STATION HEIGHT FOR A FACTOR CONTRIBUTING TO THE QUALITY WEIGHT FACTOR FOR TEMP-PS-OBS.
NDTQC	1800.	TIMESTEP (IN [S]) FOR THE THRESHOLD QUALITY CONTROL (THE QUALITY CTRL IS ALWAYS APPLIED TO OBSERVATIONS AT THE FIRST TIME WHEN THEY ARE USED)
PMINSIG	15000.	SIGNIFICANT LEVEL TEMP / PILOT DATA AT PRESSURE SMALLER THAN 15000. Pa ARE NEGLECTED
LAUTORG	.T.	.F. ==> CRESSMAN INSTEAD OF AUTOREGRESSIVE HORIZONTAL WEIGHT FUNCTION
Aircraft data (AR) – except for supplementary parameters defined below, vertical profiles parameters apply		
	(4 dimension arrays are for the fields 1:(u,v), 2:p or ps, 3:T, 4:RH)	
GNUDGAR	4*.0006	NUDGING COEFFICIENTS FOR AIRCRAFT DATA [1/S]
WTUKARA	2.5	FOR SAW-TOOTH-SHAPED TEMPORAL WEIGHTS: TEMPORAL RADIUS OF INFLUENCE TOWARDS THE PAST RELATIVE TO THE OBS. TIME
WTUKARE	0.5	FOR SAW-TOOTH-SHAPED TEMPORAL WEIGHTS: TEMPORAL RADIUS OF INFLUENCE TOWARDS THE FUTURE RELATIVE TO THE OBS. TIME
	Param. for producing multi-level reports from aircraft single-level report	
THAIRT	0.5	TEMPORAL [H] } MAXIMUM DISTANCE BETWEEN LOWEST REPORT
THAIRH	50.	HORIZONTAL [KM] } AND ANY SINGLE-LEVEL REPORT THAT IS ADDED TO A MULTI-LEVEL AIRCRAFT REPORT
THAIRV	50.	MAXIMUM VERTICAL DISTANCE [hPa] BETWEEN TWO SUCCESSIVE LEVELS WITHIN A MULTI-LEVEL AIRCRAFT REPORT
	Param. for adjusting vertical correlation scales for reports from same flight and at sufficiently small 4D-distance from one another	
LSVCORL	.T.	.T: ==> ADJUSTMENT OF CORREL. SCALES IS CONDUCTED
FSVCUT	1.	FRACTION WITH WHICH THE ADJUSTED SCALE Sadj, RATHER THAN THE SCALE Snl AS SPECIFIED IN THE NAMELIST, IS USED FOR THE DETERMINATION OF THE VERTICAL CUT-OFF IN LOG(P) OR THETA(E)-UNITS Rcutoff = Fcutoff * (FSVCUT*Sadj + (1-FSVCUT)*Snl)

NAMELIST /NUDSY/ : PARAMETERS FOR NUDGING DATA FROM SURFACE STATIONS

	(4 dimension arrays are for the fields 1:(u,v), 2:ps, 3:T, 4:RH)	
GNUDGSY	4*.0006	NUDGING COEFFICIENTS FOR SURFACE DATA [1/S]
RIFLSY	4* 100.	'CORRELATION SCALE OF AUTOREGRESSIVE HORIZONTAL STRUCTURE FUNCT.' AT THE OBS TIME (='COSAS') [KM]
RHTFSY	4* 1.	SCALING FACTOR TO THE 'COSAS' FOR THE BEGINNING AND END OF NUDGING PERIOD FOR 1 OBS RELAT. TO THE 'COSAS' AT THE OBS. TIME (AS GIVEN BY 'RIFLSY')
CUTOFR	2., 3.5.2., 2.	CUT OFF IN 'COSAS' UNITS OF THE HORIZONTAL WEIGHT FUNCTION.
FHASY	1.,4.,1.,1.,2.	SCALING FACTOR TO VERTICAL DISTANCES BETW. MODEL SURFACE AND STATION HEIGHT FOR FIS-OBS < FIS-MOD: ELEMENTS 1 – 4 FOR NUDGING WEIGHTS (SEE 'RFHASY' BELOW) ELEMENT 5 WHEN LOOKING FOR 'NEAREST' GRID POINT, TO WHICH THE OBS. REPORT WILL BE ASSIGNED
RFHASY	100.,400,2*160.	CUT-OFF AND GAUSSIAN RADIUS OF HEIGHT DIFFERENCES BETWEEN MODEL SURFACE AND STATION HEIGHT FOR A FACTOR CONTRIBUTING TO THE QUALITY WEIGHT FACTOR AS PART OF THE NUDGING WEIGHTS
ALTOPSY	4*5000.	SYNOP OBS. ABOVE HEIGHT 'ALTOPSY' ARE NOT ASSIMILATED. IF (ALTOPSY.EQ.0.) THEN SYNOP / SURF. TEMP ASSIGNED TO LAND GRID POINTS ARE NOT ASSIMIL.
QCSC	12.,500.,8.,6.	CONSTANT PARTS OF QUALITY CONTROL THRESHOLDS ('QC-THR'). (U,V):[m/s], T: [K], RH: [], PS: [Pa]
QCSTF	4*0.2	FRACTION (OF THE 'QC-THR' AT THE OBS. TIME, GIVEN BY 'QCCS') WHICH IS ADDED TO THE 'QC-THR' FOR EACH HOUR OF DIFFERENCE BETWEEN OBS. AND MODEL TIME
	(4 dimension arrays are for the fields 1:(u,v), 2:–, 3:T, 4:RH)	
DTSYOB	4* 100.	GAUSSIAN VERTICAL THETA(E) INFLUENCE 'RADIUS' AT THE GRID POINT COLUMN ASSIGNED TO THE SYNOP STATION (ACTIVE ONLY IF 'MSPRSYP'=2 !)
DPSYOB	4*1000.	SQUARE OF THE GAUSSIAN VERTICAL LN(P) INFLUENCE 'RADIUS' AT THE GRID POINT COLUMN ASSIGNED TO THE SYNOP STATION (ACTIVE ONLY IF 'MSPRSYP'=1 !)
DTSYLT	4* 1.	GAUSSIAN 'VERTICAL' THETA(E) INFLUENCE 'RADIUS' BETWEEN THE GRID PT. ASSIGNED TO THE OBS (LEVEL KE) AND THE TARGET GRID PT (AT K) (IF 'MSPRSYP'=2 !)

Variable	Default	Description
DPSYLT	4* .333	SQUARE OF GAUSSIAN 'VERTICAL' LN(P) INFLUENCE 'RADIUS' BETWEEN THE GRID PT. ASSIGNED TO THE OBS (LEVEL KE) AND THE TARGET GRID PT (AT K) (IF 'MSPRSYP'=1 !)

MSPRSYP=1	MSPRSYP=2	
DPSYOB small, DPSYLT large	DTSYOB small, DTSYLT large	: spreading primarily along σ surf.
DPSYOB large, DPSYLT small	DTSYOB large, DTSYLT small	: spreading primarily along $\theta_e/ln(p)$ surf.

WSYABL	4* 1.	FACTOR TO WEIGHTS WITHIN THE ATMOSPHERIC BOUNDARY LAYER (MORE PRECISELY THE MIXED LAYER)
THRMYMX	4* .1	IF THE LARGEST SPATIAL WEIGHT AT LAYER K FOR A GIVEN SURFACE OBS IS BELOW THIS THRESHOLD THEN THIS OBS IS NOT USED FOR SPREADING TO LAYER K-1
	Other parameters	
MSPRSYP	1	PARAMETER SPECIFYING THE SURFACE ALONG WHICH SURFACE DATA INCREMENTS ARE PRIMARILY SPREADED, I.E. THE PARAMETER WHICH SCALES THE VERTICAL DISTANCE BETWEEN THE GRID PT. ASSIGNED TO THE OBS. AND THE TARGET GRID PT. 1 : VERTICAL WEIGHTS DEPENDENT ON LN(P) DIFFERENCES ==> SPREADING PRIMARILY ALONG ISOBARS 2 : VERTICAL WEIGHTS DEPEND. ON 'TH(E)' DIFFERENCES (IF MSPRPAR EVEN: 'TH'; IF MSPRPAR ODD: 'THE') ==> SPREADING PRIMARILY ALONG ISENTROPES
LTIPLSY	.F.	.T. ==> LINEAR INTERPOLATION IN TIME OF SURFACE DATA WHICH ARE SMALLER THAN 'TIPOLMX' HOURS APART
TIPSYMX	3.0	MAX. TIME SPAN (HRS) ALLOWED FOR LINEAR INTERPOLAT. FOR SYNOP / DRIBU (TIPSYMX = 0 , IF NOT LTIPLSY)
WTUKSYA	2.5	FOR SAW-TOOTH-SHAPED TEMPORAL WEIGHTS TEMPORAL RADIUS OF INFLUENCE TOWARDS THE PAST RELATIVE TO THE OBS. TIME
WTUKSYE	0.5	FOR SAW-TOOTH-SHAPED TEMPORAL WEIGHTS TEMPORAL RADIUS OF INFLUENCE TOWARDS THE FUTURE RELATIVE TO THE OBS. TIME
RSYPMX	1.414	HORIZONTAL SEARCH RADIUS FOR GRID PTS. TO ASSIGN A SYNOP / DRIBU TO A GRID PT. (FOR 'RSYPMX' NEGATIVE, THE SEARCH IS LIMITED TO THE 4 NEIGHBOUR. GRID PTS)
MRHYES	20* 0	STATION ID'S OF SYNOP HUMID. DATA THAT ARE ALWAYS USED, I.E. IRRESPECTIVE OF RFHASY, FHASY, ALTOPSY.
MRHNO	20* 0	STATION ID'S OF SYNOP HUMID. DATA THAT NEVER USED
MUVYES	20* 0	STATION ID'S OF SYNOP WIND DATA THAT ALWAYS USED
MUVNO	20* 0	STATION ID'S OF SYNOP WIND DATA THAT ARE NEVER USED

NAMELIST /SPRRS/ : VARIOUS PARAMETERS, INCLUDING SOME RELATED TO LATERAL SPREADING OF OBS. INCREMENTS

KTOPTH	0	LOWEST MODEL LEVEL WHERE LATERAL SPREADING IS ALWAYS ALONG MODEL SURFACES
LTOPTH	.T.	.T. ==> LATERAL SPREADING NOT ALONG SIGMA LEVELS (IF MSPRPAR.GE.2) ONLY WITHIN MODEL'S SIGMA LEVELS
	(4 dimension arrays are for the fields 1:(u,v), 2:–, 3:T, 4:RH)	
TOPOBS	4*1050.	THRESHOLD [hPa] ABOVE THIS LEVEL (SMALLER PRESSURE), ONLY OBS. INCR. AT MODEL LEVELS ARE USED ('TOPOBS' IS FIXED AT 1050[hPa] IF 'MSPRPAR'.LE.1)
BOTMOD	4*1050.	THRESHOLD [hPa] BELOW THIS LEVEL (LARGER PRESSURE), ONLY OBS. INCR. AT OBS. LEVELS ARE USED ('BOTMOD' IS LARGER THAN 'TOPOBS', AND 'BOTMOD' IS FIXED AT 1050[hPa] IF 'MSPRPAR'.LE.1)
LSCADJ	4* .T.	.F. ==> LINEAR VERTICAL INTERPOLATION (IN LN(P)) INSTEAD OF VERTICAL SCALE ADJUSTMENT (BY VERTICAL AVERAGING OVER THE MODEL LAYER) FOR CONVEYING THE OBSERVATIONAL INFORMATION TO THE MODEL LEVELS (FOR COMPUT. OBS. INCR. AT MODEL LEVELS)
LYTHICK	.T.	IF .F. THEN INTERPOLATION OF MODEL VALUES TO OBS. LEVELS IS LINEAR IN LOG(PRESSURE), I.E. THE THICKNESS OF THE MODEL LAYERS IS NOT TAKEN INTO ACCOUNT
LSIGNIF	.T.	IF .F. THEN INTERPOLATION TO MODEL LEVELS ALWAYS OF OBS. INCRMENTS (INSTEAD OF OBS. VALUES, EVEN IF SUFFICIENT SIGNIFICANT-LEVEL DATA EXIST)

Variable	Default	Description
IONL, JONL	38,40	GRID PT COORDINATES FOR STANDARD OUTPUT ON DIAGNOSTIC FILE
IONL2, JONL2	38,40	2ND GRID PT COORDINATES FOR OTHER STANDARD OUTPUT
Parameters to weight different terms in the prognostic equations (only available in Euler scheme)		
+ FQADVH	1.	HORIZONTAL ADVECTION OF HUMIDITY
+ FQADVV	1.	VERTICAL ADVECTION OF HUMIDITY
+ FQDIFH	1.	HORIZONTAL DIFFUSION OF HUMIDITY
+ FQDIFV	1.	VERTICAL DIFFUSION OF HUMIDITY
+ FQRAIN	1.	HUMIDITY TENDENCY DUE TO PRECIPITATION
+ FHTHERM	1.	TOTAL ENERGY TENDENCY DUE TO THERMAL RADIATION
+ FHSOLAR	1.	TOTAL ENERGY TENDENCY DUE TO SOLAR RADIATION
+ FHADV	1.	ADVECTION OF TOTAL ENERGY
+ FHDIFH	1.	HORIZONTAL DIFFUSION OF TOTAL ENERGY
+ FHDIFV	1.	VERTICAL DIFFUSION OF TOTAL ENERGY
NAMELIST /OUTRS/ : PARAMETERS FOR DIAGNOSTIC : GENERAL AND RELATED TO VERTICAL PROFILES		
LTIMSER	.T.	.T. ==> PRINT TIME SERIES OF VERTICAL VELOCITY ON DIAGNOSTIC FILE(S)
LRSPRI	.T.	.T. ==> PRINT DATA ABOUT SURFACE PRESSURE ON DIAGNOSTIC FILES
NAMELIST /OUTSY/ : PARAMETERS FOR DIAGNOSTIC RELATED TO NUDGING OF SURFACE OBSERVATIONS		
LSYPRI	.T.	.T. ==> PRINT SURF. DATA ON STD. OUTPUT FOR CONTROL

D Modifications to the Swiss Model code

The SM code used for the present work is based on the version 2.25.1.1 of the DM/SM, with nudging extensions based on the November 1997 version of the DM nudging and with further extensions to allow the generation of synthetic wind profiler reports. With these latter extensions, both wind profiles and temperature profiles can be generated, including the simulation of observation errors. The error characteristics and the profile location, bottom, top and vertical resolution are individually specified for each synthetic profile. The observation frequency is globally specified for all simulated profiles. All these characteristics are defined in the Fortran namelist GENOBS (see below), read by the program EM.

The synthetic reports, possibly complemented with other observation reports, are stored in an Analysis Observation File (AOF); the format used by AOF is a binary format suited for observations reports which was developed at the ECMWF (Martellet, 1978). This is the native format for feeding the nudging code with observation bulletins.

A rich set of diagnostic information is available in the file YUGOBS, created in the working directory of the SM. It is also possible to have a print out of some or all of the generated profiles, including the values of the wind and temperature fields on the interleaved model levels.

Variables defined in namelist GENOBS

Variable	Type	Default	Description
YIAOFPATH	CHAR*64	' '	Path of input AOF (supplementary data)
YOAOFPATH	CHAR*64	' '	Path of output AOF (synthetic and supplementary data)
LGEN_WP	LOGICAL	false	If true: generate synthetic wind profiler data
NBTH_WP	REAL	9999.	Begin time (in hour)
NDTH_WP	REAL	9999.	Period (in hour)
NETH_WP	REAL	9998.	End time (in hour) — Define time series for
NBT_WP	INTEGER	9999	Begin time (time step) — synthetic WP observations
NDT_WP	INTEGER	9999	Period (time step)
NET_WP	INTEGER	9998	End time (time step)
ILOC_WP	INTEGER	0	Wind profile location, i-coordinate
JLOC_WP	INTEGER	0	Wind profile location, j-coordinate
UVBOT_WP	INTEGER	0	Bottom of wind profile (meter above ground)
UVTOP_WP	INTEGER	0	Top of wind profile (meter above ground)
UVRES_WP	INTEGER	0	Vertical resolution of wind profile (meter)
DDSYS_WP	REAL	0.	Bias on wind direction
DDSTD_WP	REAL	0.	Standard deviation of wind direction random error
FFSYS_WP	REAL	0.	Bias on wind velocity
FFSTD_WP	REAL	0.	Standard deviation of wind velocity random error is
FF_ERRN_WP	REAL	20.	(*ff*/FF_ERRN_WP) * FFSTD_WP , *ff* is the wind velocity in m/s
TBOT_WP	INTEGER	0	Bottom of temperature profile (meter above ground)
TTOP_WP	INTEGER	0	Top of temperature profile (meter above ground)
TRES_WP	INTEGER	0	Vertical resolution of temperature profile (meter)
TSTD_WP	REAL	0.	Standard deviation of temperature random error
TSYS_WP	REAL	0.	Bias on temperature
LPRT_WP	LOGICAL	false	If true: print generated profile in file YUGOPRT

Remark: if the vertical resolution of a profile is set to 0 the corresponding profile will not be generated.

Implementation details

No provision for WP reports exist in the original definition of the AOF format. In order to minimize the amount of modifications in the nudging code, it has been decided to consider a WP report as a special type of TEMP report. Moreover, to avoid too large truncation errors, the precision used to store the wind velocity in AOF observation records has been increased. In summary:

- WP reports are characterized by an *observation type* of value 5 (same value as for TEMP reports) and a *code type* of value 300 (new value introduced for WP).
- In the data observation records of a WP report the dew-point temperature and the pressure values are always set to undefined.
- The wind velocity is expressed in tenths of ms^{-1}.
- In the nudging code the quality control thresholds used for WP observations are those defined for TEMP.

The creation of synthetic WP reports requires the definition of a station identifier and of a station altitude:

- The station identifier of a *synthetic* WP report is the position of its definition in the corresponding namelist variable array.
- The station altitude for a *synthetic* WP report is the model orography (FIB) at the profile location.

Code for OSSE extensions has been designed in order to minimize the modifications to the existing SM code and to facilitate the creation of new modules for other types of synthetic reports. In particular the functionality of the routines PLATTE, MEDEA and GETMEM has been duplicated. The modified and new routines are:

Modified in original SM library
- unitnr.h, unidt.h, unitch.h : new Fortran units for diagnostic files and per-message scratch files
- emorg.F : call to routines genobs_init, genobs, genobs_post
- medea.F : do not close NUIN; modify some default values

Modified in nudging routines
- obcdtp.h, settyp.F, setdig.F,
  pointrs.F, prevent.F, prstat.F : add new AOF code type for wind profiler
- comana.h, namana.h, defrun.F,
  hedaof.F : new namelist variable to control production of WP reports
- multil.F : accept TEMP report of type WP with missing pressure data
- setnmb.F, comeve.h : update description of event types
- setnum.F : RFACT(3) set to 0.1 (for new representation of wind velocity)
- setiod.F : clean-up usage of Fortran unit numbers
- comiod.h, rpppmod.F : bugs correction

New header:
- comgobs.h : PARAMETERS statements, COMMON blocks and DATA statements

New routines:
- genobs_platte.F, genobs_medea.F,
  genobs_getmem.F : duplicate functionality of routines platte, medea and getmem
- genobs_init.F, genobs.F,
  genobs_post.F : generic routines to generate synthetic observations
- genwp.F : generate synthetic WP observations
- readaof.F, readobr.F : read AOF and fill arrays with observation data
- makeaof.F, makefdr.F, makeddr.F,
  makeobr_wp.F : create AOF from a set of arrays containing observation data
- merge_prof.F, usvs2df.F : other utilities

ACRONYMS AND ABBREVIATIONS

AOF	**A**nalysis **O**bservation **F**ile *(used to store observation records)*
BL radar	**B**oundary **L**ayer radar *(WP operating in the GHz band)*
COST	European **Co**operation in the Field of **S**cientific and **T**echnical Research
CWINDE	**C**OST **W**ind **I**nitiative for a **N**etwork **D**emonstration in **E**urope
DM	**D**eutschland **M**odell *(DWD operational meso-β NWP model)*
DWD	**D**eutsher **W**etter**d**ienst
ECMWF	**E**uropean **C**enter for **M**edium-Range **W**eather **F**orecasts
EM	**E**uropa **M**odel *(DWD operational meso-β NWP model, provides LBC for DM/SM)*
FASTEX	**F**ronts and **A**tlantic **S**torm **T**rack **Ex**periment
FT radar	**F**ull-**T**ropospheric radar *(WP operating in the 400MHz band)*
LBC	**L**ateral **B**oundary **C**onditions *(used in relation with a NWP model)*
MAP	**M**esoscale **A**lpine **P**rogramme
MAP SOP	**MAP S**pecial **O**bserving **P**eriod *(core of the MAP field experiment)*
NWP	**N**umerical **W**eather **P**rediction
OI	**O**ptimal **I**nterpolation *(3-D data assimilation technique)*
OSE	**O**bserving **S**ystem **E**xperiment *(based on real observations)*
OSSE	**O**bserving **S**ystem **S**imulation **E**xperiment *(based on synthetic observations)*
RASS	**R**adio **A**coustic **S**ounding **S**ystem *(complements WP to measure temperature profile)*
RUBC	**R**adiative **U**pper **B**oundary **C**ondition *(used in relation with a NWP model)*
SM	**S**wiss **M**odel *(SMI operational meso-β NWP model)*
SMI	**S**wiss **M**eteorological **I**nstitute
ST radar	**S**trato-**T**roposheric radar *(WP operating in the 50MHz band)*
VAD	**V**elocity **A**zimuth **D**isplay *(technique to derive wind profile from weather radar)*
WP	**W**ind **P**rofiling radar

REFERENCES

Arnold C.P. and Dey C.H., 1986. Observing-Systems Simulation Experiments: Past, Present, and Future. *Bull. Amer. Meteor. Soc.*, **67**, 687-695.

Bader M.J. and Graham R.J., 1996. Impact of Observations in NWP Models: Techniques and Results of Recent Studies. *Scientific Paper of the UK Meteorological Office*, **42**.

Bao J.W. and Errico R.M., 1997. An Adjoint Examination of a Nudging Method for Data Assimilation. *Mon. Wea. Rev.*, **125**, 1355-1373.

Bettems J.-M. and Binder P., 1998. The impact of an hypothetical Alpine wind profiler network on numerical weather prediction - a MAP case. *The MAP Newsletter*, **9**, 72-73.

Bettems J.-M., Binder P. and Ruffieux D., 1998. The impact of real and hypothetical wind profiler observations on numerical weather prediction - a FASTEX case. *Proc. of the 4th International Symposium on Tropospheric Profiling*, Snowmass, 2-25 Sept. 1998.

Binder P. and Rossa A., 1996. The Mesoscale Alpine Programme (MAP) – tackling current challenges in mountain meteorology. *Proc. of the 7th AMS Conf. on Mesoscale Processes*, Reading UK, 9-13 Sept. 1996, 263-265.

Davies H.C., 1976. A lateral boundary formulation for multilevel prediction models. *Quart. J. Roy. Meteor. Soc.*, **102**, 405-418.

Germann U., 1998. Vertical wind profile by SMA Doppler weather radars – A description of the product. Private communication.

Herzog H.-J., 1995. Testing a radiative upper boundary condition in a nonlinear model with hybrid vertical coordinates. *Atmos. Phys.*, **55**, 185-204.

Jacobsen I. and Heise E., 1982. A new economic method for the computation of the surface temperature in numerical models. *Beitr. Phys. Atm.*, **55**, 128-141.

Görsdorf U., 1997. The accuracy of temperature measurements with RASS. *COST-76 Profiler Workshop Proc.*, Engelberg CH, 12-16 May 1997, 231-234.

Kuo Y.H. and Guo Y.R., 1989. Dynamic Initialization Using Observations from a Hypothetical Network of Profilers. *Mon. Wea. Rev.* , **117**, 1975-1998.

Louis J.-F., 1979. A parametric model of vertical eddy fluxes in the atmosphere. *Bound.-Layer Meteor.*, **17**, 187-202.

Majewski D., 1985. Balanced initial and boundary values for a limited area model. *Contrib. Atmos. Phys.*, **58**, 147-159.

Majewski D., 1991. The Europa-Model of the Deutscher Wetterdienst. *Proc. of ECMWF Seminar on Numerical Methods in Atmospheric Models*, Reading UK, 9-13 Sept. 1991, **2**, 147-191.

Martelet J., 1978. Format of Analysis Observations files. *ECMWF Technical Note.*

Mellor G.L. and and Yamada T., 1974. A hierarchy of turbulence closure models for planetary boundary layers. *J. Atmos. Sci.*, **13**, 1791-1806.

Nash J. and Lyth D., 1997. Quality Evaluation of Time Series of Upper Winds. *COST-76 Profiler Workshop Proc.*, Engelberg CH, 12-16 May 1997, 239-242.

Newton C.W., 1954. Analysis and Data Problems in Relation to Numerical Prediction. *Bull. Amer. Meteor. Soc.*, **35**, 287-294.

NOAA, 1994. Wind Profiler Assessment Report and Recommendations for Future Use. *NOAA Report*, Silver Spring MD, 141 pp.

Oakley et al., 1997. CWINDE 97 – Report from Project Office. *COST-76 Profiler Workshop Proc.*, Engelberg CH, 12-16 May 1997, 23-26.

Ritter B. and Geleyn J.-F., 1992. A comprehensive radiation scheme for numerical weather prediction models with potential applications in climate simulations. *Mon. Wea. Rev.*, **120**, 303-325.

Schraff C.H., 1996. Data Assimilation and Mesoscale Weather Prediction: a Study with a Forecast Model for the Alpine Region. *Publications de l'Institut Suisse de Météorologie*, **56**.

Schraff Ch.H., 1997. Mesoscale Data Assimilation and Prediction of Low Stratus in the Alpine Region. *Meteorol. Atmos. Phys.*, **64**, 21-50.

Smith T.L. and Benjamin S.G., 1994. Relative Impact of Data Sources on a Data Assimilation System. *Proc. of the 10th AMS Conf. on NWP*, Portland USA, 18-22 July 1994, 491-493.

Stauffer D.R. and Seaman N.L., 1990. Use of four-dimensional data assimilation in a limited-area mesoscale model. Part I: Experiments with synoptic-scale data. *Mon. Wea. Rev.*, **118**, 1250-1277.

Tiedtke M., 1989. A comprehensive mass flux scheme for cumulus parametrization in large-scale models. *Mon. Wea. Rev.*, **117**, 1779-1800.

Van Baelen J., 1998. Wind Profilers for MAP: The French and European ST Radar Network. *The MAP Newsletter*, **8**, 25-27.

ACKNOWLEDGEMENTS

The funding for this work has been supplied by the Laboratory for Atmospheric Physics of the ETH Zurich (LAPETH), and by the Swiss Meteorological Institute (SMI) through the 'Windprofiler Pilotprojekt'. I express my gratitude to Prof. H. Richner, LAPETH, and to Dr. B. Hoegger, SMI.

Dr. Peter Binder, who initiated this project, is especially thanked for his guidance and for the numerous interesting and useful discussions we had together.

I thank also Dominique Ruffieux, SMI, for his constructive remarks and for the presentation he made during the 4th international symposium on tropospheric profiling, at Snowmass, Colorado.

Last but not least I thank Jean Quiby, head of the numerical meteorology group at the SMI, and all my colleagues for the friendly atmosphere and the constructive collaboration existing inside this group.